5-2016

# Development of Electrochemical Sensors Suitable for In Vivo Detection for Neurotransmitters

Mengjia Hu
*University of Arkansas, Fayetteville*

Development of Electrochemical Sensors Suitable for In Vivo Detection for Neurotransmitters

A dissertation submitted in partial fulfillment
of the requirements for the degree of
Doctor of Philosophy in Chemistry

by

Mengjia Hu
Wuhan University
Bachelor of Science in Chemistry, 2010

May 2016
University of Arkansas

This dissertation is approved for recommendation to the Graduate Council.

_____
Dr. Ingrid Fritsch
Dissertation Director

_____
Dr. Julie Stenken
Committee Member

_____
Dr. David Paul
Committee Member

_____
Dr. Charles Wilkins
Committee Member

**Abstract**

The electrochemical method of redox cycling was exploited to achieve new discoveries in neurotransmitter detection and to advance its suitability toward in vivo use. Redox cycling has advantages in signal amplification, selectivity of species based on their electrochemical reaction mechanisms, and limited or no background subtraction. Distinction of dopamine from norepinephrine in a mixture with an electrochemical method at unmodified electrodes was demonstrated for the first time in vitro. This ability resulted from a series of fundamental studies of redox cycling behavior of the catecholamines (dopamine, norepinephrine and epinephrine) using different electrode configurations. Taking advantage of the ECC' mechanism associated with their electrochemical oxidation and the substantially different rate constants for the first order intramolecular cyclization reaction, the catecholamines can be distinguished by monitoring the current at collector electrodes activated at different distances from the generator. In vitro detection of dopamine in the presence of multiple electrochemically-active interfering species (ascorbic acid, uric acid, L-3,4-dihydroxyphenylalanine, homovanillic acid, 3-methoxytyramine and 5-hydroxyindoleacetic acid) has also been investigated for future in vivo applications. Selective detection of physiological concentrations of dopamine at the collector electrodes using microfabricated electrode arrays was shown (with detection limits of 0.730 ± 0.013 μM and 0.086 ± 0.002 μM for dopamine with and without the presence of interfering species, respectively). In addition, two types of unique neural probes (co-planar and vertical edge microelectrode arrays) were designed with the purpose to implement the redox cycling approach in vivo. An innovative design was used to minimize the number of masks for eight layers of electrodes. Different microfabrication procedures were evaluated, with further work still needed for optimization. Also, analysis of anodic stripping voltammetry of silver-containing nanoparticles modified on electrode surfaces, performed as an interest in expanding the detection to other important neurochemicals, showed that commonly used drop-casting techniques deposit nanoparticles non-uniformly. More reproducible modification methods are needed. The work in this dissertation demonstrates the capabilities of redox cycling for multi-neurotransmitter analysis and sets the foundation for development of novel neural probes for implementing the approach. This method may also be used to obtain mechanisms and kinetics beyond the ones investigated here.

**Acknowledgements**

I would like to express my most sincere gratitude to my advisor, Dr. Ingrid Fritsch, for the invaluable support and guidance she provided throughout my graduate study. I have learned so much from her over the years, not only scientific knowledge but also the way of conducting research and communicating with other scientists. This research project would not have been possible without her idea and expertise in this field. I am truly grateful for the experience of working with her.

I would also like to thank my committee members, Dr. Julie Stenken, Dr. David Paul, and Dr. Charles Wilkins, for their insightful discussions and advices, as well as their patience and continuous support.

I greatly appreciate the training, advices and support from Errol Porter on microfabrication. Many thanks to Jerry Homesley and K.Z. Shein for their support and help on troubleshooting of instruments.

I am especially grateful for the support from current and previous members of the Fritsch group. Special thanks to Dr. Anupama Aggarwal, for introducing me to this interesting research project and providing the required training.

Lastly, I would especially like to thank my parents for their love and encouragement, as well as all of my friends for making this journey so memorable.

Research was supported partially through the National Science Foundation (CBET-1336853) and the Arkansas Biosciences Institute, the major research component of the Arkansas Tobacco Settlement Proceeds Act of 2000.

**Table of Contents**

**List of Published Papers**

Chapter 2: Redox Cycling Behavior of Individual and Binary Mixtures of Catecholamines at Gold Microband Electrode Arrays

This Chapter was published as

Hu, M.; Fritsch, I. *Anal.Chem.* **2015**, *87*, 2029-2032.

# 1. Introduction to Neurotransmitters in Brain and Methods to Detect Them

## 1.1 Introduction

Neurotransmitters, also known as chemical messengers, are chemicals released from excited presynaptic neurons and stimulate postsynaptic neurons or receptor cells. They play important roles in neurotransmission and multiple functions of the brain. Malfunction of neurotransmitters usually leads to neurological disorders or disease, such as Parkinson's disease, Huntington's disease and Alzheimer's disease.[1] To understand the origin and mechanisms of the neurological system, it is important to be able to monitor the extracellular concentrations of neurotransmitters in the mammalian brain.

There are different types of neurotransmitters in the brain, including amino acids, monoamines, and peptides. Some of these molecules are electrochemically active (e.g. catecholamines) and can be electrochemically detected. Some are not electrochemically active but can produce electrochemically detectable species with enzymatic reactions (e.g. L-glutamate and acetylcholine). Therefore, they can be detected using an enzyme-based electrochemical method. Some cannot undergo a direct oxidation-reduction reaction at an electrode, nor can be related to any enzymatic reactions (e.g. γ-aminobutyric acid), and cannot be detected by electrochemical methods.[2]

The release process of neurotransmitters in the brain is usually triggered by an action potential in the presynaptic neuron. The vesicles containing neurotransmitters will release them into the synaptic cleft by exocytosis, and then the released neurotransmitters will bind to specific receptors embedded in the postsynaptic membrane and causes depolarization of the postsynaptic neuron. After the signal has been transmitted, the neurotransmitters will be cleared from the synaptic cleft by diffusion so that its effect will not last too long, and this process for neurotransmitters like catecholamine is aided by reuptake.[3] The extracellular concentration of neurotransmitters is a result of the balance between release and clearance, which is dynamically controlled and regulated. Since they are short-lived and usually at low levels (e.g. dopamine has basal level extracellular concentrations of 5-100 nM[4] and after stimulation, overflow in the micromolar range occurs and decays with a half-life of 0.2 s in rat striatum[5]), it is difficult to monitor them. Thus, there is a need to develop new methods to selectively detect them at physiological basal concentrations.

### 1.1.1 Monoamine Neurotransmitters

The catecholamines, including dopamine (DA), norepinephrine (NE) and epinephrine (EP), are important neurotransmitters that contain one amine group and a catechol nucleus. Along with serotonin (5-HT), which also has one amine group attached to the aromatic ring, they belong to the monoamine neurotransmitters group. Monoamine neurotransmitters have been studied a lot because they are involved in many neural pathways in the brain and regulate multiple neural functions, such as movement, mood, attention and visceral function.[1]Visual representations of these pathways can be found in the literature.[6]

DA is a crucial central nervous system neurotransmitter that plays a role in cognition and motor control. It is synthesized from L-dopa using the enzyme dopa decarboxylase. There are two major dopaminergic pathways. One is between the substantia nigra and striatum. This is involved in voluntary movements. Dysfunction of this pathway may lead to Parkinson's disease. The other pathway connects the ventral tegmental area to the frontal lobe. It has different functions, including the "reward" system, which is important for the study of adaptive behavior.[1, 3]

NE can be synthesized in neurons in the locus coeruleus via an enzyme called dopamine β-hydroxylase to remove the β-hydroxyl group on DA. It has pathways from locus coeruleus projecting to the cerebral cortex, the thalamus and the hypothalamus, the olfactory bulb, the cerebellum, the midbrain and the spinal cord. It is involved in regulation of functions such as attention and arousal, because it increases the level of excitatory activity.[1, 3]

EP is in the last of the biosynthesis line of catecholamines that can be converted from NE by the enzyme phentolamine N-methyltransferase. EP is localized to the hypothalamus and brainstem/medulla in brains of various species including mammals.[7] It serves as a neurotransmitter in the brain as well as being released in the bloodstream and is related to the fight-or-flight response of the autonomic nervous system.

The three catecholamines have similar molecular structure and they all undergo similar 2-electron oxidation at physiological pH, which makes it difficult to distinguish them by simple electrochemical methods. The potential at which they start to oxidize in vivo is around +0.2 V vs a Ag/AgCl (3 M NaCl) reference electrode when scanning the electrode from -0.2 V to +0.6 V using a carbon paste electrode.[8, 9] Different catecholamines can coexist in certain regions of the brain or other organs in the body.[10, 11] It is important to have a method with high spatial and temporal resolution that distinguish them from each other.

Efforts have been made toward the differentiation of catecholamines based on their electrochemical oxidation mechanism. An ECC' mechanism has been proposed for the three catecholamines,[12, 13] and is schematically shown in Figure 1.1. This process starts with a two-electron transfer step at the electrode (E), in which catecholamines oxidize to form an *o*-quinone (OQ). The OQ undergoes an intramolecular cyclization process (C) and internal oxidation-reduction in solution to form the leucoaminochrome (LAC). The apparent rate constants for this intramolecular cyclization reaction for the three catecholamines are substantially different ($k_{DA}$ = 0.13 ± 0.05 $s^{-1}$, $k_{NE}$ = 0.98 ± 0.52 $s^{-1}$, $k_{EP}$ = 87 ± 10 $s^{-1}$, in phosphate buffer at pH 7.4),[14] which provides the opportunity of differentiation between them. LAC can engage in a homogenous reaction (C') with another molecule in the OQ form, resulting in an additional two-electron oxidization to the aminochrome (AC), while the OQ reduces back to the original catecholamine. It has been reported that AC also undergoes a two-electron reduction and its $E_{1/2}$ value is about -0.207 V vs. Ag/AgCl (saturated KCl) for EP.[12, 15] This is more negative than the reduction potential of OQ, and thus will not interfere with the reduction signal arising from electrochemical conversion of OQ back to the catecholamine form.

### 1.1.2 Electrochemically-Active Interfering Species in the Brain

Neurotransmitters do not function by themselves in a simple environment. Instead, they exist in a complicated biological matrix containing different substances, some of which are electrochemically active, and therefore can create interferences in electrochemical detection. Ascorbic acid (AA) is one that has been of most concern for in vivo electrochemical detection of DA. It serves as antioxidant in the brain to clear oxygen or nitrogen based radicals and serves as a neuromodulator for DA- and glutamate-mediated neurotransmission. It exists in millimolar concentrations which are about $10^4$-$10^5$ times of DA in some regions of the brain.[16, 17] AA undergoes a two-electron oxidation followed by a chemical hydration process (EC mechanism).[18] The chemical hydration process has fast kinetics and the hydrated product is not electrochemically active. Thus, an irreversible or quasi-reversible electrochemical behavior is observed.

Other electrochemically active species include uric acid (UA), L-3,4-dihydroxyphenylalanine (L-dopa), a precursor to DA, and metabolites of catecholamines: 3,4-dihydroxyphenylacetic acid (DOPAC), homovanillic acid (HVA), and 3-methoxytyramine (3-MT).[9] The metabolites of 5-HT, 5-hydroxyindoleacetic acid (5-HIAA) also coexist with catecholamines in certain regions of the brain.

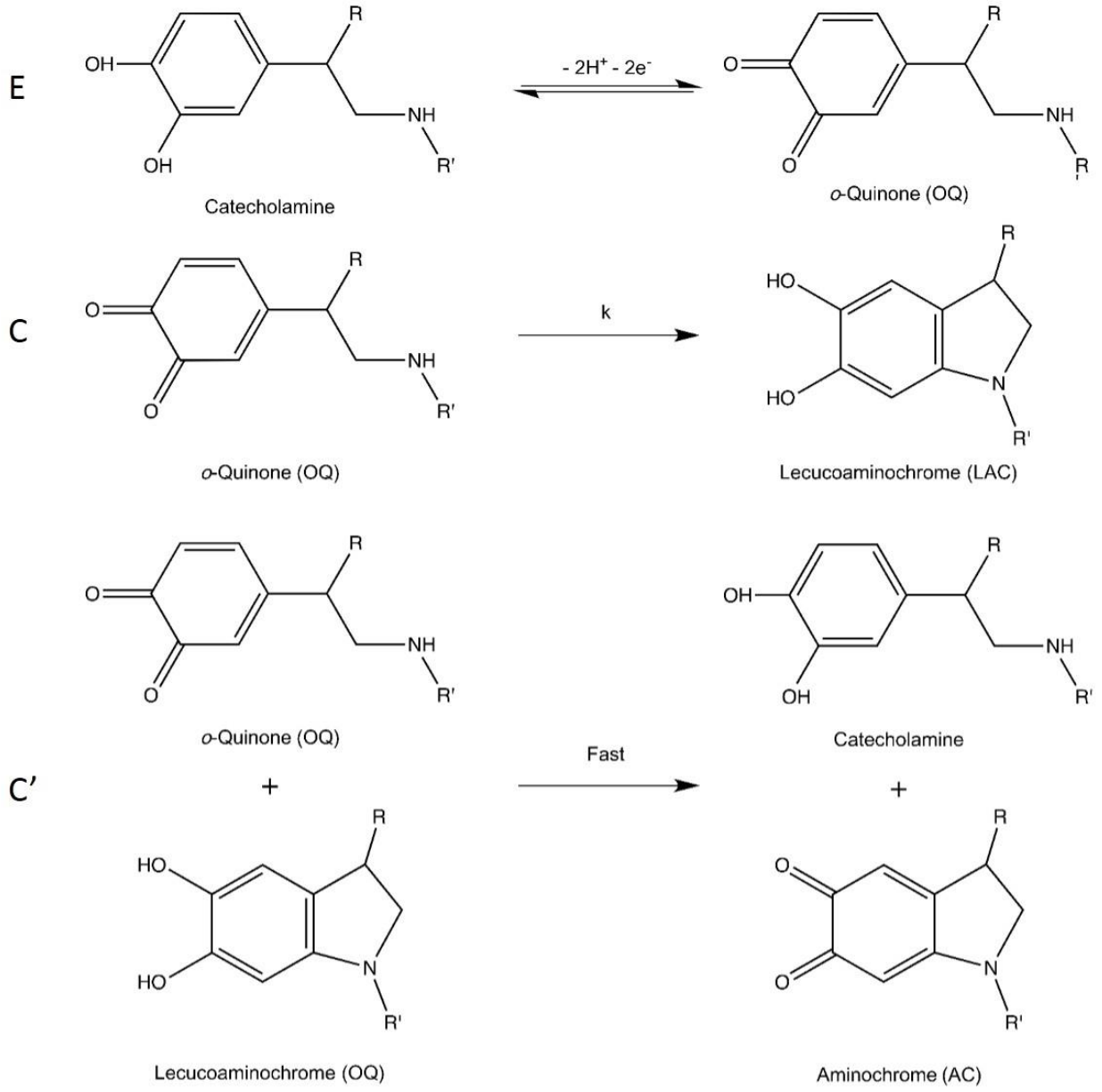


**Figure 1.1** Schematic representation of the ECC' mechanism of the electrochemical oxidation of catecholamines: DA, R=H, R'=H; NE, R=OH, R'=H; EP, R=OH, R'=$CH_3$. (Reaction mechanism proposed by Ciolkowski et al.[13])

Most of the electrochemically interfering species mentioned above have similar electrode potentials to those of catecholamines, especially AA and DOPAC, which have similar oxidation potential in vivo.[9] Thus, with a simple electrochemical method, such as cyclic voltammetry (CV) or chronoamperometry (CA) using unmodified electrodes, these species cannot be distinguished from catecholamines. Consideration of improvements to electrochemical detection is needed.

Selective detection of catecholamines in the presence of these interfering species by electrochemistry can be achieved with electrode modification, which eliminates some interfering species (e.g. Nafion can be used to eliminate the DOPAC signal because DOPAC is negatively charged at physiological pH and repelled by Nafion[19]) or shifts the oxidation or reduction peaks of the analyte. Species can also be selectively detected by examining the shapes of their voltammograms and the unique oxidation and reduction peak potentials.

### 1.1.3 In Vivo Detection Methods of Neurotransmitters

A lot of effort has been spent toward investigating chemical communication between neurons in the brain using in vivo detection of neurotransmitters with high sensitivity and selectivity. Most detection methods are used in combination with traditional neurochemical tools to provide complete information about the in vivo environment. Three predominant approaches in this field include microdialysis, electrochemistry, and spectroscopy.[9]

Microdialysis is an important sampling method for analyzing extracellular fluid and is widely used for in vivo neurochemistry studies. It uses a microdialysis probe with a semi-permeable membrane to collect extracellular fluid, and the tips of the probe are typically 200–400 μm in diameter. The semi-permeable membrane will let small molecules like the amine neurotransmitters pass through the membrane according to their concentration gradient. The perfusion inside the probe with a slow rate (< 3 μl/min) will generate a stream and carry the analyte to the detector. As a sampling method, microdialysis must be coupled with different separation and detection techniques such liquid chromatography, mass spectrometry and electrochemical detection which can help achieve a high degree of chemical selectivity and sensitivity.[20, 21]

There are advantages and disadvantages involved with in vivo microdialysis of the brain. Implementation of the probe is relatively easy and a variety of neurotransmitters can be studied at the same time. Also, the probe can be used to infuse known compounds such as drug molecules, which make it good

for preclinical and clinical applications.[2, 20] However, microdialysis provides worse spatial and temporal resolution than electrochemical sensors. The typical spatial resolution for typical microdialysis is about 0.1 $mm^3$ as it generally has a larger probe size. The temporal resolution is usually between 10 to 30 min, and it depends on the sampling efficiency, which is related to membrane properties and perfusion flow rate, and properties of the detection method. The relatively low temporal and spatial resolution make it inadequate for measuring transient signals with precise location information. In addition, there is also the problem of tissue damage, which has brought about concerns regarding its accuracy.[21, 22]

Electrochemical detection of neurotransmitters has been studied since the 1970s. Detection of catecholamines with AA as a major interfering species has been reported.[8] Selective detection of all the neurotransmitters presented in the extracellular fluid of the brain is a major challenge for in vivo voltammetry. Several methods including CA, differential normal pulse voltammetry (DPV) and fast-scan voltammetry (FSCV) are used, where FSCV is one of the most popular methods.[4, 9]

Carbon-fiber microelectrodes are mostly used for in vivo voltammetry since they have relatively small sizes (5-15 μm diameter or even smaller), which causes little tissue damage.[23, 24] Detection of DA by FSCV using carbon-fiber microelectrodes in vivo has been developed over several decades. Sub-second DA release in rat striatum has been studied by FSCV with background subtraction. Because FSCV is performed with a very high scan rate (300 V/s to 600 V/s), it can eliminate the AA oxidation signal due to its slow kinetics. Selectivity over other species can be achieved by using specific applied waveforms that can cause shifts in the peak potentials. The voltammogram of different species can be distinguished by their oxidation and reduction peak position and shape, which is determined by the redox potential, electrochemical reversibility, and electron transfer kinetics of the species.[4, 9] Quantitative measurement of individual components within a mixture of neurochemicals including DA, 5-HT, DOPAC, HVA, 3-MT, L-dopa, UA and AA has been made in Wightman's laboratory.[25] However, NE cannot be distinguished from DA in a mixture by simple FSCV. Instead, they have made in vivo detection of NE and DA simultaneously by inserting two carbon-fiber electrodes in different regions of the brain to examine differences in the dynamics of their extracellular concentrations.[26]

FSCV is suitable for monitoring the phasic DA because of its high temporal resolution, but problems will arise when used for long-term measurement of basal levels. Because of the large capacitive current

produced during the fast scan rate experiment, a large non-faradaic background current is produced and this background current at a carbon electrode surface is stable for minutes so that it can be subtracted. But over longer times, the background current will drift, which may produce problems when trying to measure the basal level signal for extended periods.[4, 27] Another problem for this technique is that catecholamines may adsorb to carbon electrodes, which results in an increase in the observed signal and a slower time response of the electrode. The problem of slower time response could be solved by deconvolution of the CV data.[28, 29]

Spectroscopic techniques such as positron emission tomography (PET) and functional magnetic resonance imaging (fMRI) can also be used to monitor neurotransmitter activity, which are noninvasive and can provide spatially resolved images for neuronal activity of the intact brain.[22] PET uses chemical agents that emit positrons to image changes of extracellular DA levels. But it is not widely used because of its low temporal (<10 s) and spatial resolution (<1 $cm^3$), as well as its high cost. The fMRI method takes advantages of hydrogen spins and has been applied for various behavioral studies. Resolution of approximately 4 mm has been achieved by fMRI in human subjects.[9]

### 1.1.4 Redox Cycling

The electrochemical method redox cycling has the advantages of no background subtraction,[30] signal amplification, and selectivity of species with different electrochemical reaction mechanisms. These features make it a promising technique for in vivo neurotransmitter detection. Its application for detection of DA in the presence of interfering species using different electrode configurations has been studied in vitro both in stationary and flow systems.[31-37] Normally, electrode arrays with two or more sets of closely spaced electrodes are used for redox cycling studies. In redox cycling, species generated (by oxidation or reduction of the analytes) at one set of electrodes (generator) diffuse to their neighboring electrodes (collector), and can be converted back to their original form at the collector (by reduction or oxidation, respectively). A schematic of this process is shown in Figure 2.1. This process can be repeated for multiple cycles if the generated species remain electrochemically active when it reaches the collector, this helps to amplify the signal. With decreasing gap between the generator and the collector electrodes, better amplification and collection at the collector can be achieved, because there is less time for diffusional loss of the generated

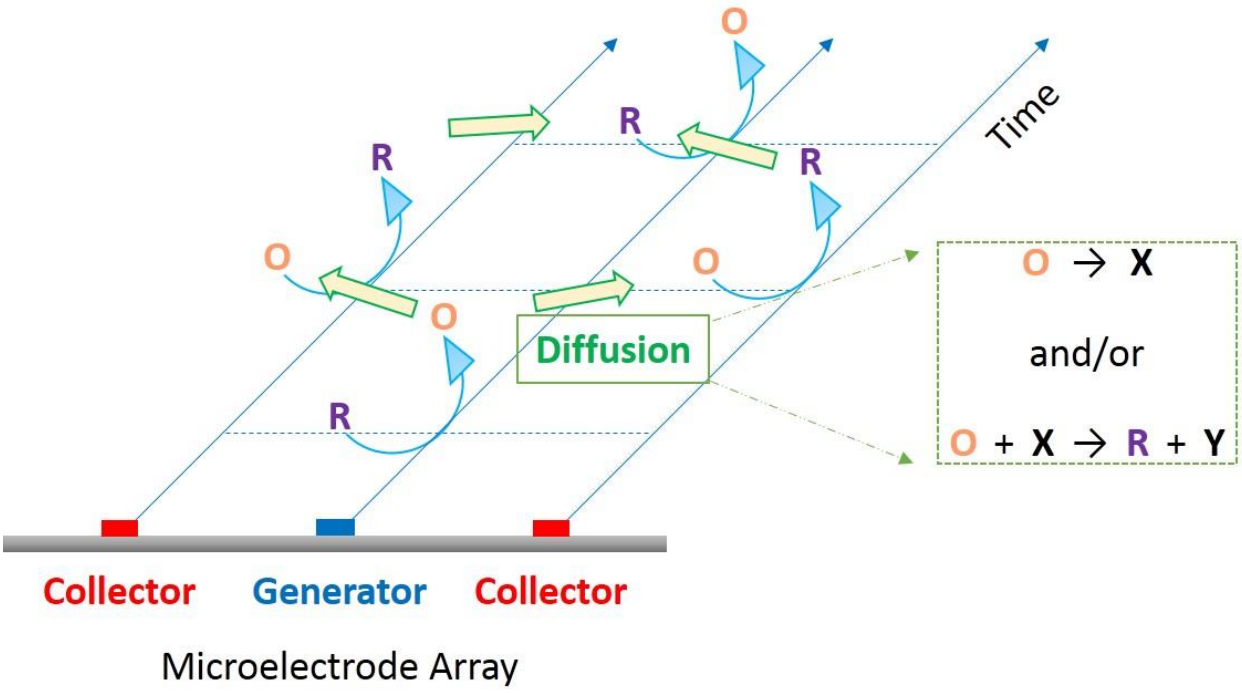


**Figure 1.2** Illustration of redox cycling at a microelectrode array with a representative cross-section of three electrodes in the array. The process shown here along the timeline involves an electrochemically-reversible analyte in its reduce form (R) that is oxidized to the form (O) at the generator and diffuses to the collector where it is reduced back to R. If O undergoes following chemistry (as shown in the green box: the product of the following chemistry, X, is not electrochemically active; or O can be reduced back to R in solution by homogeneous reaction with other species), it will take place during its diffusion to the collector. Therefore, distance can be related to reaction time in a redox cycling experiment.

product. The effect of the width of electrodes, gaps between the generator and collector, and placement of the electrodes on redox cycling efficiencies has been reported by Niwa et al.[31]

However, if the generated species are not electrochemically active when they reach the collector (e.g. due to reactions occurring during the time it takes to diffuse between the electrodes), the collector signal will be silent, which provides selectivity. This process is also affected by the spacing between the generator and the collector–with increased spacing more species are lost to the surrounding solution and thus cannot be recycled. To better understand the redox cycling system, the amplification factor ($A_f$, the ratio of the generator current with redox cycling to that without redox cycling) and collection efficiency ($C_e$, the ratio of collector current to generator current during redox cycling) are used to characterize the redox cycling efficiency.

The effect of the spacing between the generator and the collector on redox cycling efficiencies has been studied using a generation-collection simulation model before.[38] It has been proposed that when the time for a generated species to diffuse to the collector is much greater than that of the half-life of the following homogeneous reaction (if there is one), the $C_e$ will approach zero. This provides the opportunity of selective detection of species with different electrochemical reaction kinetics. For instance, in the ECC' mechanism of catecholamine oxidation, with the C reaction as the rate determining step, we can simplify this system by ignoring the C' reaction for the moment. Based on the apparent rates obtained from literature for the C reaction,[14] half-lives of catecholamines are calculated to be $t_{DA}$ = 5300 ms; $t_{NE}$ = 710 ms; $t_{EP}$ = 8.0 ms, which differ by at least one order of magnitude between each other. Therefore, by setting the redox cycling configuration with specific gaps between the generator and the collector, where the diffusion time for the OQ is much smaller than the half-life of one species (e.g. DA) but close to or greater than that of another species (e.g. NE), the three catecholamines can be differentiated from each other by monitoring the collector signal. This can be used to study other systems with EC mechanisms, such as the electrochemical oxidation of AA.

It has been demonstrated previously in our research group that DA can be selectively detected in the presence of 100 µM AA by redox cycling and the detection limit on at the collector electrode of arrays of micro band electrodes (4-µm wide with 4-µm gaps and 2-mm long) under redox cycling conditions is 452 ± 26.0 nM.[39, 40] This detection limit is sufficient for in vivo detection, and encourages further study with redox

cycling using this geometry. However, for an in vivo environment, there are additional interfering species and the presence of other neurotransmitters. Therefore, it of interest to study selective detection of DA in complicated matrices containing interfering species, as well as simultaneous detection of different neurotransmitters.

### 1.1.5 Electrode Modification

Electrode modification has been used for electrochemical biosensors for multiple reasons. A major purpose of electrode modification includes protecting the electrode surface from fouling caused by the biological environment, providing catalytic properties, and better sensitivity because of concentration of the analyte and selectivity because of exclusion of interfering species.[41-43]

Different materials have been explored for electrode modification, among which nanoparticles have drawn a lot of attention. Nanoparticle-modified or nanostructured electrodes have been used for neurotransmitter detection, because of their small size, catalytic activity, and good conductivity.[41, 44] Different compositions of nanoparticles and modification procedures have been investigated. Simultaneous detection of DA and other biological analytes, such as 5-HT, EP, AA and UA, has been reported previously.[45-47]

There are several problems with nanoparticle modification. First of all, nanoparticles containing electrochemically-active compositions could interfere with the target electrochemistry. Also, modification procedures without precise control may lead to uneven distribution of nanoparticles and different surface morphologies of the modified electrode surface. Characterization methods are needed to better understand and control the nanoparticle modification process.

### 1.1.6 Microfabricated Devices for In Vivo Applications

Devices with dimensions and physical properties suitable for tissue insertion are needed for in vivo applications of the electrochemical method of redox cycling. To minimize tissue damage, the diameter of the insertion part of the neural probe should not be bigger than 100 μm. Also, the probe should have enough mechanical strength, which is related to the material used and the shape of the probe, to survive the insertion procedure.[48] Microfabricated neural probes have been developed for years for different applications in neurological and biomedical fields.[49] Various designs and materials used have been

reported.[50-53] However, it is still challenging to make small-sized electrode arrays on a tiny probe tip to achieve redox cycling. Novel probe design and an optimized fabrication procedure are desired.

### 1.2 Overview of the Studies Described in this Dissertation

The main objective of this project is to develop novel strategies of electrochemical detection and devices to achieve quantification of neurotransmitters of interest in the brain with low detection limits. To achieve this goal, fundamental studies have been performed and are described in this dissertation. These include the evaluation of the redox cycling behavior of catecholamines, the application of redox cycling for DA detection in presence of multiple interfering species, and initiating the fabrication of neural probes that are suitable for in vivo detection by redox cycling.

Chapter 2 demonstrates the fundamental study of redox cycling behavior of individual and binary mixtures of the three different catecholamines using microfabricated band electrode arrays in vitro. Six pairs of alternating generator and collector electrodes, 4.0 μm wide and 2.00 mm long microbands with 4.0 μm gaps, were used. Different redox cycling efficiencies were observed for different catecholamines, depending on the intramolecular cyclization rates of their oxidation products. The redox cycling behavior of their binary mixtures also indicates the existence of homogeneous reactions between the oxidation products and cyclization products of the different catecholamines. This chapter was published as a letter in *Analytical Chemistry*.[54]

As a follow-up to Chapter 2, the redox cycling behavior of individual DA, NE and their mixture is further studied in Chapter 3. Four generator-collector gap conditions (4, 12, 20, and 28 μm) were investigated using the same microfabricated chip as in Chapter 2, but with a different electrode configuration (alternating three collectors with two generators). The collection efficiency during redox cycling for NE had a greater dependence on the gap width than DA, and the collector current of NE becomes silent at big gap widths (20 and 28 μm). The collector signal of the DA-NE mixture approaches that of DA alone with the increasing gap.

Chapter 4 focuses on the application of redox cycling for the detection of DA in the presence of multiple interfering species, including AA, UA, L-dopa, HVA, 3-MT, and 5-HIAA. The same microfabricated chip and electrode configurations as in Chapter 2 were used. Under the conditions used here, all of the interfering species investigated only showed activity at the generator but not at the collector while DA

showed signals at both. Calibration curves of DA with and without the presence of interfering species have been made.

In Chapter 5, the design and fabrication procedure for an SU-8 based neural probe with dimensions suitable for in vivo neurotransmitter detection is described. Two types of microelectrode arrays, including a co-planar microband array and an edge microband array, were designed and placed on the same set of masks. The same mask can be used for the different fabrication procedures used for the two types of arrays. However, the fabrication procedure and materials used still need to be optimized.

Chapter 6 is a study of the electrochemical characterization of silver containing nanoparticles (including Ag nanocubes(Ag C), Ag nanocuboctahedrons (Ag CT), Au nanocages (Au NC) and Ag nanospheres (Ag NP)) modifying an electrode surface. This study is intended to begin investigations of incorporating nanomaterials at the electrodes for enhanced sensing and for application to a wider range of analytes. Two approaches of electrode modification with nanoparticles were investigated (drop casting with and without coverage of a Nafion film) with anodic stripping voltammetry for analysis. Stripping votammograms of the nanoparticles were irreproducible and indicate that methods other than simple drop casting should be used for such analysis.

Each chapter in this dissertation is written in a format that is compatible for publication in peer-reviewed journals. Chapter 3 is followed by a chapter containing supporting information that is labeled as Chapter 3.S.

**1.3 References**

(1) Fix, J. D. In *Neuroanatomy* Anonymous ; Lippincott Williams & Wilkins:Philadelphia, 2008; pp 283-297.

(2) Zhang, M. Y.; Beyer, C. E. *J.Pharm.Biomed.Anal.* **2006**, *40*, 492-499.

(3) Bear, M. F., Connors, B. W. and Paradiso, M. A. *Neuroscience : Exploring the Brain,* ed.; Lippincott Williams & Wilkins:Philadelphia,PA; 2007.

(4) Robinson, D. L.; Venton, B. J.; Heien, M. L.; Wightman, R. M. *Clin.Chem.* **2003**, *49*, 1763-1773.

(5) Yavich, L.; Forsberg, M. M.; Karayiorgou, M.; Gogos, J. A.; Mannisto, P. T. *J.Neurosci.* **2007**, *27*, 10196-10202.

(6) Purves, D., Augustine, G. J., Fitzpatrick, D., Hall, W. C., LaMantia, A., McNamara, J. O. and Williams, S. M. In *Neuroscience* Anonymous ; Sinauer Associates, Inc:Massachusetts, 2004; pp 149.

(7) Mefford, I. N. *Prog.Neuro-Psychopharmacol.Biol.Psychiatry.* **1988**, *12*, 365-388.

(8) Kissinge.Pt; Hart, J. B.; Adams, R. N. *Brain Res.* **1973**, *55*, 209-213.

(9) Robinson, D. L.; Hermans, A.; Seipel, A. T.; Wightman, R. M. *Chem.Rev.* **2008**, *108*, 2554-2584.

(10) Greco, S.; Danysz, W.; Zivkovic, A.; Gross, R.; Stark, H. *Anal.Chim.Acta.* **2013**, *771*, 65-72.

(11) Cooper, B. R.; Wightman, R. M.; Jorgenson, J. W. *Journal of Chromatography B: Biomedical Sciences and Applications.* **1994**, *653*, 25-34.

(12) Hawley, M.; Tatawawadi, S.; Piekarski, S.; Adams, R. *J.Am.Chem.Soc.* **1967**, *89*, 447-450.

(13) Ciolkowski, E. L.; Maness, K. M.; Cahill, P. S.; Wightman, R. M.; Evans, D. H.; Fosset, B.; Amatore, C. *Anal.Chem.* **1994**, *66*, 3611-3617.

(14) Ciolkowski, E. L.; Cooper, B. R.; Jankowski, J. A.; Jorgenson, J. W.; Wightman, R. M. *J.Am.Chem.Soc.* **1992**, *114*, 2815-2821.

(15) Zhang, Z.; Huang, J.; Wu, X.; Zhang, W.; Chen, S. *J Electroanal Chem.* **1998**, *444*, 169-172.

(16) Harrison, F. E.; May, J. M. *Free Radical Biology and Medicine.* **2009**, *46*, 719-730.

(17) Dunnett, S. B. *Dopamine,* ed.; Elsevier:Amsterdam ; Boston; 2005.

(18) Xing, X.; Bae, I. T.; Shao, M.; Liu, C. *J Electroanal Chem.* **1993**, *346*, 309-321.

(19) Vreeland, R. F.; Atcherley, C. W.; Russell, W. S.; Xie, J. Y.; Lu, D.; Laude, N. D.; Porreca, F.; Heien, M. L. *Anal.Chem.* **2015**, *87*, 2600-2607.

(20) Darvesh, A. S.; Carroll, R. T.; Geldenhuys, W. J.; Gudelsky, G. A.; Klein, J.; Meshul, C. K.; Van der Schyf, Cornelis J. *Expert opinion on drug discovery.* **2011**, *6*, 109-127.

(21) Watson, C. J.; Venton, B. J.; Kennedy, R. T. *Anal.Chem.* **2006**, *78*, 1391-1399.

(22) Schltz, K. N.; Kennedy, R. T. *Annu.Rev.Anal.Chem.* **2008**, *1*, 627-661.

(23) Nesbitt, K. M.; Jaquins-Gerstl, A.; Skoda, E. M.; Wipf, P.; Michael, A. C. *Anal.Chem.* **2013**, *85*, 8173-8179.

(24) Nesbitt, K. M.; Varner, E. L.; Jaquins-Gerstl, A.; Michael, A. C. *ACS chemical neuroscience.* **2014**, *6*, 163-173.

(25) Heien, M. L.; Johnson, M. A.; Wightman, R. M. *Anal.Chem.* **2004**, *76*, 5697-5704.

(26) Park, J.; Takmakov, P.; Wightman, R. M. *J.Neurochem.* **2011**, *119*, 932-944.

(27) Wilson, G. S.; Johnson, M. A. *Chem.Rev.* **2008**, *108*, 2462-2481.

(28) Bath, B. D.; Michael, D. J.; Trafton, B. J.; Joseph, J. D.; Runnels, P. L.; Wightman, R. M. *Anal.Chem.* **2000**, *72*, 5994-6002.

(29) Venton, B. J.; Troyer, K. P.; Wightman, R. M. *Anal.Chem.* **2002**, *74*, 539-546.

(30) Niwa, O.; Kurita, R.; Liu, Z. M.; Horiuchi, T.; Torimitsu, K. *Anal.Chem.* **2000**, *72*, 949-955.

(31) Niwa, O.; Morita, M.; Tabei, H. *Electroanalysis.* **1991**, *3*, 163-168.

(32) Niwa, O.; Morita, M.; Tabei, H. *Electroanalysis.* **1994**, *6*, 237-243.

(33) Niwa, O.; Morita, M. *Anal.Chem.* **1996**, *68*, 355-359.

(34) Kurita, R.; Tabei, H.; Liu, Z.; Horiuchi, T.; Niwa, O. *Sensors Actuators B: Chem.* **2000**, *71*, 82-89.

(35) Vandaveer, W. R.; Woodward, D. J.; Fritsch, I. *Electrochim.Acta.* **2003**, *48*, 3341-3348.

(36) Dam, V. A. T.; Olthuis, W.; van den Berg, A. *Analyst.* **2007**, *132*, 365-370.

(37) Ma, C.; Contento, N. M.; Gibson, L. R.; Bohn, P. W. *Anal.Chem.* **2013**, *85*, 9882-9888.

(38) Shea, T. V.; Bard, A. J. *Anal.Chem.* **1987**, *59*, 2101-2111.

(39) Aggarwal, A. *Studies Toward the Development of a Microelectrode Array for Detection of Dopamine through Redox Cycling,* Ph.D ed.; University of Arkansas:Fayetteville, AR; 2011.

(40) Aggarwal, A.; Hu, M.; Fritsch, I. *Analytical and bioanalytical chemistry.* **2013**, *405*, 3859-3869.

(41) Luo, X.; Morrin, A.; Killard, A. J.; Smyth, M. R. *Electroanalysis.* **2006**, *18*, 319-326.

(42) Lange, U.; Roznyatovskaya, N. V.; Mirsky, V. M. *Anal.Chim.Acta.* **2008**, *614*, 1-26.

(43) Ahuja, T.; Kumar, D. *Sensors Actuators B: Chem.* **2009**, *136*, 275-286.

(44) Saha, K.; Agasti, S. S.; Kim, C.; Li, X.; Rotello, V. M. *Chem.Rev.* **2012**, *112*, 2739-2779.

(45) Goyal, R. N.; Gupta, V. K.; Oyama, M.; Bachheti, N. *Talanta.* **2007**, *72*, 976-983.

(46) Mathiyarasu, J.; Senthilkumar, S.; Phani, K. L. N.; Yegnaraman, V. *Journal of nanoscience and nanotechnology.* **2007**, *7*, 2206-2210.

(47) Zhang, Y.; Ren, W.; Zhang, S. *Int J Electrochem Sci.* **2013**, *8*, 6839-6850.

(48) Hetke, J. F.; Anderson, D. J.; Wise, K. D. *Engineering in Medicine and Biology Society, 1996. Bridging Disciplines for Biomedicine. Proceedings of the 18th Annual International Conference of the IEEE.* **1997**, *18*, 266-267.

(49) Fekete, Z. *Sensors Actuators B: Chem.* **2015**, *215*, 300-315.

(50) Tseng, T. T.; Monbouquette, H. G. *J Electroanal Chem.* **2012**, *682*, 141-146.

(51) Pongrácz, A.; Fekete, Z.; Márton, G.; Bérces, Z.; Ulbert, I.; Fürjes, P. *Sensors Actuators B: Chem.* **2013**, *189*, 97-105.

(52) Altuna, A.; Gabriel, G.; de la Prida, Liset Menéndez; Tijero, M.; Guimerá, A.; Berganzo, J.; Salido, R.; Villa, R.; Fernández, L. J. *J Micromech Microengineering.* **2010**, *20*, 064014.

(53) Cheung, K. C.; Renaud, P.; Tanila, H.; Djupsund, K. *Biosensors and Bioelectronics.* **2007**, *22*, 1783-1790.

(54) Hu, M.; Fritsch, I. *Anal.Chem.* **2015**, *87*, 2029-2032.

## 2. Redox Cycling Behavior of Individual and Binary Mixtures of Catecholamines at Gold Microband Electrode Arrays

## 2.1 Abstract

The electrochemical redox cycling (RC) behavior of individual and binary mixtures of three catecholamines are investigated using gold microelectrode arrays in vitro. Catecholamines showed reversible or irreversible responses during RC depending on their oxidation products' cyclization rate. The RC behavior of the binary mixtures supports the disproportionation reaction of catecholamines, which has been previously reported, but not under RC conditions or with mixtures. This fundamental study provides insights on the effects of complicated mechanisms and kinetics on RC and sets the foundation for future applications of RC for in vivo multi-neurotransmitter analysis.

## 2.2 Redox Cycling Behavior of Individual and Binary Mixtures of Catecholamines at Gold Microband Electrode Arrays

As an important group of neurotransmitters, catecholamines (dopamine, DA, norepinephrine, NE, and epinephrine, EP) have been studied for years because of their crucial role in prefrontal cortical function[1] and neurological diseases such as Parkinson's,[2,3] Huntington's,[4] Alzheimer's, and schizophrenia.[5] The three catecholamines have similar molecular structures and can coexist in biological samples. Therefore, detection techniques that are able to distinguish between different catecholamines are important for neurological studies.

One of the most used methods for in vivo analysis of catecholamines is microdialysis coupled with various separation and detection techniques. Microdialysis is good for monitoring basal level neurotransmitter concentrations with slow changes but suffers from low temporal and spatial resolution as well as tissue damage[6] caused by its relatively large probe size.[7,8] Also, the reuptake process of DA limits the ability of DA to diffuse to the microdialysis probe and thus may alter the results.[9] Another often-used approach involves electrochemistry using 5−30 μm diameter carbon fiber electrodes to monitor fast transient signals. Carbon nanotube fiber[10] and carbon nanotube yarn electrodes[11] have also been used to minimize biofouling or provide high temporal resolution. Fast scan cyclic voltammetry (FSCV) in particular is the most widely used electrochemical technique for this purpose because it provides a means for both quantitation and qualitative assessment of the environment surrounding the electrode probe.[12] A key drawback for this technique, however, is that it generates a high background current that needs to be subtracted out. This makes it unsuitable for basal level detection. To overcome this limitation, fast-scan controlled-adsorption voltammetry has been developed to monitor tonic dopamine and is alternated with FSCV to monitor phasic dopamine every 5 min.[13] Future applications on other catecholamines and mixtures still need to be evaluated.

In addition to DA, the other two catecholamines EP and NE can coexist in the extracellular fluid of the brain and other biological samples, along with their metabolites and interfering species. Simultaneous detection of NE and EP in adrenal medullary chromaffin cells[14] as well as DA and serotonin by FSCV have been reported before,[15] and the disadvantages of FSCV persist. There remains a need to develop methods

with high spatial and temporal resolution with low background for simultaneous and selective neurotransmitter detection.

The electrochemical method of redox cycling (RC) has been explored for DA detection in the presence of ascorbic acid (AA) within micro/nanofluidic channels[16] and with simple interdigitated array electrodes.[17] This method provides signal amplification and the ability to distinguish species based on their electron transfer kinetics (electrochemically reversible vs quasi-reversible and irreversible species), by careful selection of the applied potentials and the diffusion time frames, the latter of which is related to the separation between the electrodes. Its additional advantage of low charging current, which arises because it is a steady state technique, leads to possible applications of detecting not only transient changes that are evoked by behavior or controlled stimuli but also basal levels simultaneously. In vitro studies have been performed with different designs of electrodes while none of them have been applied in vivo yet. Its application for in vitro DA detection in the presence of AA has been reported.[17–21] The detection limit varies depending on geometry and design of electrodes. With the design used here, a detection limit of 454 ± 26 nM has been achieved previously.[20] Also, a detection limit of 10 nM by others has been demonstrated with planar and vertically separated interdigitated microelectrode arrays (MEAs.)[17] The chemical systems for which RC has been evaluated have been limited to DA and AA. Fundamental studies to establish the RC behavior of additional catecholamines, their mixtures, and interfering species are important for future applications.

In the case of detecting catecholamines, electrodes at anodic potentials are defined as generator electrodes (GE), and those at cathodic potentials are defined as collector electrodes (CE). The amplification factor ($A_f$, the ratio of the generator current with RC to that without RC, Eq 1) and collection efficiency ($C_e$, the ratio of collector current to generator current during RC, Eq 2) are used to characterize the RC system.[21]

$$A_f = \frac{i_{GE/CE}}{i_{GE}} \quad (1)$$

$$\%C_e = 100\% \left( \frac{i_{CE}}{i_{GE/CE}} \right) \quad (2)$$

where $i_{GE}$ is the generator current without RC, $i_{GE/CE}$ is the generator current with RC, and $i_{CE}$ is the collector current.

In this work we discuss the RC behavior of individual and binary mixtures of three catecholamines: DA, NE, and EP on microfabricated gold band MEAs in vitro, which has not been reported previously. Effects of the disproportionation reaction of catecholamines on their RC behavior are investigated. This knowledge will help to ascertain the suitability of and possible new opportunities for RC for chemical analysis in the brain.

The 1 in. × 1 in. silicon chip-based MEAs used here contain 18 individually addressable gold microband electrodes which are 2.00 mm long, 4.0 μm wide, and separated by 4.0 μm gaps. In this particular study, six alternating microbands are shorted together and used as GE and CE, respectively, as shown in Figure 2.1, activating a total of 12 electrodes. A bipotentiostat equipped with a faraday cage and a picoamp booster (CHI 750A, CH Instruments, Austin, TX) was used for all electrochemical experiments. Replicate experiments were performed, and data are reported as the average ± 1 standard deviation.

A solution containing a model compound (5 mM hexaammineruthenium(III) chloride in 0.1 M KCl) was used to electrochemically characterize the electrodes before and after catecholamine studies to inspect the electrode performance. The unmodified gold electrodes used here, especially the ones used as the GE, could be fouled by catecholamines, and this effect is monitored by the changes in electrochemical behavior of the model compound. A three-electrode system was used with a Ag/AgCl (saturated KCl) reference electrode and a Pt wire auxiliary electrode. Cyclic voltammetry (CV) was performed at the GE, which was cycled between 0.350 V and −0.200 V with a scan rate of 0.020 V/s. For the case without RC, the CE remained at an open circuit. During RC, the CE was held at −0.200 V. An average Af of 2.7 ± 0.3 and Ce of 80% ± 5% were achieved with the MEA system used here.

CV was also used to study the RC behavior of 50 μM concentrations of the individual catecholamines and their binary mixtures in aCSF buffer (100 mM NaCl, 5.0 mM KCl, 1.2 mM $NaH_2PO_4$, 5.0 mM $NaHCO_3$, 10 mM glucose, 2.5 mM HEPES, 1.2 mM $MgSO_4$, 1.0 mM $CaCl_2$) at 7.4 pH using the same sets of GE and CE as were used with the model compound. The GE was cycled between −0.150 and 0.550 V at a scan rate of 0.020 V/s. During RC, the CE was held at −0.010 V. Representative results are shown in Figure 2.2 and Table 2.1.

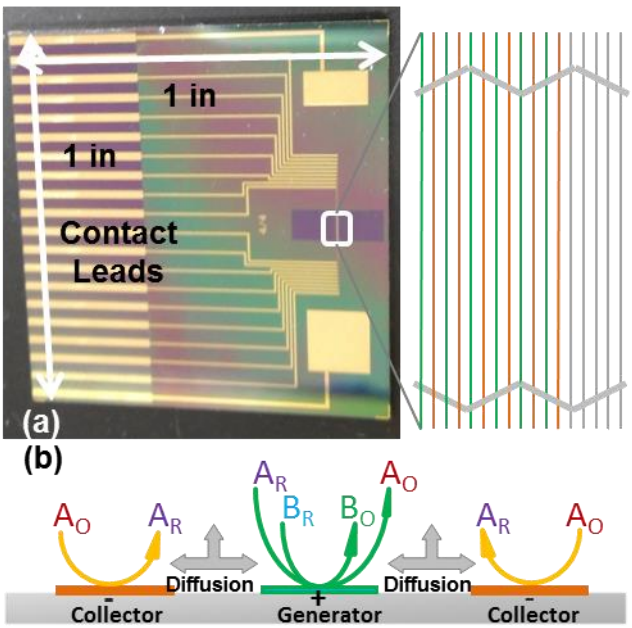


**Figure 2.1** (a) Photographic image of the microfabricated chip (on left) in which six pairs of alternating GE (green) and CE (orange) are activated (expanded schematic on right); (b) Representative cross-sectional diagram of RC: electrochemically reversible species in the reduced form, $A_R$, oxidize at the generator to form $A_O$, diffuse to the collector and then reduce back; electrochemically irreversible species in the reduced form, $B_R$, can only oxidize at the generator to form $B_O$.

CV responses of binary mixtures with and without RC are overlaid in Figure 2.2 with responses from the individual species that were run before or after the binary mixture, which aided in accounting for fouling effects when comparing mixtures with individual signals. For individual catecholamines, DA and NE showed reversible or quasi-reversible RC behavior with an amplified GE signal. DA has an average $A_f$ of 1.5 ± 0.3 and $C_e$ of 48% ± 16%, while NE has an average $A_f$ of 1.2 ± 0.1 and $C_e$ of 35% ± 10%, which are lower than that of DA. However, EP appears to be irreversible with a CE signal almost equal to the aCSF background current and no amplification at the GE with RC. With different $A_f$ and $C_e$, the GE signals with RC for the same concentration of different catecholamines showed better differentiation than those without RC.

Without RC, the GE signal of the DA-NE mixture approximately equals the sum of the GE currents of the individual DA and NE (with an error of 2.44%); GE and CE signals with RC also follow the same trends (with an error of 2.78% and −5.75%, respectively (Figure 2.2 c, b, and a). This result is expected because the structures of DA and NE only differ by a β-hydroxyl group and have similar standard electrode potentials. The theoretical calculated standard potential is about +0.555 V for DA vs Ag/AgCl (saturated KCl)[22] and about +0.554 V for NE vs Ag/AgCl (saturated KCl).[23] An equimolar DA-EP mixture also produces a GE signal without RC that is close to the sum of individual signals (with an error of −0.09%) (Figure 2.2 f). However, with RC, the GE and CE signals of the mixture are less than the sum of the individual signals, by 7.24 nA (11.28% of the mixture GE current) and 6.67 nA (42.67% of the mixture CE current), respectively (Figure 2.2 e,d). The equimolar NE-EP mixture exhibits results similar to the DA-EP mixture, as shown in Figure 2.2 g−i, where the mixture CE signal with RC also lies in between NE and EP individual signals. In both DA-EP and NE-EP mixtures, the values of $A_f$ and $C_e$ lie between those obtained for the individual species.

The diminished collector signal of the DA-EP and NE-EP mixtures compared to DA and NE alone, respectively, may be explained by the disproportionation reaction that occurs after electrochemical oxidation of catecholamines. A mechanism was proposed by Adams and co-workers in the 1960s, which evaluated the electrochemical oxidation of catecholamines in vitro.[24] It was suggested that the catecholamine is first converted to its o-quinone form by applying an oxidizing potential at the electrode. Then, when pH > 3 (which is the case under physiological conditions), the o-quinone deproto- nates and undergoes intramolecular cyclization to form the leucoaminochrome. The cyclized product can then oxidize

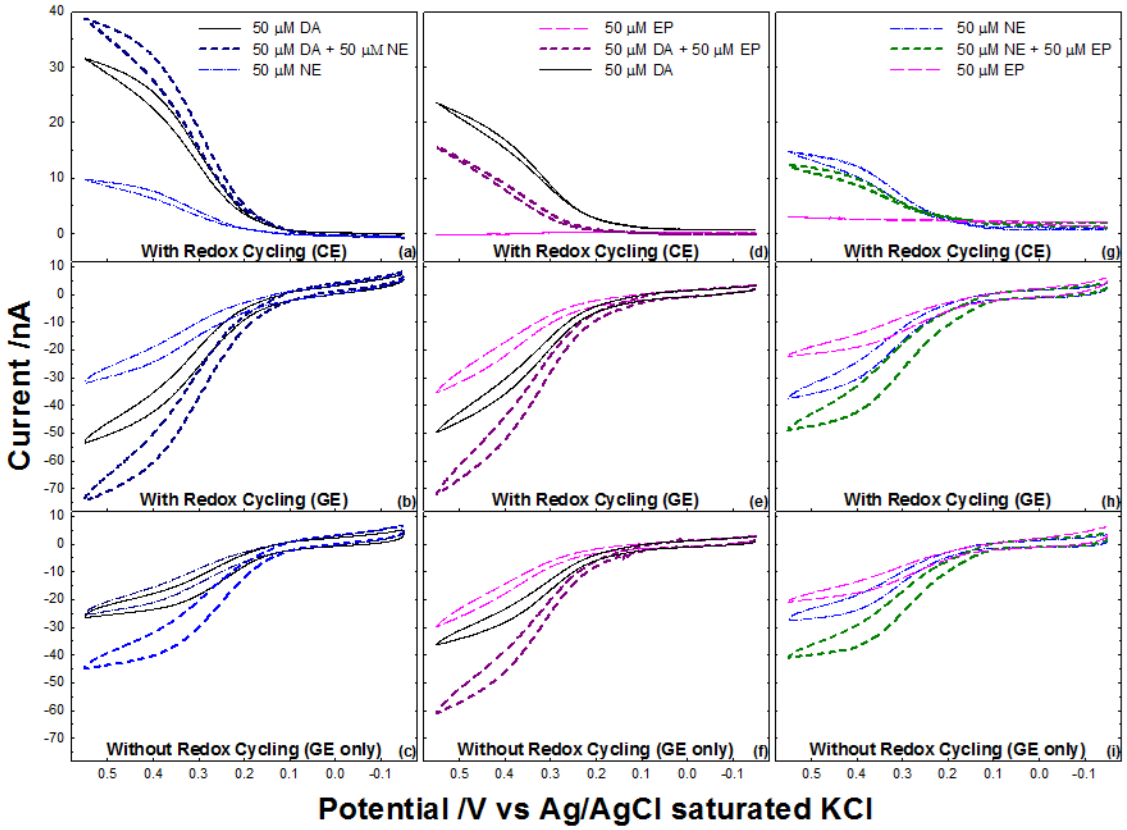


**Figure 2.2** CV responses at 0.02 V/s of individual catecholamines (50 µM) and their binary mixtures (50 µM each) in aCSF buffer, with RC and without. Six microbands served as the generator and six intermediate, alternating microbands served as the collector (−0.01 V). (The order of samples listed in each legend represents the order in which the CV experiments were performed to obtain these data.)

**Table 2.1 Comparison of currents, $A_f$, and $C_e$ for binary mixtures (50 μM each) and individual components (50 μM).***

| Catecholamine | $i_{GE}$ (nA) | $i_{GE/GC}$ (nA) | $i_{CE/GC}$ (nA) | $A_f$ | $C_e$ (%) |
|---|---|---|---|---|---|
| **DA** | 20.13 | 42.41 | 29.81 | 2.11 | 70.29 |
| **DA-NE** | 36.44 | 63.28 | 36.85 | 1.74 | 58.23 |
| **NE** | 15.42 | 19.11 | 9.16 | 1.24 | 47.94 |
| **EP** | 24.45 | 27.74 | 0.35 | 1.13 | 1.28 |
| **DA-EP** | 54.88 | 64.17 | 15.63 | 1.17 | 24.36 |
| **DA** | 30.48 | 43.67 | 21.95 | 1.43 | 50.26 |
| **NE** | 25.79 | 32.85 | 13.67 | 1.27 | 41.60 |
| **NE-EP** | 36.89 | 42.91 | 10.50 | 1.16 | 24.46 |
| **EP** | 14.85 | 13.96 | 1.03 | 0.94 | 7.37 |

* The three sets of results shown were performed with different chips, so that the absolute current for each species is different between sets, but the relative currents for the individual species and their mixture can be compared within a set.

to the aminochrome by reacting with the o-quinone form of a catecholamine and regenerate the starting catecholamine. The intramolecular cyclization rates for different catecholamines are quite different, thus providing the possibility of distinguishing them by the degree of the cyclization reaction. The apparent rate constants for this cyclization were determined by chronoamperometry at glassy carbon electrodes: $k_{DA} = 0.13 \pm 0.05\ s^{-1}$, $k_{NE} = 0.98 \pm 0.52\ s^{-1}$, $k_{EP} = 87 \pm 10\ s^{-1}$, in phosphate buffer at pH 7.4. It has been reported that with a scan rate of 10 V/s, NE and EP can be resolved by the shape of their cyclic voltammograms, because this gives EP enough time to be cyclized but not for NE.[14]

Under the RC conditions used here, oxidation and reduction reactions happen at different electrodes (GE and CE, respectively), and the time for the oxidized species to be reduced is controlled by the diffusion time between the GE and CE. The diffusion time of a molecule in two dimensions can be approximated by $t = x^2/(4D)$ where x is the edge to edge distance between the neighboring GE and CE and D is the diffusion coefficient.[25] By applying the parameters used in this experiment, where $x = 4.0\ \mu m$, $D = 6 \times 10^{-6}\ cm^2/s$ for DA in aqueous solution,[26] the diffusion time is calculated to be 6.7 ms. During this diffusion time frame, most of the o-quinone form of DA and NE remain uncyclized when they reach the CE and can be reduced while EP is almost all in its cyclized form, which is inactive at the electrode. By changing the gap between GE and CE, we should be able to control the diffusion time, thus limiting the progress of the intramolecular cyclization reaction. This approach may make it possible to differentiate among all three catecholamines based on their intramolecular cyclization rates. More studies are needed to develop this concept further.

This fundamental study provides information on the effects of the disproportionation reaction of catecholamines on their RC behaviors and insight into distinguishing them based on their intramolecular cyclization rates and the diffusion time during RC. With advantages of low background current and ability to offer continuous detection, RC holds promise for possible in vivo neurotransmitter detection applications. (RC using chronoamperometry, instead of the slow CV used here for fundamental characterization, would allow real time monitoring for those applications.) The concepts described herein can also be applied more generally to other chemical systems to study mechanisms and kinetics of species that undergo electron transfer followed by homogeneous chemical reactions.

## 2.3 Acknowledgement

Research was supported partially through the National Science Foundation (Grants CHE-0719097 and CBET-1336853) and the Arkansas Biosciences Institute, the major research component of the Arkansas Tobacco Settlement Proceeds Act of 2000. We are grateful to Anupama Aggarwal and Vishal Sahore for fabricating the MEAs.

## 2.4 References


(1) Arnsten, A. F. T.; Pliszka, S. R. *Pharmacol. Biochem. Behav*. **2011**, 99, 211−216.

(2) Vazey, E. M.; Aston-Jones, G. Front. *Behav. Neurosci*. **2012**, 6.

(3) Lotharius, J.; Brundin, P. *Nat. Rev. Neurosci*. **2002**, 3, 932−942.

(4) Jakel, R. J.; Maragos, W. F. *Trends Neurosci*. **2000**, 23, 239−245.

(5) Friedman, J. I.; Adler, D. N.; Davis, K. L. *Biol. Psychiat*. **1999**, 46, 1243−1252.

(6) Khan, A. S.; Michael, A. C. TrAC, *Trends Anal. Chem*. **2003**, 22, 503−508.

(7) Watson, C. J.; Venton, B. J.; Kennedy, R. T. *Anal. Chem*. **2006**, 78, 1391−1399.

(8) Kennedy, R. T. *Curr. Opin. Chem. Biol*. **2013**, 17, 860−867.

(9) Nesbitt, K. M.; Jaquins-Gerstl, A.; Skoda, E. M.; Wipf, P.; Michael, A. C. *Anal. Chem*. **2013**, 85, 8173−8179.

(10) Harreither, W.; Trouillon, R. I.; Poulin, P.; Neri, W.; Ewing, A. G.; Safina, G. Anal. Chem. **2013**, 85, 7447−7453.

(11) Jacobs, C. B.; Ivanov, I. N.; Nguyen, M. D.; Zestos, A. G.; Venton, B. J. *Anal. Chem*. **2014**, 86, 5721−5727.

(12) Robinson, D. L.; Venton, B. J.; Heien, M. L. A. V.; Wightman, R. M. *Clin. Chem*. **2003**, 49, 1763−1773.

(13) Atcherley, C. W.; Wood, K. M.; Parent, K. L.; Hashemi, P.; Heien, M. L. *Chem. Commun*. **2015**, DOI: 10.1039/C4CC06165A.

(14) Ciolkowski, E. L.; Cooper, B. R.; Jankowski, J. A.; Jorgenson, J. W.; Wightman, R. M. *J. Am. Chem. Soc*. **1992**, 114, 2815−2821.

(15) Swamy, B. E. K.; Venton, B. J. *Analyst* **2007**, 132, 876−884.

(16) Goluch, E. D.; Wolfrum, B.; Singh, P. S.; Zevenbergen, M. A. G.; Lemay, S. G. *Anal. Bioanal. Chem*. **2009**, 394, 447−456.

(17) Niwa, O.; Morita, M.; Tabei, H. *Electroanalysis* **1991**, 3, 163− 168.

(18) Oleinick, A.; Zhu, F.; Yan, J.; Mao, B.; Svir, I.; Amatore, C. *ChemPhysChem* **2013**, 14, 1887−1898.

(19) Ma, C.; Contento, N. M.; Gibson, L. R.; Bohn, P. W. *Anal. Chem*. **2013**, 85, 9882−9888.

(20) Aggarwal, A.; Hu, M.; Fritsch, I. *Anal. Bioanal. Chem*. **2013**, 405, 3859−3869.

(21) Vandaveer, W. R., IV; Woodward, D. J.; Fritsch, I. *Electrochim. Acta* **2003**, 48, 3341−3348.

(22) Song, Y.; Song, Y.; Xie, W.; Shi, D. Russ. *J. Phys. Chem*. **2006**, 80, 1467−1474.

(23) Song, Y. *Spectrochim. Acta, Part A: Mol. Biomol. Spectrosc*. **2007**, 67, 1169−1177.

(24) Hawley, M. D.; Tatawawadi, S. V.; Piekarski, S.; Adams, R. N. *J. Am. Chem. Soc*. **1967**, 89, 447−450.

(25) Bard, A. J.; Faulkner, L. R. *Electrochemical Methods: Fundamentals and Applications*; Wiley: New York, **1980**.

(26) Gerhardt, G.; Adams, R. N. *Anal. Chem*. **1982**, 54, 2618−2620.

# 3. Application of Electrochemical Redox Cycling: Toward Differentiation of Dopamine and Norepinephrine

### 3.1 Abstract

The electrochemical redox cycling behavior of dopamine (DA), norepinephrine (NE), and their mixture was investigated using coplanar gold microband electrode arrays at four generator-collector gap conditions (4, 12, 20, and 28 μm). This method provides opportunity for differentiating the catecholamines in mixtures by monitoring the current at collector electrodes activated at different distances from generator electrodes. It takes advantage of the ECC' mechanism associated with the electrochemical oxidation of catecholamines, in which DA and NE have rate constants that differ by a factor of 7.5 for the first order intramolecular cyclization (C) following electron transfer (E). Collector electrodes activated at different distances from the generators were used to examine the process of the following chemistry at different time points, because spatial relationships are related to temporal ones through diffusion. Solutions of artificial cerebral spinal fluid containing 50 μM DA, 50 μM NE, and a DA-NE mixture of 50 μM of each were examined. The collection efficiency during redox cycling for NE had a greater dependence on gap width than DA, and the collector current of NE became silent at ~20 μm. The collector current of the mixture approaches that of DA alone with increasing gap, suggesting that differentiation of DA and NE may be possible. The collector current of the mixture is further affected by the homogenous reaction (C') between oxidized and cyclized products of DA and NE, and drops below that of DA alone. This may be used for differentiation in more complicated chemical systems.

### 3.2 Application of Electrochemical Redox Cycling: Toward Differentiation of Dopamine and Norepinephrine

Catecholamines–dopamine (DA), norepinephrine (NE) and epinephrine (EP)–are important neurotransmitters because of their roles in neurological functions and related diseases.[1-3] In vitro differential analysis of catecholamines in biological specimens such as brain samples and biological fluids has been developed for diagnosis and treatment of diseases. Common methods involve separation by chromatography coupled with different detection techniques.[4-7] The co-secretion of different catecholamines in the same region of an organ necessitates simultaneous detection in vivo.[8, 9] Electrochemistry has been applied for in vivo analysis of individual catecholamines and carries certain advantages. However, due to their similarity in chemical structure and oxidation potential, it is difficult to simultaneously identify different catecholamines by simple electrochemical methods. Here, we study the redox cycling approach, which is promising for in vivo detection, to address the key challenge in differentiating DA and NE from each other by using a microband electrode array. Taking advantage of the ECC' mechanism of their electrochemical oxidation, these two species can be distinguished by the spatial distribution of their oxidized form that survives the post-oxidative following chemistry whose temporal dependence is highly species-specific.

Electrochemical detection of individual catecholamines,[10-12] and investigation of their oxidation processes have been pursued for decades.[13, 14] The ECC' mechanism is schematically shown in Figure 3.1. In this pH-dependent process, the catecholamine first undergoes a two-electron oxidation reaction at the electrode (E), producing an *o*-quinone (OQ). The OQ undergoes an intramolecular cyclization process (C) and internal oxidation-reduction to form the leucoaminochrome (LAC). The apparent intramolecular cyclization rates for the three catecholamines are different ($k_{DA} = 0.13 \pm 0.05\ s^{-1}$, $k_{NE} = 0.98 \pm 0.52\ s^{-1}$, $k_{EP} = 87 \pm 10\ s^{-1}$, in phosphate buffer at pH 7.4),[15] which provides the opportunity of differentiation. LAC can engage in a homogenous reaction (C') with another molecule in the OQ form, resulting in an additional two-electron oxidization to the aminochrome (AC), while the OQ reduces back to the original catecholamine. It has been reported that AC also undergoes a two-electron reduction and its $E_{1/2}$ value is about -0.207 V vs. Ag/AgCl (saturated KCl) for EP.[13, 16] This is outside the potential window used here, and thus electrochemical reduction of AC to LAC is not considered.

Taking advantage of the differences in the rate constants of different catecholamines for the intramolecular cyclization reaction, simultaneous and differential detection of NE and EP in adrenal medullary chromaffin cells has been demonstrated at a carbon fiber electrode,[15] based on the difference in the shape of the voltammograms at a selected scan rate (10 V/s). At this time scale, most $OQ_{EP}$ molecules cyclize while some $OQ_{NE}$ remain, so that the additional reduction peak for $AC_{EP}$ to $LAC_{EP}$ can be observed at a more negative potential. At 10 V/s and a frequency of 1 cyclic voltammogram per second, this method is limited by the relatively low temporal resolution for monitoring secretion at single cells, which occurs on a tens millisecond time scale. Another method for simultaneous NE-EP detection involves a faster scan rate (800 V/s) with a more positive switching potential to obtain an additional wave for the oxidation of the secondary amine of EP. This does not occur for NE, which is a primary amine.[17] The higher scan rate is limiting in the requirement for greater background subtraction. Electrochemical studies that differentiate between DA and NE have not yet been reported.

The electrochemical redox cycling method used here has been developed for in vitro detection of DA in the presence of interferences using different electrode configurations and shows specific advantages.[10, 18-21] Electrode arrays with closely spaced microelectrodes are used instead of a single electrode. The analytes are oxidized or reduced at one set of electrodes (generator electrodes), the generated species diffuse to electrodes nearby (collector electrodes) where they can be reduced or oxidized back, respectively, to their original form. This recycling process amplifies the signal and provides selectivity based on the electro activity of the species reached the collector. The redox cycling efficiency of an electrochemical system can be characterized by the amplification factor ($A_f$), which equals the ratio of the generator current with redox cycling to that without redox cycling. Another important parameter is the collection efficiency ($C_e$), which equals the ratio of collector current to generator current.[19] The redox cycling efficiency is affected by the spacing of generator and collector electrodes. As the gap increases, more species are lost to the surrounding solution by diffusion, and longer time is provided for following chemistry, which all lead to decreasing redox cycling efficiency.

We previously examined the redox cycling efficiency of DA, NE and EP using a microband electrode array with a 4 μm gap between generator and collector electrodes.[23] Because of its fast intramolecular cyclization rate, EP showed very low efficiency and therefore could be differentiated at the collector. DA

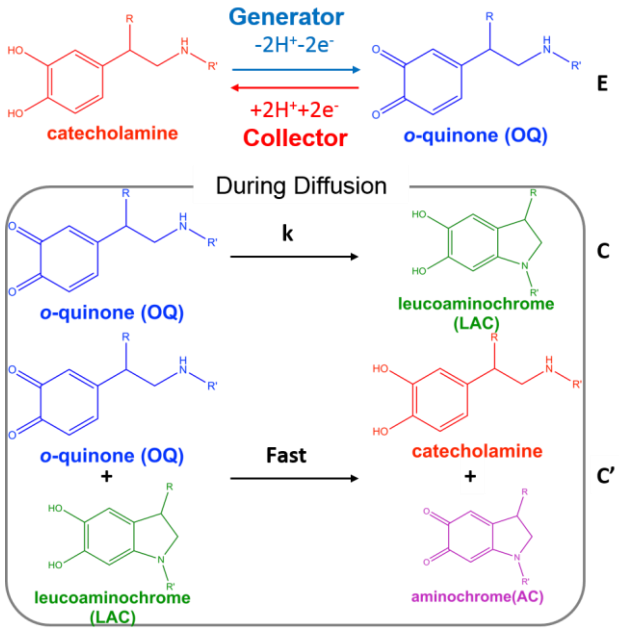


**Figure 3.1** Schematic of electrochemical oxidation of catecholamines and following chemistry (the ECC' mechanism) for: DA, R=H, R'=H; NE, R=OH, R'=H; EP, R=OH, R'=$CH_3$.

and NE, however, showed similar redox cycling performance. Here, we take advantage of their different intramolecular cyclization rates and the ability to manipulate the chemical reaction time by changing the separation between generation and collection sites to examine the extent of differentiation between DA and NE.

Cyclic voltammetry (CV) was used to study the redox cycling behavior of individual 50 µM DA, 50 µM NE and their 50 µM:50 µM mixture in pH 7.4 artificial cerebral spinal fluid (aCSF) for four different gap widths on microelectrode arrays with 2.00 mm long, 4.0 µm wide band electrodes and 4.0 µm gaps. Electrode configurations are shown in Figure 3.2. Without redox cycling, the generator electrodes were scanned between -0.150 V and 0.550 V at 0.020 V/s. With redox cycling, the collector electrodes were held at -0.010 V while the generator electrodes were scanned. Details of the device, electrochemical setup, and chemicals used can be found in the Supporting Information.

Figure 3.3 shows representative CV responses. When the collectors remain off (Figure 3.3 (i)-(l),), the plateau current at the generators for solutions containing either DA or NE alone are similar in magnitude. The response from a solution containing their mixture is approximately equal to the sum of individual results for all gap conditions (with an average error of -1.14% ± 62.30%). Detailed data analyses are provided in the Supporting Information (Table 3.S1). The additive nature of the generator currents for the individual components in a mixture is consistent with our previous results acquired with six pairs of alternating generator and collector with 4-µm gaps.[23]

When the collectors are activated (Figure 3.3 (a)-(h)), the recycling phenomenon is observed for both species at all gaps. At the 4 µm gap, DA exhibits a higher $A_f$ relative to that of NE, while that for the DA-NE mixture lies in the middle, which is consistent with our previous results.[23] With increasing gap width, $A_f$ of DA, NE, and their mixture all decrease due to increasing diffusional loss and more extensive following reaction chemistry because of the longer transit time. At large gap widths (20, 28 µm), the amplification effect is barely observed, mainly due to diffusional loss. For all four gap widths, generator signals with redox cycling for the DA-NE mixture is close to the sum of the results for the individual species (with an average error of 2.38% ± 37.01%). Detailed data analyses are provided in the Supporting Information (Table 3.S2). This indicates that with or without redox cycling, the generator provides information about the total concentration of catecholamines.

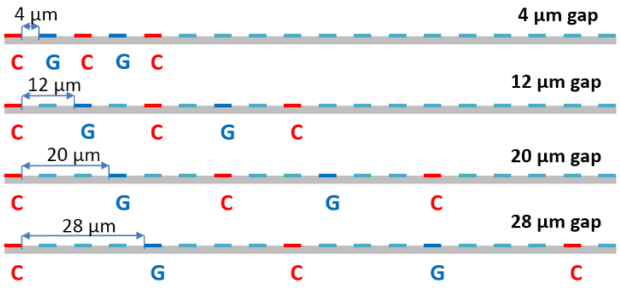


**Figure 3.2** Schematic of electrode configurations for four different edge-to-edge gap conditions, 4, 12, 20 and 28 µm, in which two electrodes are shorted as the generator (G) and three alternating electrodes are shorted as the collector (C).

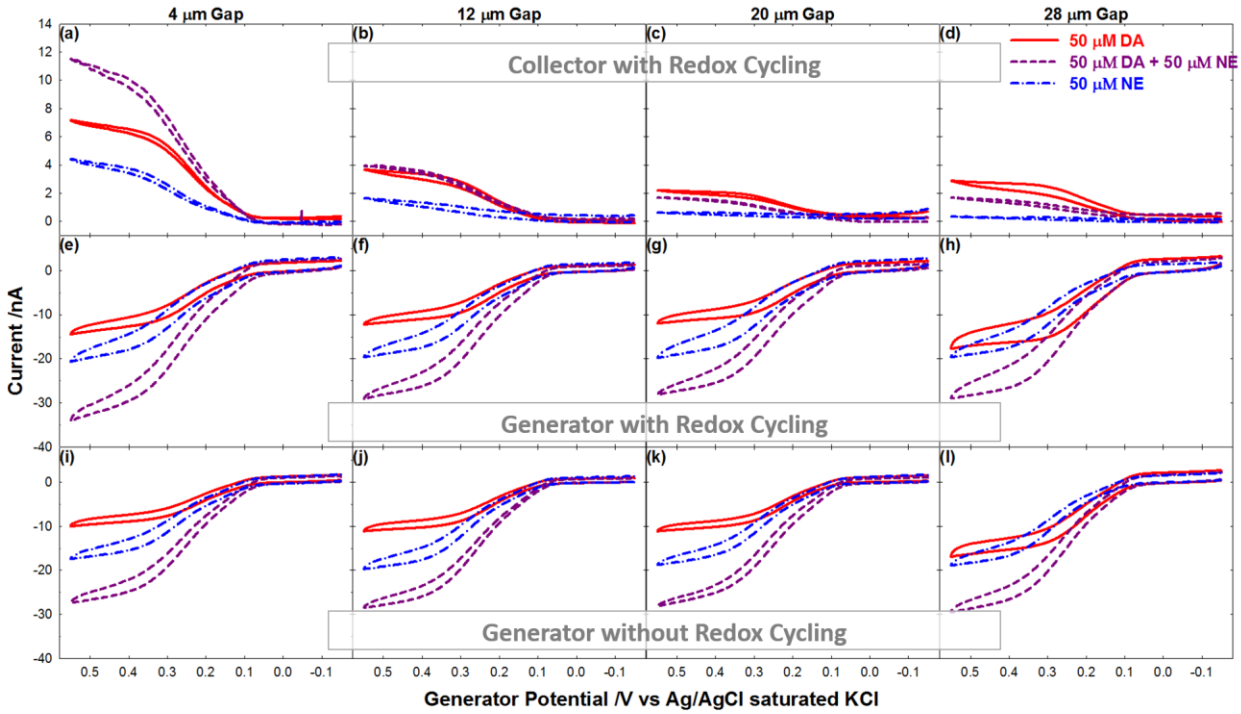


**Figure 3.3** CV responses at 0.020 V/s in solutions of 50 µM DA (red, solid), 50 µM NE (blue, dash-dot) and their binary mixtures (50 µM of each, purple, dash) in aCSF buffer, with and without redox cycling for four gap conditions: 4, 12, 20 and 28 µm. The generator electrodes were scanned from -0.150 V to 0.550 V while collector electrodes were held at -0.010 V during redox cycling.

Collector current and $C_e$ were also investigated. Table 3.1 lists averages plus/minus one standard deviation of $C_e$ from experiments performed on three different chips. Both DA and NE exhibit decreasing collector current with increasing electrode separation (Figure 3.3 (a)-(d)), where that for NE is more dramatic than for DA. With increasing gap width, the collector response for the mixture approaches that for solutions containing only DA, which is similar to the behavior of the DA-EP and NE-EP mixtures at the 4-µm gap reported previously[23]. At a large gap width (~20 µm), the collector signal for NE becomes silent. For all gap widths, DA shows a relatively higher $C_e$ than NE, and $C_e$ for their mixture lies in middle. $C_e$ for DA, NE, and their mixture all decrease with increasing gap width, while $C_e$ for NE has a greater dependence on gap width than DA. Detailed data analyses are provided in the Supporting Information (Table 3.S3).

A generation-collection simulation model was proposed previously to study similar systems. According to Shea et al.,[22] when the time for a generated species to diffuse to the collector is much greater than that of the half-life of the following homogeneous reaction, the $C_e$ will approach zero. For the ECC' mechanism of catecholamines oxidation, with the C reaction as the rate determining step, we simplified this system by ignoring the C' reaction for the moment. Based on the apparent rates obtained from literature for the C reaction, half-lives of catecholamines are calculated to be $t_{DA}$ = 5300 ms; $t_{NE}$ = 710 ms; $t_{EP}$ = 8.0 ms. The diffusion times for the OQ to diffuse across different gap widths in one dimension may be calculated by $t_x = x^2/(2D)$[24]: $t_4$ = 13 ms; $t_{12}$ = 120 ms; $t_{20}$ = 330 ms; $t_{28}$ = 650 ms, where x is the edge-to-edge gap width and D is the diffusion coefficient of DA in aqueous solution ($D = 6.0 \times 10^{-6}$ $cm^2/s$,[25] used for all catecholamines in this approximate calculation). As can be seen, $t_{DA} >> t_{28}$, $t_{NE} \approx t_{28}$ and $t_{EP} \approx t_4$. Thus, relatively high $C_e$ values for DA at all four gap widths, relatively high $C_e$ values for NE at the smaller gap widths but low values at the larger gap widths, and low $C_e$ values for EP at all four gap widths are expected. This trend is consistent with our previous results at the 4-µm gap and the experimental results shown above.

The DA-NE mixture system is complicated by the possibility of homogenous reactions between products generated from different catecholamines. According to the approximate calculation mentioned above, at small gap widths, small amounts of $LAC_{DA}$ and $LAC_{NE}$ are produced, thus the C' reaction depends on LAC. Mixing DA with NE will not measurably affect the progress of this reaction and the collector current is addible. With increasing gap widths, there is more time for the homogenous reactions to take place before

**Table 3.1 Normalized $C_e$ in solutions of aCSF buffer containing 50 µM DA, 50 µM NE and 50 µM each in a binary mixture.**

| Gap | DA | Mixture | NE |
|---|---|---|---|
| **4 µm** | 120.13 ± 15.45% | 82.22 ± 10.74% | 56.29 ± 12.01% |
| **12 µm** | 76.77 ± 4.82% | 40.52 ± 8.62% | 18.93 ± 4.84% |
| **20 µm** | 61.01 ± 17.32% | 28.36 ± 10.22% | 10.49 ± 5.44% |
| **28 µm** | 37.78 ± 6.22% | 16.90 ± 3.81% | 6.04 ± 2.49% |

* Due to limitations in quality control of microfabrication from electrode-to-electrode and chip-to-chip, the electrodes used for each gap condition have slightly different areas. Thus, the data are normalized against the average response obtained with the model compound before and after DA and NE studies for each gap condition.

the OQ reaches the collector electrode. At larger gap widths, less OQ will be available to react with LAC, and thus the reaction C' depends on OQ rather than LAC. Mixing DA with NE provides the opportunity for extra $LAC_{NE}$ to react with $OQ_{DA}$ so that less OQ species reach the collector, decreasing the collector current. More quantitative studies about the effects of different concentrations and the ratio of DA to NE, as well as computer simulation are needed to further understand the mixture system.

In this fundamental study, we investigated the redox cycling behavior of DA, NE and their mixture at different gap widths. Based on our previous study,[23] the phenomena described here also apply to EP. By translating the gap width between generator and collector electrodes as a reaction time in a redox cycling experiment, the distinct detection of three catecholamines can be based on their different intramolecular cyclization rates, and therefore the survival time of their OQ form. This survival time follows the trend of DA > NE > EP, which indicates that EP will be silent at the collector at small gap widths, and NE will be silent at larger gap widths where DA can still be detected. When mixed together, any interactions between DA and NE did not affect the generator signal with statistical significance. Thus, the signal at the generator corresponds to the sum of the signals of the individual species, which provides information about the total catecholamine concentration. The interaction between DA and NE start to play a role and affect the collector current of the mixture with increasing gap widths (20 and 28 μm gap in this study). More investigations are needed to map the relationship among the collector current, the concentration of each individual component, and the gap conditions, so that decoding the composition of a mixture of catecholamines is possible.

### 3.3 Acknowledgement

Research was supported partially through the National Science Foundation (CBET-1336853) and the Arkansas Biosciences Institute, the major research component of the Arkansas Tobacco Settlement Proceeds Act of 2000. We are grateful to Anupama Aggarwal and Vishal Sahore for contributing toward fabrication of the microelectrodes.

### 3.4 Supporting Information

Supporting information includes description of device, electrochemical setup, and chemicals used, as well as summaries and ANOVA tests of processed data of generator alone, generator and collector with redox cycling signals for 50 μM DA, NE and DA-NE mixture of 50 μM of each from three repetitive experiments. This material is available free of charge via the Internet at http://pubs.acs.org.

### 3.5 References


(1) Arnsten, A. F.; Pliszka, S. R. *Pharmacology Biochemistry and Behavior.* **2011**, *99*, 211-216.

(2) Lotharius, J.; Brundin, P. *Nature Reviews Neuroscience.* **2002**, *3*, 932-942.

(3) Vazey, E. M.; Aston-Jones, G. *Frontiers in behavioral neuroscience.* **2012**, *6*

(4) Raggi, M. A.; Sabbioni, C.; Nicoletta, G.; Mandrioli, R.; Gerra, G. *Journal of separation science.* **2003**, *26*, 1141-1146.

(5) Diao, P.; Yuan, H.; Huo, F.; Chen, L.; Xiao, D.; Paau, M. C.; Choi, M. M. *Talanta.* **2011**, *85*, 1279-1284.

(6) Mu, C.; Zhang, Q.; Wu, D.; Zhang, Y.; Zhang, Q. *Biomedical Chromatography.* **2015**, *29*, 148-155.

(7) Sima, I. A.; Casoni, D.; Sârbu, C. *Talanta.* **2013**, *114*, 117-123.

(8) Greco, S.; Danysz, W.; Zivkovic, A.; Gross, R.; Stark, H. *Anal.Chim.Acta.* **2013**, *771*, 65-72.

(9) Cooper, B. R.; Wightman, R. M.; Jorgenson, J. W. *Journal of Chromatography B: Biomedical Sciences and Applications.* **1994**, *653*, 25-34.

(10) Niwa, O.; Morita, M.; Tabei, H. *Electroanalysis.* **1991**, *3*, 163-168.

(11) Robinson, D. L.; Venton, B. J.; Heien, M. L.; Wightman, R. M. *Clin.Chem.* **2003**, *49*, 1763-1773.

(12) Wang, Y.; Wang, S.; Tao, L.; Min, Q.; Xiang, J.; Wang, Q.; Xie, J.; Yue, Y.; Wu, S.; Li, X. *Biosensors and Bioelectronics.* **2015**, *65*, 31-38.

(13) Hawley, M.; Tatawawadi, S.; Piekarski, S.; Adams, R. *J.Am.Chem.Soc.* **1967**, *89*, 447-450.

(14) Ciolkowski, E. L.; Maness, K. M.; Cahill, P. S.; Wightman, R. M.; Evans, D. H.; Fosset, B.; Amatore, C. *Anal.Chem.* **1994**, *66*, 3611-3617.

(15) Ciolkowski, E. L.; Cooper, B. R.; Jankowski, J. A.; Jorgenson, J. W.; Wightman, R. M. *J.Am.Chem.Soc.* **1992**, *114*, 2815-2821.

(16) Zhang, Z.; Huang, J.; Wu, X.; Zhang, W.; Chen, S. *J Electroanal Chem.* **1998**, *444*, 169-172.

(17) Pihel, K.; Schroeder, T. J.; Wightman, R. M. *Anal.Chem.* **1994**, *66*, 4532-4537.

(18) Niwa, O.; Morita, M.; Tabei, H. *Electroanalysis.* **1994**, *6*, 237-243.

(19) Vandaveer, W. R.; Woodward, D. J.; Fritsch, I. *Electrochim.Acta.* **2003**, *48*, 3341-3348.

(20) Ma, C.; Contento, N. M.; Gibson, L. R.; Bohn, P. W. *Anal.Chem.* **2013**, *85*, 9882-9888.

(21) Aggarwal, A.; Hu, M.; Fritsch, I. *Analytical and bioanalytical chemistry.* **2013**, *405*, 3859-3869.

(22) Shea, T. V.; Bard, A. J. *Anal.Chem.* **1987**, *59*, 2101-2111.

(23) Hu, M.; Fritsch, I. *Anal.Chem.* **2015**, *87*, 2029-2032.

(24) Bard, A. J. and Faulkner, L. R. In *Electrochemical Methods: Fundamentals and Applications* Anonymous ; Wiley:New York, 1980; pp 147.

(25) Gerhardt, G.; Adams, R. N. *Anal.Chem.* **1982**, *54*, 2618-2620.

## 3.S Supporting Information: Application of Electrochemical Redox Cycling: Toward Differentiation of Dopamine and Norepinephrine

Supporting information includes description of device, electrochemical setup, and chemicals used, as well as summaries and ANOVA tests of processed data of generator alone, generator and collector with redox cycling signals for 50 μM DA, NE and DA-NE mixture of 50 μM of each from three repetitive experiments.

### 3.S1 Device, Electrochemical Setup, and chemicals used

Microfabricated 1 in. × 1 in. model chips containing 18 individually-addressable gold microband electrodes that are 2.00 mm long, 4.0 µm wide and separated by 4.0 µm gaps were used here. Microfabrication details are described elsewhere.[1,2] A bipotentiostat equipped with a Faraday cage and a picoamp booster (CHI 760B, CH Instruments, Austin, TX) was used to perform the electrochemical experiments. A Ag/AgCl (saturated KCl) reference electrode and Pt wire auxiliary electrode were employed. As shown in Figure 3.2 of the main document, two shorted generator microbands and three shorted collector microbands, in an alternating arrangement, served as the first and second sets of working electrodes, respectively. They were activated to have a specified gap width (4, 12, 20 and 28 µm, edge to edge distance between the neighboring generator and collector electrodes).

All chemicals were used as received unless otherwise stated. Water (ACS reagent grade, 18 MΩ cm or greater) was obtained from Ricca Chemical (Arlington, TX, USA). Before and after redox cycling studies involving catecholamines, all working electrodes were characterized by cyclic voltammetry (CV) using a solution of 1.0 mM potassium ferricyanide (EM Science, Gibbstown, NJ, USA) in 100.0 mM KCl (BDH, Radnor, PA, USA). The supporting electrolyte consisted of artificial cerebral spinal fluid (aCSF) buffer (100 mM NaCl (EMD, Gibbstown, NJ, USA), 5.0 mM KCl, 1.2 mM NaH2PO4 (Alfa Aesar, Ward Hill, MA, USA), 5.0 mM NaHCO3 (J.T.Baker, Phillipsburg, NJ, USA), 10 mM glucose (BDH), 2.5 mM HEPES (Alfa Aesar), 1.2 mM MgSO4, 1.0 mM CaCl2 (Alfa Aesar)) at 7.4 pH. (−)-Norepinephrine, ≥ 98%, crystalline was obtained from Sigma, St. Louis, MO, USA and dopamine hydrochloride, 98.5% from Alfa Aesar.

### 3.S2 Generator without and with redox cycling

The percentage differences between the sum of the generator signals (current value measured at the plateau of the sigmoidal cyclic voltammetric response) for the individual components ($i_{G,DA}$ and $i_{G,NE}$, for 50 µM DA and 50 µM NE in separate solutions) and the generator signal for the mixture ($i_{G,Mixture}$ for 50 µM DA + 50 µm NE combined in a single solution) were calculated for each gap condition using eq.3.S-1,

$$\text{Percentage difference} = \frac{(i_{G,DA} + i_{G,NE}) - i_{G,Mixture}}{i_{G,Mixture}} \times 100\% \qquad \text{(3.S-1)}$$

Results for the generator current without redox cycling and with redox cycling are listed in Table 3.S1 and Table 3.S2, respectively.

**Table 3.S1. Percentage difference between the sum of the generator currents without redox cycling for the individual components and the mixture, following eq. 3.S-1.**

| Gap(μm) / Repeats | 4 | 12 | 20 | 28 | Average |
|---|---|---|---|---|---|
| **#1** | 10.83% | -63.67% | 9.10% | 33.52% | -2.56% |
| **#2** | 2.24% | -28.71% | 2.14% | 2.11% | -5.56% |
| **#3** | -8.00% | 2.63% | 2.47% | 21.68% | 4.70% |
| **Average** | 1.69% | -29.92% | 4.57% | 19.11% | -1.14% |

The ANOVA test at the 95% confidence level ($F_{column} = 3.514 < F_{table} = 4.066$ and $F_{row} = 0.153 < F_{table} = 4.256$) indicates that there is no statistically significant difference among replicates and different gap conditions for generator current without redox cycling.

**Table 3.S2. Percentage difference between the sum of the generator currents with redox cycling for the individual components and mixture, following eq. 3.S-1.**

| Gap(μm) / Repeats | 4 | 12 | 20 | 28 | Average |
|---|---|---|---|---|---|
| **#1** | 9.31% | -0.96% | 3.07% | 25.74% | 9.29% |
| **#2** | -1.86% | -26.47% | 5.28% | -2.94% | -6.50% |
| **#3** | -1.78% | 0.51% | -1.40% | 20.05% | 4.34% |
| **Average** | 1.89% | -8.97% | 2.31% | 14.28% | 2.38% |

The ANOVA test at the 95% confidence level ($F_{column} = 2.109 < F_{table} = 4.066$ and $F_{row} = 1.781 < F_{table} = 4.256$) indicates that there is no statistically significant difference among replicates and different gap conditions for the generator current with redox cycling.

These results suggest that the generator signal is not affected by the following chemistry interactions between DA and NE. Thus, the current at the generator can provide information of the total concentration of the catecholamines.

**3.S3 Collector with redox cycling**

The percentage differences between the collector signal for the DA alone ($i_{C,DA}$, for 50 μM DA) and that for the DA-NE mixture ($i_{C,Mixture}$, for 50 μM DA + 50 μM NE) were calculated for each gap condition using eq. 3.S-2 and are listed in Table 3.S3.

$$\text{Percentage difference} = \frac{i_{C,DA} - i_{C,Mixture}}{i_{C,Mixture}} \times 100\% \qquad \text{(3.S-2)}$$

**Table 3.S3. Percentage difference between the sum of the generator currents without redox cycling for the individual components and the mixture, following eq. 3.S-2.**

| Gap(μm) / Repeats | 4 | 12 | 20 | 28 | Average |
|---|---|---|---|---|---|
| **#1** | 10.83% | -63.67% | 9.10% | 33.52% | -2.56% |
| **#2** | 2.24% | -28.71% | 2.14% | 2.11% | -5.56% |
| **#3** | -8.00% | 2.63% | 2.47% | 21.68% | 4.70% |
| **Average** | 1.69% | -29.92% | 4.57% | 19.11% | -1.14% |

The ANOVA test at the 95% confidence level ($F_{column} = 5.978 > F_{table} = 4.066$ and $F_{row} = 0.239 < F_{table} = 4.256$) indicates that there is no statistically significant difference between replicates of the collector current for a fixed gap condition. However, there is a significant difference among different gap conditions——with increasing gap width, the collector current of the DA-NE mixture approaches and then drops below that for the DA alone.

### 3.S4 References

(1) Aggarwal, A. *Studies toward the Development of a Microelectrode Array for Detection of Dopamine through Redox Cycling*. University of Arkansas, Fayetteville, AR, 2011.

(2) Aggarwal, A.; Hu, M.; Fritsch, I. *Analytical and bioanalytical chemistry* **2013**, *405*. 3859-3869.

# 4. Detection of Dopamine Using Redox Cycling in the Presence of Electrochemically-Active Physiological Interfering Species

## 4.1 Abstract

Electrochemical detection of dopamine (DA) in the presence of electrochemically-active, interfering species known to coexist in the brain, including ascorbic acid (AA), uric acid (UA), L-3,4-dihydroxyphenylalanine (L-dopa), homovanillic acid (HVA), 3-methoxytyramine (3-MT) and 5-hydroxyindoleacetic acid (5-HIAA), under redox cycling conditions was investigated on gold microband arrays with an alternating generator and collector electrode configuration. With the opportunity for amplified signals and continuous monitoring, but without the need for background subtraction so that basal level detection may be possible, redox cycling is unique compared to electrochemical approaches used for in vivo DA detection. Therefore, it is of interest to evaluate its performance in solutions with interfering species similar in composition to those in the brain to determine its appropriateness for in vivo applications. Under conditions used in this study, the interfering species investigated are active at the generator and silent at the collector electrodes, while DA and its oxidized form are active at both. This behavior suggests that it may be possible to isolate the detection of DA in their presence at the collector. However, relatively smaller collector signals were observed compared to those for DA in the absence of the interfering species, presumably due to homogeneous reactions in solution between the oxidized product of DA and the interfering species during the diffusion time between the generator and collector electrodes.

## 4.2. Introduction

Dopamine (DA) is a crucial neurotransmitter in the central nervous system. Dopaminergic system dysfunction is related to neurological disorders such as Parkinson's disease,[1] Huntington's disease,[2] and drug addiction.[3] Monitoring the DA concentration in the extracellular fluid of the brain is of great importance for understanding its function in neurological systems. Methods for selective DA detection in the presence of other neurotransmitters and their metabolites as well as neuromodulators need to be developed for this purpose. Here, we investigate the performance of redox cycling for selective detection of DA in the presence of electrochemically-active species that are often at relatively higher concentrations and may interfere with this detection method.

Ascorbic acid (AA) is an interfering species of most concern for in vivo electrochemical detection of DA. It serves as antioxidant in the brain to clear oxygen or nitrogen based radicals and serves as a neuromodulator for DA- and glutamate-mediated neurotransmission. It exists in millimolar concentrations[4] which are about 10,000-100,000 times of DA in some regions of the brain.[5] Other electrochemically-active species including uric acid (UA), L-3, 4-dihydroxyphenylalanine (L-dopa), a precursor to DA, and metabolites of catecholamines: 3, 4-dihydroxyphenylacetic acid (DOPAC), homovanillic acid (HVA), and 3-methoxytyramine (3-MT). Another important neurotransmitter (serotonin, 5-HT) and its metabolites (5-hydroxyindoleacetic acid, 5-HIAA) and can coexist with DA in certain regions of the brain. Most of these interfering species have similar electrode potentials to that of DA, especially AA and DOPAC, which have an oxidation potential in vivo of +0.2 V vs a Ag/AgCl (3 M NaCl) reference electrode at a carbon paste electrode in Teflon tubing.[5, 6] Thus, with simple electrochemical methods, such as cyclic voltammetry (CV) or chronoamperometry (CA) using unmodified electrodes, the signals for these species cannot be distinguished from that for DA.

In vivo detection of DA is usually performed with fast scan cyclic voltammetry (FSCV) or microdialysis coupled with different detection techniques. A 5-30 μm diameter carbon fiber electrode (with 25–400 μm exposed electrode length) that is used in FSCV provides good spatial resolution and minimal tissue damage. The fast scan rate (usually from 300 V/s to 600 V/s) enables this technique to monitor quick transients of neurotransmitter concentrations; however, the high scan rate also creates high background current, which makes it unsuitable for monitoring basal levels.[7] Microdialysis, on the other hand, is good for basal level

detection of multiple analytes, but it suffers from greater tissue damage[8-10] and low temporal and spatial resolution because of its large probe diameter of 200 – 400 mm with a 1 – 4 mm sampling length.[11]

The electrochemical method of redox cycling has been explored for use in the field of DA detection in vitro before.[12-17] This method provides signal amplification and the ability of distinguishing between species with different electrochemical kinetics.[18, 19] Its advantage in low background current also leads to possible application of detecting of not only transients of DA that are evoked by behavior or controlled stimuli, but also basal levels of DA in the brain. In vitro studies of DA detection with and without the presence of up to 100-fold excess concentration of AA have been demonstrated previously by our group,[16] but redox cycling has not been applied in vivo. Devices containing microelectrode arrays with a size small enough for implantation in vivo are needed to apply this method in vivo. An understanding of the performance in more complicated matrices like those found in vivo is also needed. It is this latter point that this paper addresses.

The redox cycling system used in here consists of one set of electrodes scanning or poised at anodic potential (generator electrodes) where DA (the analyte) can be oxidized to its o-quinone form ($DA_O$) and a neighboring set of electrodes poised at cathodic potential (collector electrodes) where the $DA_O$ can be reduced back to DA. Each analyte molecule will be recycled between the generator and the collector more often as the generator and collector electrodes are brought closer together, thus providing an amplified signal. However, if the oxidized form of the analytes are not active upon arrival at the collector, they will not contribute toward a signal there and cannot be recycled, which is the case for the interfering species we investigated here. The amplification factor, which is the ratio of the generator current with redox cycling to that without redox cycling, $A_f$, and the collection efficiency, which is the ratio of collector current to generator current during redox cycling, $C_e$, are used to characterize the redox cycling effect.

The redox cycling behavior of DA in presence of the interfering species AA, UA, L-dopa, HVA, 3-MT and 5-HIAA is investigated here. Based on the difference in their electrochemical reaction kinetics, DA in presence of these interfering species can be selectively detected by monitoring the collector current. This approach has been demonstrated before in the presence of AA. However, with high concentrations of these interfering species, homogeneous chemical reactions with $DA_O$ can take place during the time it takes to diffuse to the collector, which decreases the efficiency of the redox cycling. This problem should be minimized by decreasing the spacing between the generator and the collector so that more $DA_O$ survives

because of a shorter trip. Here, we quantify the impact on redox cycling of DA for these different interfering species at a fixed spacing. Simultaneous detection of two other interfering species DOPAC and 5-HT is not addressed in this paper. As a reversible species, DOPAC oxidizes and re-reduces at a similar potential as DA, and thus cannot be simply discriminated from DA by redox cycling. However, DOPAC is negatively charged at physiological pH, so modifying the electrodes with a negatively charge polymer film, such as Nafion, could prevent DOPAC from diffusing to GE thus eliminate its signal.[20] 5-HT is also electrochemically reversible and it can severely foul the electrode. Electrode modification with films such as poly (3, 4-ethylene dioxythiophene) (PEDOT) could be used to protect electrodes from fouling.[21] However, permeation into thick films can decrease the diffusion coefficient of species, and thus decrease the magnitude of the current (sensitivity). Further study is needed to consider the impact of these two species on DA detection by redox cycling.

## 4.3. Experimental

### 4.3.1 Materials and chemicals

All chemicals were used as received unless otherwise stated. Hexaammineruthenium(III) chloride (Ru 32.8%), dopamine hydrochloride (98.5%), L-(+)-AA (99+%), uric acid (99%), 3,4-Dihydroxy-L-phenylalanine (98+%), homovanillic acid (98+%), HEPES, (ACS grade) were obtained from Alfa Aesar (Ward Hill, MA, USA). The 3-methoxytyramine HCl was obtained from Bachem (Bubendorf, Switzerland). The 5-hydroxyindo-3-acetic acid (99%) was obtained from Acros Organics (Fair Lawn, NJ, USA). Potassium chloride and sodium chloride were obtained from EMD Chemicals (Gibbstown, NJ, USA). Sodium hydrogen phosphate monobasic was obtained from J.T. Baker (Phillipsburg, NJ, USA). Calcium chloride, sodium sulfate, sodium hydrogen carbonate, magnesium sulfate, and glucose were obtained from Aldrich Chemical (St. Louis, MO, USA). Water (ACS reagent grade, 18 MΩ cm or greater) was obtained from Ricca Chemical (Arlington, TX, USA). DA and the interfering species were dissolved in pH 7.4 aCSF (artificial cerebrospinal fluid) buffer, which is considered to approximately represent the extracellular fluid composition in the mammalian brain.

### 4.3.2 Microelectrode array design and fabrication

Microelectrode arrays consisting of 18 individually addressable gold microband electrodes that are 4.0 µm wide, 2.00 mm long and separated by 4.0 µm gaps were used for the redox cycling studies.

Photographic image of the microfabricated chip and expanded view of the microarray is shown in Figure 4.1 A and B, respectively. Detailed fabrication procedures are described elsewhere.[22] Briefly, an 80 nm film of gold was evaporated onto a $SiO_2$-coated wafer with 8 nm chromium as adhesion layer. The electrode pattern was created by photolithography using positive photoresist S1805 (Rohm and Haas Electronic Materials LLC, Marlborough, MA, USA) followed by wet etching. Benzocyclobutene (BCB) served as an insulator for the leads. It was spin-coated and patterned, so that only the electrode array would be exposed to the solution and an edge connector could interface the chip via the contact pad region to the potentiostat. Residual BCB was cleaned away from those regions by reactive ion etching (with 32.0 sccm $O_2$ and 8.0 sccm $SF_6$ gas flow rate at 250.0 mTorr with a power of 200 W for 10 s) and individual chips were released by dicing.

#### 4.3.3 Redox cycling

Six alternating microbands were shorted together and used as the generator and the collector, respectively. Schematics of this alternating generator and collector electrodes configuration is shown in Figure 4.1 C.All experiments were performed with a bipotentiostat (CHI 750A, CH Instruments, Austin, TX), equipped with a Faraday cage and a picoamp boosterA three-electrode system was used for DA detection, where a Ag/AgCl (saturated KCl), a Pt wire, and the electrodes in the array served as reference, auxiliary, and working electrodes, respectively.

The redox cycling behavior of the array was characterized using 1.0 mM $K_3[Fe(CN)_6]$ (in 100.0 mM KCl), an electrochemically reversible model compound, by CV with a scan rate of 0.020 V/s before and after it was used for DA detection. Both CV and CA were used for detection of DA in aCSF buffer (100 mM NaCl, 5.0 mM KCl, 1.2 mM $NaH_2PO_4$, 5.0 mM $NaHCO_3$, 10 mM glucose, 2.5 mM HEPES, 1.2 mM $MgSO_4$, 1.0 mM $CaCl_2$) at 7.4 pH. Without redox cycling, the collector was not activated, but the generator was either scanned with CV from -0.150 V to 0.550 V and back at a scan rate of 0.020 V/s or held using CA at 0.550 V. With redox cycling, the collector was also held at -0.010 V to reduce the oxidized DA. Replicate experiments were performed and data are reported as the average of the replicates plus/minus one standard deviation.

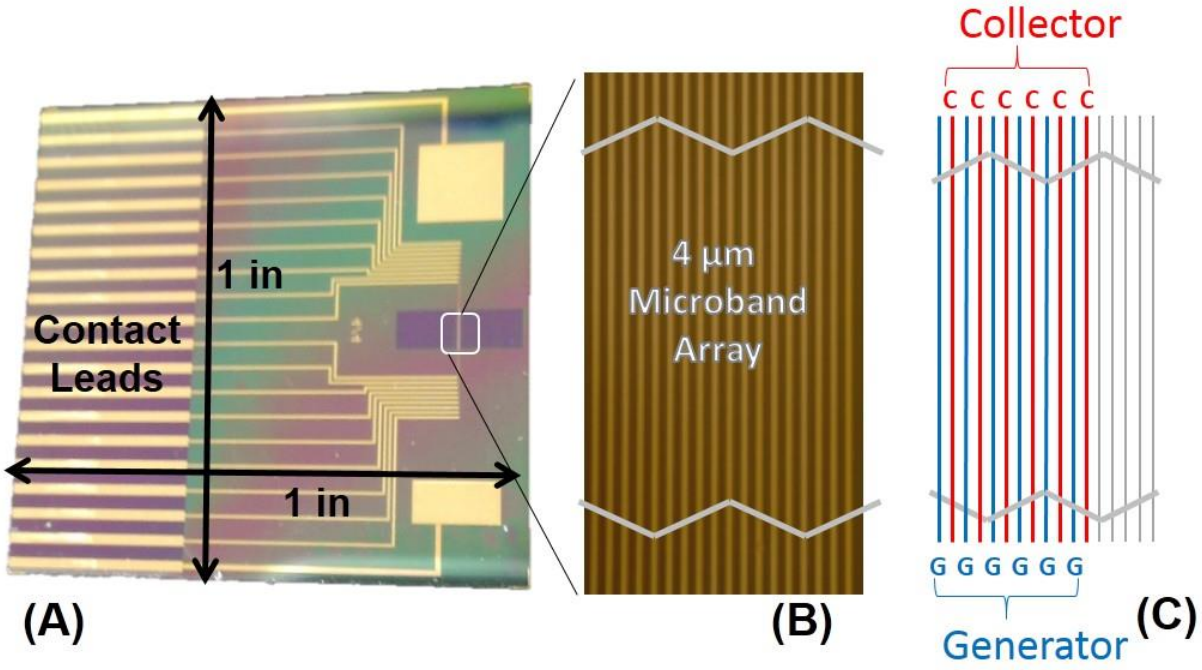


**Figure 4.1** Photographic image of the microfabricated chip (A) with expanded view the array containing 18 microband electrodes that are 2.00 mm long, 4.0 µm wide and separate by 4.0 µm gaps (B), and schematics of alternating generator and collector electrodes configuration: six pairs of generator (blue) and collector (red) (C)

### 4.4. Results and discussion

Representative CV results of the electrodes characterized in a solution containing the model compound, 1.0 mM $K_3[Fe(CN)_6]$ in 100.0 mM KCl, before the array was used for DA detection is shown in Figure 4.2. Peak-shaped CV responses were obtained by the generator without redox cycling. This is caused by overlapping diffusion layers of the neighboring microband electrodes for the time scale of this experiment, which makes it behave like a macroelectrode. With redox cycling, both the generator and the collector showed sigmoidally-shaped CV responses because of the alternating configuration of microelectrodes poised at different potential. The alternating generator-collector configuration used here showed good redox cycling efficiency. An average $A_f$ of 1.9 ± 0.5 and $C_e$ of 66% ± 19% were observed. Better amplification and collection efficiency have been reported with a redox cycling system using different electrode configurations (up to 4.5× amplification with 4 µm wide electrodes and 2 µm gaps in microband arrays[23] or about 10× amplification with recessed ring-disk nanoelectrode arrays[17]). Possible reasons include higher redox species concentration used and closer spacing of electrodes.[23, 24]

The redox cycling behavior of DA and of each individual interfering species were examined by CV. A representative CV response for 10 µM DA is shown in Figure 4.3. The voltammogram for the collector with redox cycling and the generator with and without redox cycling all exhibited sigmoidal shapes with a plateau between +0.300 V and +0.550 V. An average $A_f$ of 1.9 ± 0.4 and $C_e$ of 64% ± 3% were observed. The $A_f$ and $C_e$ of DA were smaller than those for the model compound, due to chemistry following the electrochemical oxidation. An ECC' mechanism has been proposed with a reversible electron transfer step (E) followed by an intramolecular cyclization of the oxidation product (C) and a bimolecular homogenous chemical reaction (C'). The amount of oxidized species available for recollection is decreased by forming electrochemically-inactive species both through cyclization and reduction via the homogenous reaction.[23,24] The effect of this mechanism has been discussed previously for all three catecholamines.[19]

AA and UA have been studied as the main interfering species in DA detection. They are present in extracellular fluid of the brain with concentrations higher than that of DA (100 to 1000 times of that for DA in striatum).[25, 26] Both AA and UA showed redox cycling behavior with low amplification and collection, with an $A_f$ of 0.9 for AA and 1.1 for UA; $C_e$ of 2% for AA and 12% for UA. Representative CV responses of

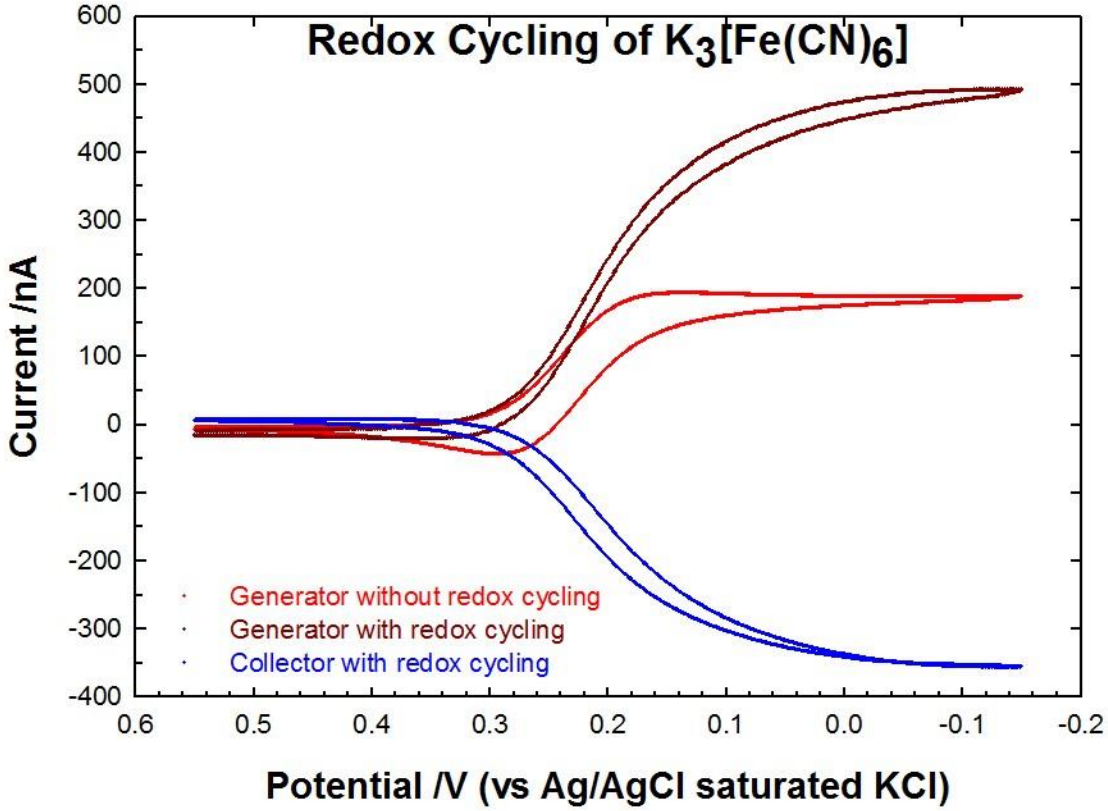


**Figure 4.2** Redox cycling behavior of electrodes as obtained by CV in a solution of 1.0 mM $K_3[Fe(CN)_6]$ and 100.0 mM KCl: generator without redox cycling (red, dashed), generator with redox cycling (brown, solid), and collector with redox cycling (blue, solid)

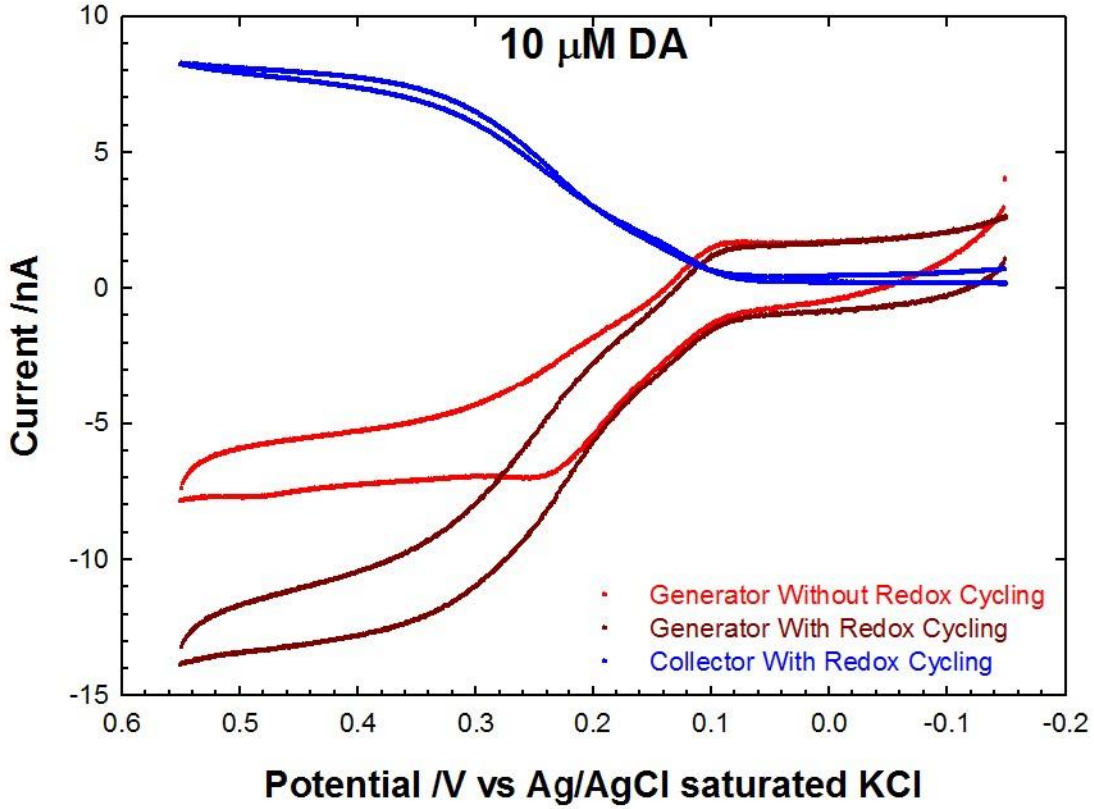


**Figure 4.3** Redox cycling behavior of electrodes as obtained by CV in a solution of 10 μM DA in aCSF buffer: generator without redox cycling (red, dashed), generator with redox cycling (brown, solid), and collector with redox cycling (blue, solid)

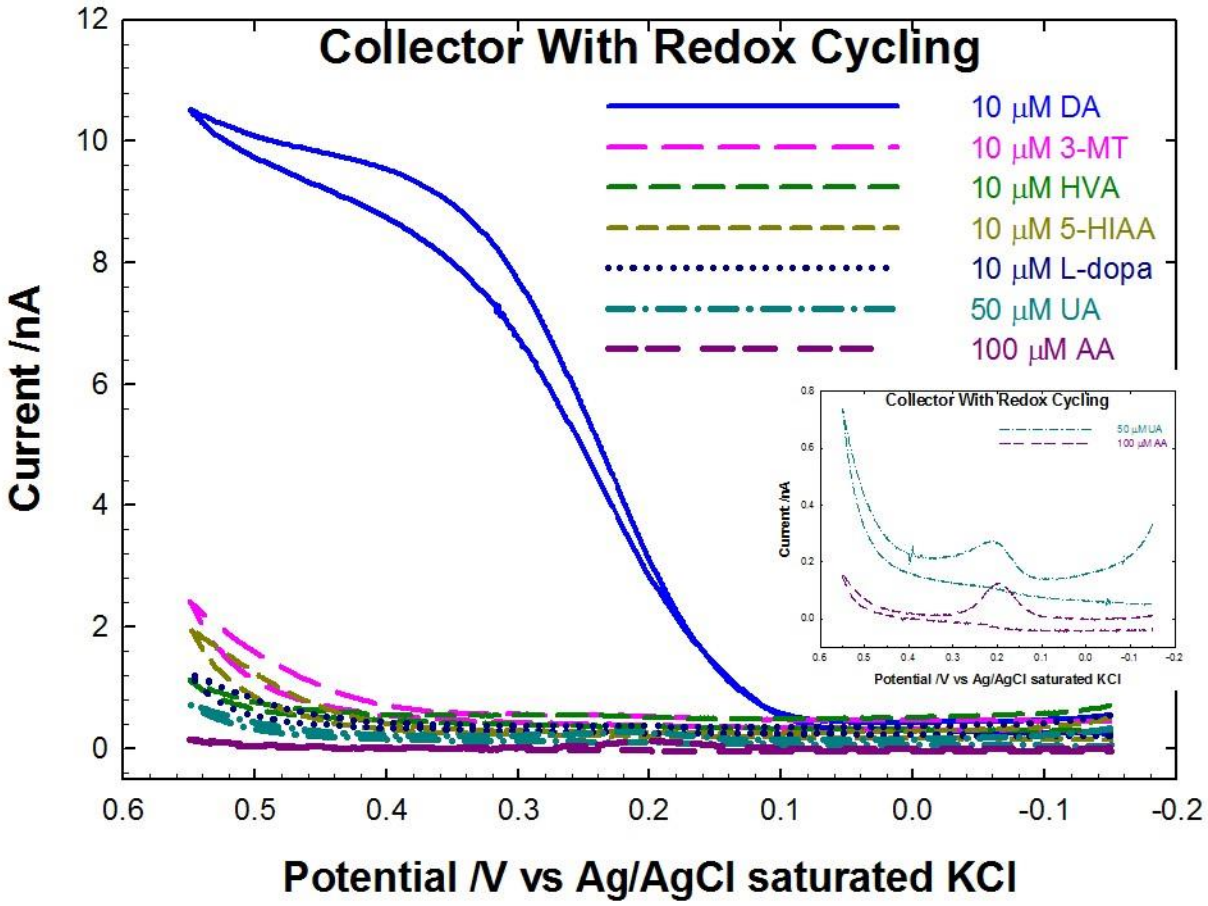


**Figure 4.4** Redox cycling behavior of collector electrodes as obtained by CV in solutions containing aCSF buffer and the following: 100 μM AA (purple, double dash), 50 μM UA (dark cyan, dash-dot), 10 μM 3-MT (magenta, long-dash), HVA (green, medium-dash), 5-HIAA (golden, short-dash), and L-dopa (dark blue, dotted) overlaid with 10 μM DA (blue, solid). Inset showed signals from UA and AA with expanded scale.

100 µM AA and 50 µM UA at the collector with redox cycling are shown as examples in the inset of Figure 4.4. Note that the peak at +0.2 V is due to contamination of the solution, this peak is with low current compared to the collector current from DA, so that it will not contribute to the total collector current. HVA, L-dopa, 3-MT and 5-HIAA present in extracellular fluid of the brain with relative low concentrations compare to AA and UA.[25] Currents from CV responses at +0.550 V were used to calculate the redox cycling efficiency. They have similar redox cycling behavior with silent collector signals as those of UA and AA but slightly different collecting efficiencies (16%, 12%, 12%, 23% for HVA, L-dopa, 3-MT and 5-HIAA, respectively). Responses for the collector with redox cycling using CV in solutions containing 10 µM HVA, L-dopa, 3-MT and 5-HIAA are shown in Figure 4.4, overlaid with the signal from 10 µM DA for comparison. The low collector current for these interfering species compared to the same or lower concentration of DA suggest the possibility of differential detection of DA at the collector.

The redox cycling behavior of DA in presence of interfering species in the solution was investigated. Representative CV responses of 10 µM DA and a mixture of 100 µM AA, 50 µM UA, 5 µM HVA, 1 µM L-dopa, 5 µM 5-HIAA and 1 µM 3-MT are shown in Figure 4.5. The concentrations of interfering species were chosen based on the concentrations of a typical standard solution used for microdialysis probe calibration.[27] In the mixture of DA with the interfering species, the generator responses with and without redox cycling are higher than the sum of individual responses. However, the collector response is lower than for DA alone. This could be caused by homogenous chemical reactions between the oxidized form of DA and the interfering species, as shown by the reaction schemes in eq 4.1 and 4.2,

$$DA \rightleftharpoons DA_O + 2e^- + 2H^+ \quad (4.1)$$

$$DA_O + X \rightarrow DA + Y \quad (4.2)$$

where X represents the interfering species in solution and Y represents the product from the homogenous redox reaction. As the reaction shown in eq 4.2 happens during diffusion between the generator and collector electrodes, less $DA_O$ will be available for reduction at the collector, thus decreasing the signal there. Likewise, more reduced DA becomes available so that the signal at the generator increases. This reaction is complicated, with a lot of unknown constants, combination of experimental studies and digital simulations is needed to further understand this system.

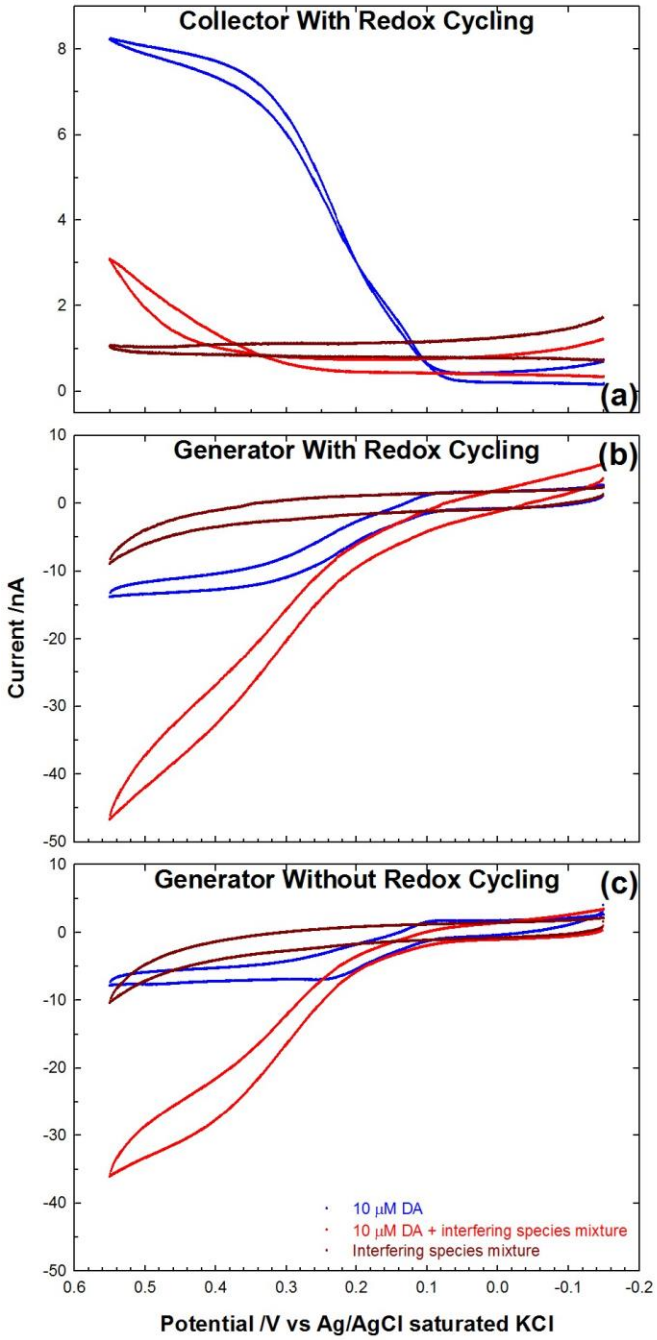


**Figure 4.5** Redox cycling behavior of electrodes as obtained by CV in solutions of aCSF buffer containing 10 µM DA (blue, solid), 10 µM DA in the presence of the mixture of interfering species (red, dashed) including 100 µM AA, 50 µM UA, 5 µM HVA, 1 µM L-dopa, 5 µM 5-HIAA and 1 µM 3-MT, and the mixture of interfering species alone (brown, solid): (a) collector with redox cycling, (b) generator with redox cycling, and (c) generator without redox cycling

As a more quantitative method compared to CV, CA results with three replicates were used to make calibration curves of DA alone in aCSF buffer and DA also in the presence of the mixture containing 100 µM AA, 50 µm UA, 5 µM HVA, 1 µM L-dopa, 5 µM 5-HIAA and 1 µM 3-MT (Figure 4.6). Redox cycling responses using CA exhibit a similar trend as those for CV. Equations for the least squares best fit lines to the data are shown in the figures. The detection limits are determined by three times the standard deviation of the blank signal and divided by the slope. Detection limits are reported as ± one standard deviation (calculated by detection limit multiply with standard deviation of slope then divided by the slope). The detection limits for DA alone and DA in the presence of the interfering species at the collector were found to be 0.730 ± 0.013 µM and 0.824 ± 0.016 µM, respectively, using standard deviation of aCSF alone for both. These results are within the same order of magnitude compared to the results reported previously using the same type microelectrode arrays but different electrode configurations (0.417 ± 0.067 µM for DA and 0.454 ± 0.026 µM for DA in presence of 100 µM AA).[16] When use the standard deviation of the interfering species mixture for the calculation of detection limit of DA in presence of interfering species, a lower detection limit is achieved: 0.086 ± 0.002 µM, due the lower standard deviation of the data set from DA in presence of interfering species. The calibration here only used one chip with sequential replicates, and the error from fabrication of the electrode arrays are not considered. Lower detection limits of DA in the presence of AA have been achieved by redox cycling systems with other electrode configurations: $10^{-8}$ M DA has been quantitatively measured using closely spaced interdigitated arrays with 50 electrodes that are 3 µm wide with 2 µm gaps;[12] and a 20 nM detection limit of DA was obtained with recessed ring−disk nanoelectrode arrays.[17] This indicates that by decreasing the electrode width and gap and increasing the number of electrodes, better redox cycling efficiencies with lower detection limits can be obtained.

**4.5. Conclusions**

Redox cycling behavior of DA in the presence of multiple electroactively-interfering species, AA, UA, L-dopa, HVA, 3-MT and 5-HIAA, was investigated using microelectrode arrays with 4.0 µm wide electrodes and 4.0 µm gaps. DA showed reversible redox cycling behavior while all the interfering species were irreversible at the collector electrode under the conditions used here. When mixed together, collector signals of DA were affected by the interfering species. This may be due to the homogeneous chemical reactions that occur between the oxidized form of DA and the interfering species during the diffusion time

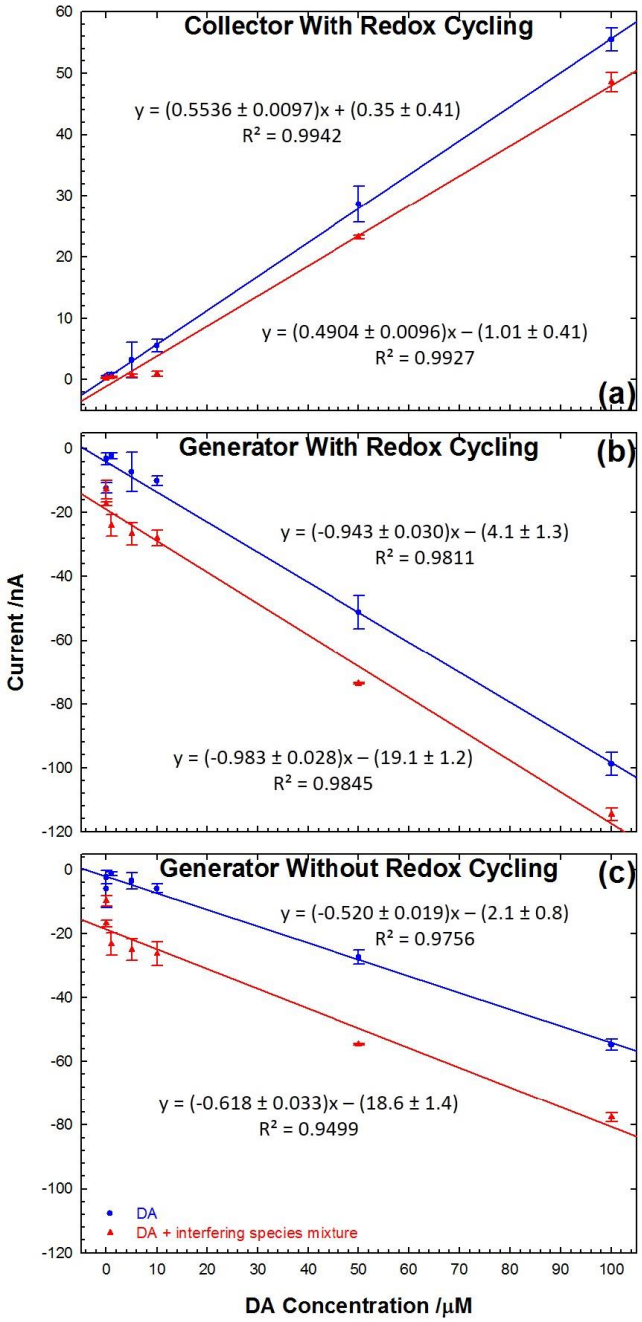


**Figure 4.6** Calibration curves obtained using CA of a solution of aCSF containing DA (blue, solid) and DA in the presence of interfering species (red, dashed) including 100 µM AA, 50 µM UA, 5 µM HVA, 1 µM L-dopa, 5 µM 5-HIAA and 1 µM 3-MT: (a) collector with redox cycling, (b) generator with redox cycling, and (c) generator without redox cycling.

between the generator and collector. Future studies of the mechanism and kinetics of these following chemical reactions are needed. Based on the kinetics, it is possible that microelectrode arrays can be designed with a specific geometry and gap between the generator and collector electrodes so that the oxidized species of DA can be collected before it reacts significantly with the interfering species. Digital simulations of this system will be performed to optimize the microelectrode array design.

### 4.6 Acknowledgments

Research was supported partially through the National Science Foundation (CBET-1336853) and the Arkansas Biosciences Institute, the major research component of the Arkansas Tobacco Settlement Proceeds Act of 2000. We are grateful to Anupama Aggarwal and Vishal Sahore for contributing toward fabrication of the microelectrodes.

**4.7 References**


(1) Lotharius, J.; Brundin, P. *Nature Reviews Neuroscience.* **2002**, *3*, 932-942.

(2) Jakel, R. J.; Maragos, W. F. **2000**, *23*, 239-245.

(3) Volkow, N.; Fowler, J.; Wang, G.; Baler, R.; Telang, F. **2009**, *56*, 3-8.

(4) Harrison, F. E.; May, J. M. *Free Radical Biology and Medicine.* **2009**, *46*, 719-730.

(5) Robinson, D. L.; Hermans, A.; Seipel, A. T.; Wightman, R. M. *Chem.Rev.* **2008**, *108*, 2554-2584.

(6) Kissinge.Pt; Hart, J. B.; Adams, R. N. *Brain Res.* **1973**, *55*, 209-213.

(7) Robinson, D. L.; Venton, B. J.; Heien, M. L.; Wightman, R. M. *Clin.Chem.* **2003**, *49*, 1763-1773.

(8) Khan, A. S.; Michael, A. C. *TrAC Trends in Analytical Chemistry.* **2003**, *22*, 503-508.

(9) Nesbitt, K. M.; Jaquins-Gerstl, A.; Skoda, E. M.; Wipf, P.; Michael, A. C. *Anal.Chem.* **2013**, *85*, 8173-8179.

(10) Nesbitt, K. M.; Varner, E. L.; Jaquins-Gerstl, A.; Michael, A. C. *ACS chemical neuroscience.* **2014**, *6*, 163-173.

(11) Kennedy, R. T. **2013**, *17*, 860-867.

(12) Niwa, O.; Morita, M.; Tabei, H. *Electroanalysis.* **1991**, *3*, 163-168.

(13) Niwa, O.; Morita, M.; Tabei, H. *Electroanalysis.* **1994**, *6*, 237-243.

(14) Vandaveer, W. R.; Woodward, D. J.; Fritsch, I. *Electrochim.Acta.* **2003**, *48*, 3341-3348.

(15) Goluch, E. D.; Wolfrum, B.; Singh, P. S.; Zevenbergen, M. A. G.; Lemay, S. G. **2009**, *394*, 447-456.

(16) Aggarwal, A.; Hu, M.; Fritsch, I. *Analytical and bioanalytical chemistry.* **2013**, *405*, 3859-3869.

(17) Ma, C.; Contento, N. M.; Gibson, L. R.; Bohn, P. W. *Anal.Chem.* **2013**, *85*, 9882-9888.

(18) Shea, T. V.; Bard, A. J. *Anal.Chem.* **1987**, *59*, 2101-2111.

(19) Hu, M.; Fritsch, I. *Anal.Chem.* **2015**, *87*, 2029-2032.

(20) Crespi, F.; M ├╢bius, C. **1992**, *42*, 149-161.

(21) Atta, N. F.; Galal, A.; Ahmed, R. A. **2011**, *158*, F52-F60.

(22) Aggarwal, A. *Studies Toward the Development of a Microelectrode Array for Detection of Dopamine through Redox Cycling,* Ph.D ed.; University of Arkansas:Fayetteville, AR; 2011.

(23) Dam, V. A. T.; Olthuis, W.; van den Berg, A. *Analyst.* **2007**, *132*, 365-370.

(24) Niwa, O.; Morita, M.; Tabei, H. *Anal.Chem.* **1990**, *62*, 447-452.

(25) Zetterström, T.; Sharp, T.; Marsden, C.; Ungerstedt, U. *J.Neurochem.* **1983**, *41*, 1769-1773.

(26) Sun, C.; Lee, H.; Yang, J.; Wu, C. *Biosensors and Bioelectronics.* **2011**, *26*, 3450-3455.

(27) Bazzu, G., Biosa, A., Farina, D., Spissu, Y., Calia, G., Dedola, S., Rocchitta, G., Migheli, R., Serra, P. A. and Desole, M. S. In *Neurotrophic Factors* Anonymous ; Springer:2012; pp 365-381.

# 5. Design and Microfabrication of SU-8 Based Micro Probe with Dimensions Suitable for In Vivo Detection of Dopamine

## 5.1 Abstract

A polymer-based neural probe containing a band electrode array that is intended for in vivo detection of neurotransmitters was designed and several microfabrication procedures were evaluated. Two types of neural probes were conceived: one with a co-planar microband array on the lateral surface of the shaft and the other with a nanoband array along the vertical edge at the tip. A highly efficient plan was devised to make use of as few as a single “metal layer” mask for both types of electrode configurations. It involves rotating the mask by 90° to pattern up to four sets of sequentially-deposited layers of metal and insulator. Different microfabrication strategies were used to optimize the co-planar and edge array probes. Due to the physical properties of the SU-8 polymer used here, multiple problems were encountered during fabrication of both types of probes. Possible causes of the problems and future optimization of the fabrication process are discussed.

## 5.2 Introduction

As a popular technique for recording and influencing neural activities, microfabricated neural probes have been developed for different applications in neurological and biomedical fields.[1] Although it is invasive, it offers high temporal and spatial resolution. Different materials have been studied for microfabrication of neural probes, among which silicon is the most popular one. However, this material has the disadvantages of rigidity and brittleness, which makes the fabricated probe easy to break and cause tissue damage.[2] Another type of neural probe is made of flexible polymers[3] (e.g. polyimide, SU-8), which avoids the brittleness problem. The polymer-based probe also has the advantages of lower-cost and an easier fabrication process.

In order to apply the electrochemical method of redox cycling to in vivo neurotransmitter detection, a probe with dimensions appropriate for insertion is needed. Probes with an interdigitated array (IDA) of microelectrodes was designed and fabricated previously in the Fritsch laboratory.[4] These silicon based IDA probes contain 260 µm × 260 µm or 260 µm × 100 µm gold microband electrode array areas containing 140 µm or 50 µm long, 4 µm wide microband electrodes, with 4 µm gaps between adjacent electrodes, and on a shaft that is 670 µm wide and 980 µm long. The fabricated IDA probes were characterized in vitro using the model compound $[Ru(NH_3)_6]^{3+}$ and a detection limit of about 500 nM was obtained on certain designs.[4] However, there are several problems for this IDA probe design. One is that the length of the probe tip is not long enough to reach the target location in the rat brain. According to neuroanatomy diagrams, the striatum, which is a structure of common interests for in vivo dopamine detection, is located about 4 mm deep in the rat brain. Also, the width of the probe tip is still too big for insertion, which makes it unsuitable for in vivo studies.

Many factors need to be considered in designing neural probes suitable for in vivo studies. The probe size is critical for minimizing tissue damage when the probe needs to be implanted. However, there is a tradeoff between probe size (length and thickness) and mechanical strength. Smaller probes may produce less tissue damage, but it would be easier to bend or break during insertion. Thinner and longer probes are also not easy to fabricate and handle. Increasing sharpness of the probe tip by using shallow diffusion of the needle shape at the probe tip may help improve the insertion properties of the probe.[5]

The substrate material used for the neural probe plays an important role on performance. In general, two major types materials are used for neural electrode probes. Most reported in the literature are silicon-based. The Michigan array and the Utah array are two of the most popular silicon-based devices made for simultaneous recording of multiple sites of interest in the brain. The rapid development in silicon micromachining technologies has resulted in silicon-based devices to be explored for applications for years. Silicon-based microelectrodes have the advantages of good reproducibility and low variability, they can also be used for devices with multiple functions integrated onto them. This makes it promising for applications that provide high-resolution recording and stimulation in complex neurological studies.[1]

To achieve a small probe thickness, either a specific kind of ultrathin silicon wafer was used,[6] or a wafer-thinning process was performed. There are several ways to thin the wafer. For example, deep boron diffusion into silicon defining the shank of the probe is carried out before the wafer is used. After all the other fabrication processes are complete, the wafer is thinned from the backside (the side opposite to that where the electrodes are patterned) using an isotropic wet etch, and then an ethylene diamine pyrocatechol etch is used to release the probes.[3] The front side of the probes can be thinned and patterned by deep reactive ion etching (DRIE). The back side of the wafer can be thinned with wet silicon etching.[7]

To avoid the complicated wafer thinning process, polymer based neural probes can be used. The thickness of a polymer-based probe is relatively easier to control. Commonly used polymers include polyimide, benzocyclobutene (BCB), and SU-8.[2, 3] Polyimide has the advantages of good insulation resistance, dielectric strength, and high mechanical flexibility. It can be pattern by standard microfabrication procedures and has been etched by dry etch techniques such as reactive ion etching (RIE).[8] As negative photoresists, BCB and SU-8 have been used a lot as an insulation layer between conducting layers in microfabrication processes. Compared to polyimide and BCB, SU-8 also allows the fabrication of devices over a wider thickness range, and thus provides better control of the rigidity of the device by adjust the thickness of the probe throughout the length of the probe tip.[2] Different microfabrication strategies and applications have been reported for these polymer-based neural probes. However, most of the devices are only used for voltage recordings in neurophysiological studies. Its suitability for electrochemical detection remains untested.

## 5.3 Experimental Section

### 5.3.1 Chemicals and Materials

A 125 cm diameter, single crystal, 625 ± 25 μm thick silicon wafer (N type, 1-0-0-orientation) with 2 μm ± 5% $SiO_2$ layer grown thermally on one side was commercially obtained (SQ 12775, Silicon Quest International, Inc., Santa Clara, CA). Chromium plated tungsten rods (2 in. long x 0.050 in. diameter, CC/ION 40040) (Kurt J. Lesker Company, Jefferson Hills, PA), pieces from Canadian Maple Leaf gold coin with 99.99% purity on a molybdenum notched heating boat (Kurt J. Lesker Company) and aluminum pellets (99.99%, from Alfa Aesar, Ward Hill, MA) on a molybdenum boat were used as metal evaporation sources.

The S1805 positive photoresist (Rohm and Haas Electronic Materials LLC, Marlborough, MA) and AZ 300 MIF developer (AZ Electronic Materials, Somerville, NJ) were used as received. The OmniCoat, SU-8 3050, SU-8 2000.5, and SU-8 developer were obtained from MicroChem (Newton, MA). Chromium etchant (HTA enterprise,CEP 200) and gold etchant (Transene, GE8148) were also used as received.

### 5.3.2 Device Design

The AutoCAD designs and corresponding chrome masks for SU-8 based neural microelectrode arrays were made. As shown in Figure 5.1, the whole wafer was divided into four quarters and two different types of microelectrode arrays (co-planar and edge microelectrode arrays) were distributed evenly along with alignment marks on each quarter with central symmetry. All neural probes were designed to share similar shape with a pointed probe tip and an arc shaped shaft to reduce insertion shear forces. Two configurations were designed for co-planar microelectrode arrays. Planar probe A (Figure 5.2 A) has 9 individually-addressable microband electrodes, each is 100 μm long, 4 μm wide with 4 μm gap between neighboring electrodes. Planar probe B (Figure 5.2 B) is similar to planar probe A, only with the 2nd and 4th bands missing, so that redox cycling can be performed with different gaps between generator and collector electrodes without other metal (which can equilibrate redox species in solution over its entire area) present in the gap. Co-planar probes are designed to fit a Molex zero insertion force (ZIF) edge connector with 1.00 mm pitch and 9 circuits (part number 52610-0972). The other type is vertical edge microelectrode arrays with three electrodes on each layer: one on the pointed part of the probe tip and two on the sides of the shaft near the probe tip (Figure 5.3 A). To ensure the exposure of metal layers on the vertical edge plane, the electrode areas on the probe tip and sides are designed in a way such that the metal layer goes

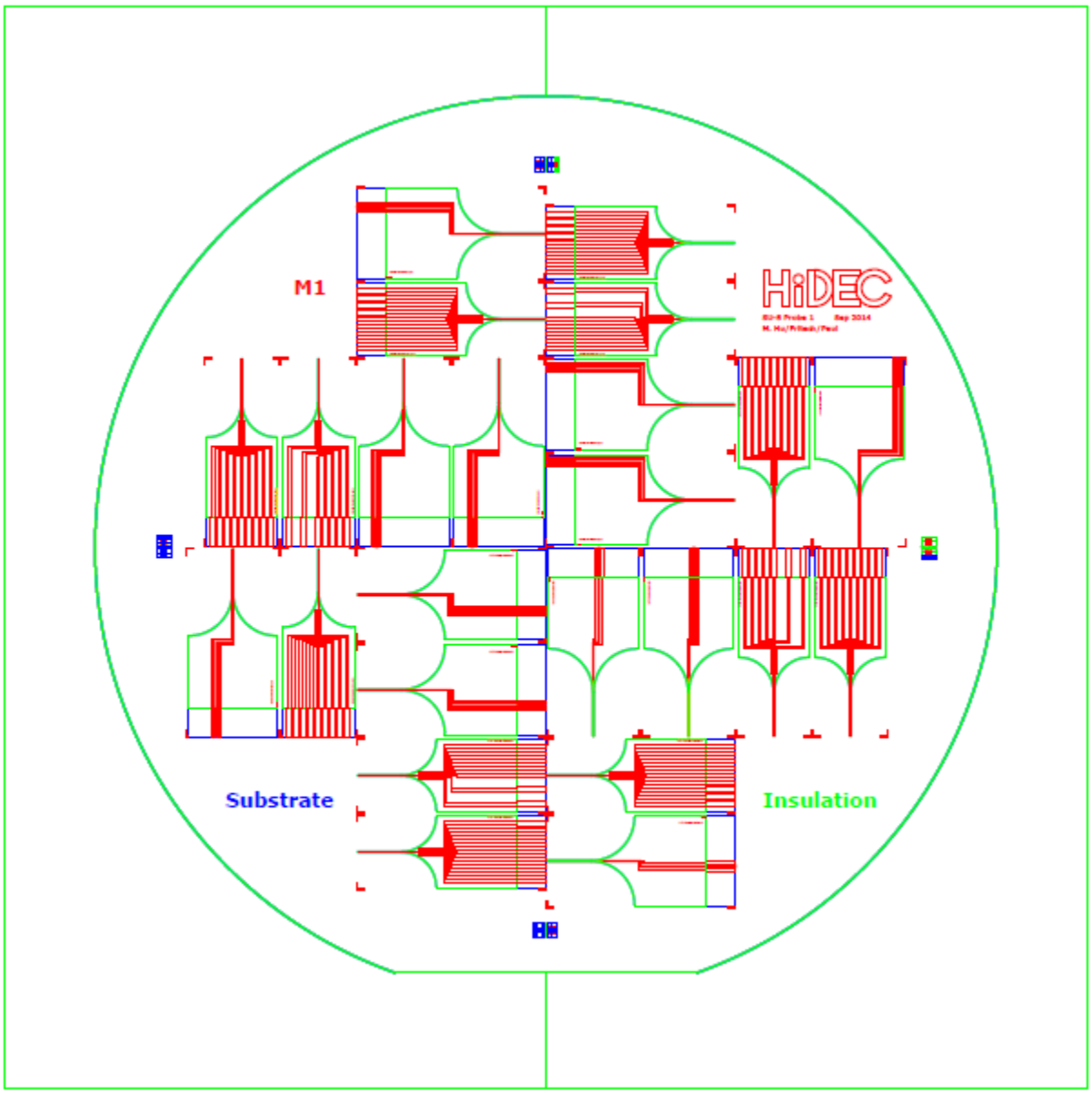


**Figure 5.1** Overlay of the AutoCAD designs for three layers: a substrate layer (blue), a metal layer (red), and an insulation layer (green). The substrate and insulation layers are designed for dark field masks, in which all enclosed features are clear. The metal layer is designed for a clear field mask, in which all enclosed features are filled. This design is made for a 125 cm-diameter wafer using a 150 cm by 150 cm mask plate.

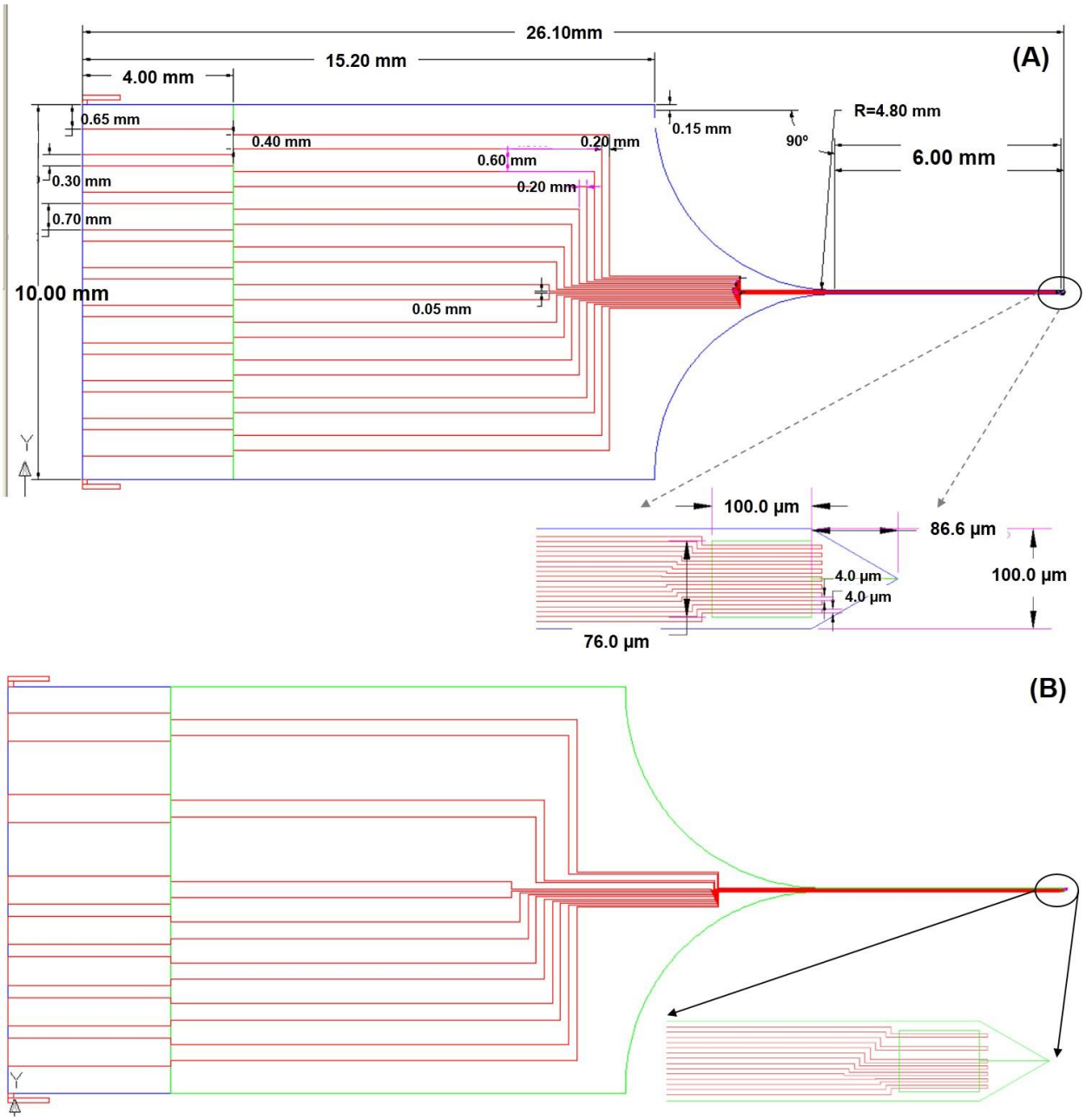


**Figure 5.2** AutoCAD drawing of co-planar microelectrode arrays with dimensions labeled. The devices contain three layers: a substrate layer (blue), a metal layer (red), and a insulation layer (green). Both co-planar and edge array designs share the same probe shape and size: a 10.0 mm × 15.2 mm main body part connected with an arc shaped shaft and a needle shaped insertion part that is 6.0 mm long and 0.1 mm wide. (A) Planar probe A contains 9 individual addressable microband electrodes that are 100 µm long, 4 µm wide with 4 µm gap between neighboring electrodes; (B) Planar probe B is a modified version of planar probe A with the 2$^{nd}$ and 4$^{th}$ electrode removed.

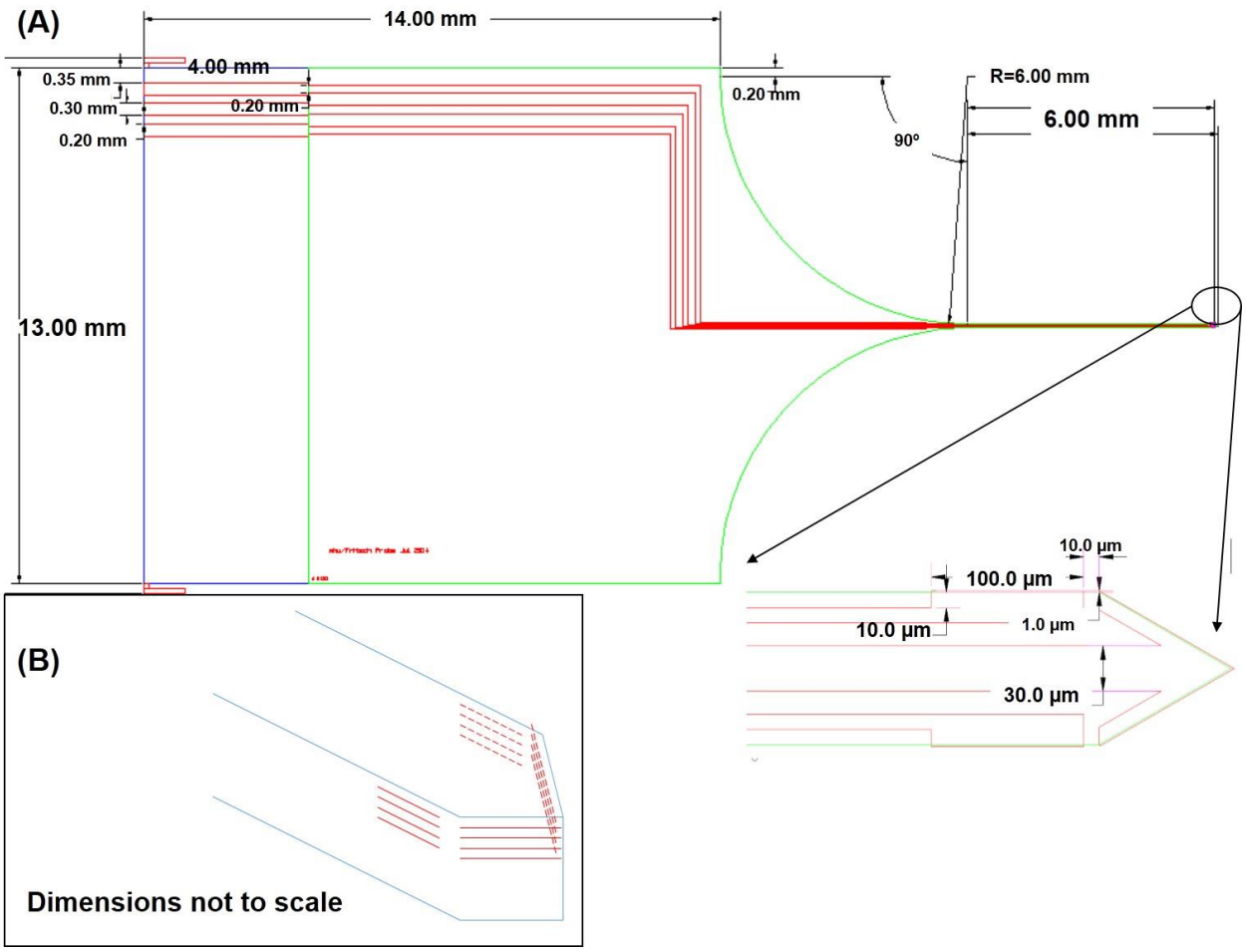


**Figure 5.3** (A) AutoCAD drawing of vertical edge microelectrode arrays with dimensions labeled. The devices contain three layers: a substrate layer (blue), a metal layer (red), and a insulation layer (green). The shape is similar to that of the co-planar probe design, but wider to accommodate more leads: a 13.0 mm × 14.0 mm main body part connected with an arc shaped shaft and a needle shaped insertion part that is 6.0 mm long and 0.1 mm wide. Each metal layer in this design will produce three electrodes on the vertical plane: one on probe tip (arrow shaped that is 101.7 µm long on each side) and two on the edges of the probe tip (100 µm long). (B) Schematic illustration of probe tip part of the vertical edge array: electrode areas that will be exposed on the vertical plane are shown as red lines. Three sets of microband electrode arrays can be obtained including one set on each side of the probe and one set with angled microbands on the probe tip. Note that the dimensions here are not to-scale.

beyond the probe tip frame defined by the substrate layer (the electrodes were extended for 1 μm from the edge of probe tip frame). A 3D schematic illustration of the probe tip for this design is shown in Figure 5.3 B. This type of probe is designed to fit a Molex ZIF edge connector with 0.50 mm pitch and 24 circuits (part number 52559-2452).

A total of four chrome masks were made, including one “substrate layer” mask, two “metal layer” masks, and one “insulation layer” mask. The two “metal layer” masks contain the same number and placement of the two types of probe designs so that they can both be used for the production of the two types of probes and use the same set of the “substrate layer” and “insulation layer” masks. The positions of the leads on the vertical edge microelectrode array probe on the two “metal layer” masks are different, however, so that all eight electrodes can be individually addressable. By rotating the metal layer mask for 90 degrees each time, the two “metal layer masks” can produce edge microband array probes with up to eight metal layers (4 layers from each mask) in the array on the vertical edge.

### 5.3.3 Fabrication Procedures

The SU-8 polymer serves as both substrate and insulation layers during fabrication. As a negative photoresist, SU-8 can be easily patterned by photolithography. Different types of SU-8 have different viscosities, thus providing the possibility of a wide range of substrate thicknesses and therefore flexibility of the structure.[2] Fabrication procedures were designed for co-planar microelectrode array probes (Figure 5.4) and edge microelectrode array probes (Figure 5.5) based on microfabrication processes described in the literature.[2, 8] The proposed procedures were tested and optimized, unless otherwise indicated. The process that was used is as follows. All photolithography processes were performed at the High Density Electronics Center at the University of Arkansas.

For both procedures, silicon wafers with 2 μm thick silicon dioxide layers on both sides were used as the carrier wafers. These were cleaned prior to use to remove contamination from the environment, as well as residues left from prior usage. The organic clean step of the RCA cleaning procedure (named after the inventors RCA (Radio Corporation of America) Laboratories) was used for removing organic contaminates that could affect the fabrication process. Wafers were immersed in a solution of 5:1:1 volume ratio mixture of DI water: $NH_4OH$: $H_2O_2$ at 75 °C for 10 min. Then the wafers were rinsed immediately with DI water followed by a spin-rinse-dry (SRD) process to remove residual cleaning solution. Al pellets on molybdenum

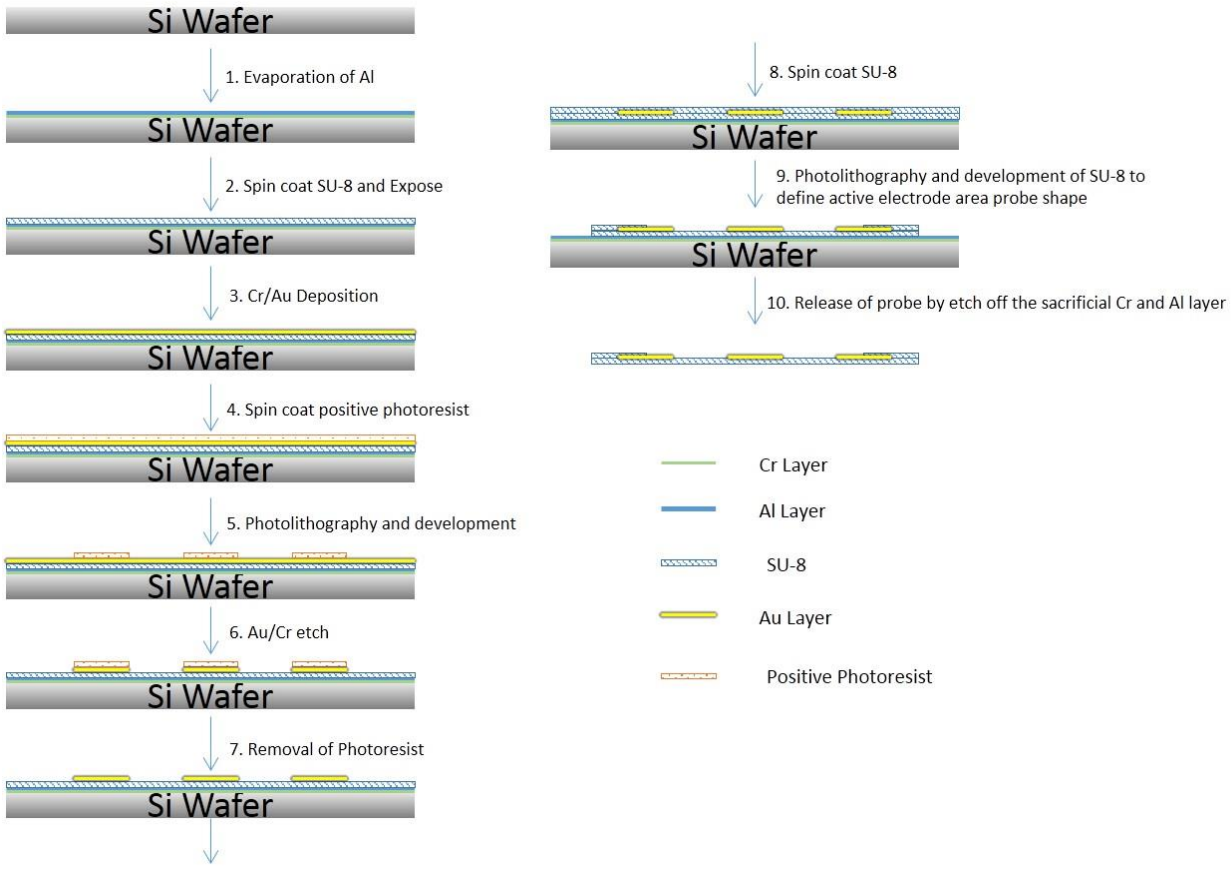


**Figure 5.4** Schematic of fabrication process flow for making the probes containing the co-planar microelectrode arrays.

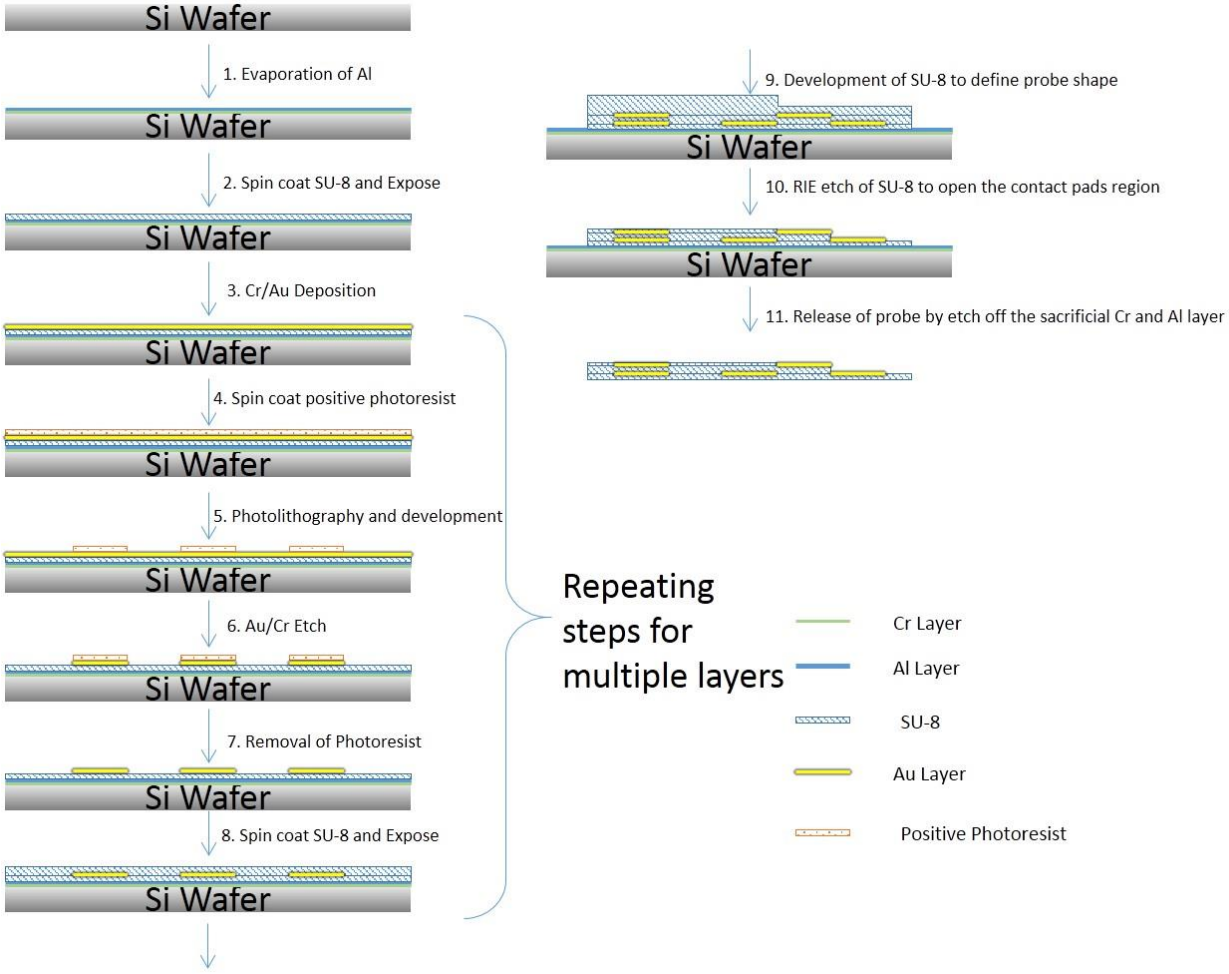


**Figure 5.5** Schematic of fabrication process flow for the probes containing the vertical edge microelectrode arrays. During the repeating steps for multiple layers of electrodes, the “metal layer” mask is rotated 90 degrees after patterning each metal layer to make the subsequent layer. Each “metal layer” mask can be used to make up to four layers of electrodes, A total of eight layers of electrodes can be obtained with the use of both “metal layer” masks.

boat were used as metal sources for thermal evaporation of the Al sacrificial layer (50 nm) using an Edwards 306 Auto thermal evaporator, fitted with a piezoelectric crystal thickness monitor.

For both fabrication procedures, a thick SU-8 layer (SU-8 3050), which is about 90 µm thick, is then applied (spin at 1250 rpm for 30 s) to the Al-coated carrier wafer and spin coated at 1500 rpm. OmniCoat was applied as an adhesion layer prior to applying the SU-8 at 2500 rpm for 30 s. The wafer was baked at 200 °C for 6 min before the OmniCoat application and 1 min after. This layer is then patterned by exposure to UV light (365 nm) through the "substrate layer" mask using a Suss MA150 Contact Aligner. The exposure time was calculated by exposure dose divided by the UV light intensity (number obtained from a weekly updated logbook). Optimization of the exposure as well as the pre-exposure, post-exposure baking and curing parameters are discussed in the Results and Discussions section.

A Cr adhesion layer and a Au layer were then deposited on the thick SU-8 substrate layer by thermal evaporation (using an Edwards 306 Auto thermal evaporator) using pieces from 99.99% gold coin and chromium-plated tungsten rods as Au and Cr metal sources, respectively. For co-planar microelectrode arrays, 8.0 nm Cr and 80.0 nm Au were deposited. The deposition rate for both metals was controlled to be 0.2 – 0.4 nm/s. This bimetallic layer was then patterned by standard photolithography procedures using either of the two "metal layer" masks. The adhesion promoter, hexamethyldisilazane (HMDS), was applied onto the dehydrated wafer by spin coating at 2500 rpm for 30 s. The positive photoresist S1805 was then applied by spin coating at 6000 rpm for 30 s to get a thickness of 0.5 µm. The wafer with the S1805 coating was baked at 115 °C for 90 s and 45 °C for 30 s before exposure. Exposure dose was calculated using the constant (35 mJ/µm $cm^2$) multiplied by the photoresist thickness (0.5 µm). The metal layers were then etched by gold and chromium wet etches. A 0.5 µm thick layer of SU-8 (SU-8 2000.5) was applied by spin coating at 2500 rpm for 30 s and patterned by exposure through the "insulation layer" mask to expose the active electrode areas and contact pads. An oxygen plasma was used to clean the residual organics from the surface using the RIE instrument (PlasmaTherm SLR 720 Reactive Ion Etch) with a 117 sccm gas flow and 150 W for 1 min. Finally, to release the fabricated devices, the unexposed part of the thick SU-8 layer was developed by SU-8 developer and individual devices could be released by etching the Al sacrificial layer away with 0.6 M NaOH. The carrier wafer could then be cleaned and reused for other processes.

Optimization of parameters for the dehydration process, exposure and wet etching, are discussed in the Results and Discussions section.

The fabrication process for the edge microelectrode arrays is similar to that of the co-planar microelectrode arrays probes. To obtain the vertical edge array from multiple metal layers, the Cr, Au deposition, the thin SU-8 layer deposition, and patterning process of the metal layer and thin SU-8 layer were repeated multiple times, with 10.0 nm Cr, 250.0 nm Au from each deposition and photolithography of the thick SU-8 layer using “substrate layer” mask or simple blank exposure. This process is intended to produce multiple stacked metal layer-substrate layers (up to 8). However, due to problems occurring during the fabrication process, a maximum of two metal layers was produced. As is proposed, upon successful production of multiple metal-insulation layers, RIE is intended to be used to expose the contact pads because it has some selectivity of organic substrate over metal substrate.[9] The electrode width and gap depends on the thickness of Au layer and insulation layer, respectively, which is less than 1 μm.

**5.4 Results and Discussion**

There are several challenges in the process of producing both types of probes by following the proposed microfabrication procedure shown in Figure 5.4 and Figure 5.5. Efforts have been made toward solving the problems that occurred and optimizing the parameters used in the steps. The major problem lies in the thick SU-8 process that causes difficulties in resolving the small features of metal layer on top of it. It is also unstableness in that it bends and cracks during the fabrication process.

For step 2 shown in Figure 5.4 and Figure 5.5, different exposure and baking parameters for the thick SU-8 layer have been evaluated. It has been reported that SU-8 devices show negative (toward the substrate) or positive out-of-plane curvature depending on the exposure dose, baking temperature, and baking time.[10] Curved devices will not fit well into an edge connector, create problems for precise insertion in tissue, and cause poor adhesion to a carrier wafer during fabrication. Among the parameters tested, a total exposure dose of 240 mJ/cm$^2$, pre-exposure bake at 65°C for 5 min, at 95 °C for 12 min and post-exposure bake at 65 °C for 1 min, at 95 °C for 3 min, without the curing process produced the best results so far with less bending of released devices or cracking of blanket-exposed SU-8 substrate layer.

When the “substrate layer” mask was used in step 2 for both procedures, the metal layer deposited (step 3 in both procedures shown in Figure 5.4 and Figure 5.5) on the un-exposed thick layer of SU-8 forms

an uneven surface with wrinkles. This is caused by the soft un-exposed SU-8 that can expand during deposition and shrink in the vacuum environment evaporation. This uneven surface makes it hard to pattern the metal layer (step 5 for both procedures) with small features, because it interferes with the mask making a uniform contact with the surface. Details will be discussed later in this section. An alternative approach of blanket exposing the entire thick SU-8 layer has been tried. In this way, deposition of a smooth Cr/Au layer coated on the hard, exposed surface of SU-8 was possible. The drawback of this alternative approach is that the probe shape cannot be defined by photolithography, so that a more complicated process would be needed. Different methods, including solvent removal and chemical removal of thick SU-8 layers have been reported previously. RIE is only good for removal of thin SU-8 films.[11] To reduce the thickness of exposed SU-8 that would need to be removed, a 2-step exposure for the substrate layer was used so that the area to be removed was not crosslinked throughout the entire thickness. With this approach, the thick SU-8 layer was exposed with a dose of 180 mJ/cm$^2$ using the substrate mask and a second, blanket exposure was performed with dose of 60 mJ/cm$^2$ without the mask.

The dehydration temperature and time before applying the HMDS (in step 4 of both procedures) and the second, thin SU-8 layer (in step 8 of both procedures) were optimized. Normally, baking at a relatively high temperature (≥ 200 °C) for a long time (10 min) is used to make sure the wafer is completely dehydrated. However, at this high temperature, exposed SU-8 layer is not stable and peels off the carrier wafer or forms cracks, especially when covered with metal layers. The dehydration temperature and time also affect the un-exposed SU-8 substrate layer. After a long baking time at a high temperature, it takes a longer time for the un-exposed SU-8 to develop, and it might not even develop at all. Among the parameters that were tried, the dehydration by baking on a hot plate of 115 °C for 90 s worked well and showed no difference to results obtained without the thick SU-8 layer underneath.

During the photo-patterning step of the metal layers (step 5 for both procedures), the larger electrodes (the lateral dimensions for the edge microelectrode arrays, ≥ 10 µm) are less sensitive to variation in exposure and developing parameters. The 4-µm features did not resolve under the same conditions as those used with the plain silicon substrate alone. Features on some areas of the wafer were more resolved than others. As shown in Figure 5.6, at the probe tip where a rough gold surface surrounds it, small features with 4 µm sizes are not completely resolved (Figure 5.6 A and B), compared to the well-

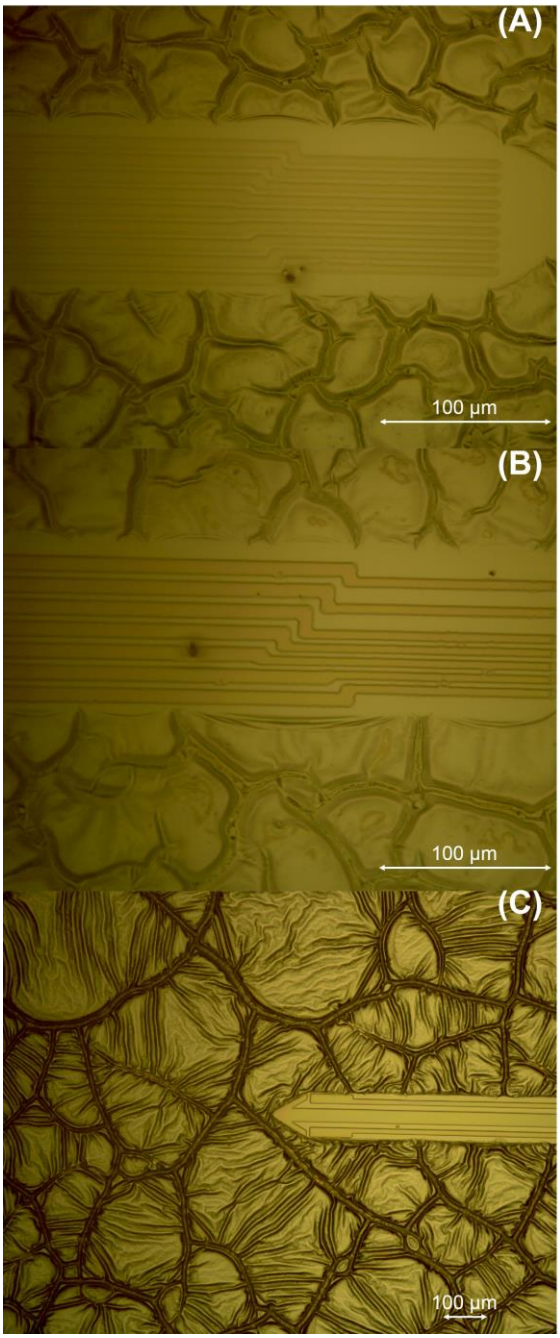


**Figure 5.6** Microscope images showing the probe tip area with patterned positive photoresist on a Cr/Au layer that had been deposited onto the patterned thick SU-8 substrate layer. Images were taken for probes on the same wafer under the same fabrication conditions. Electrode arrays with 4 µm band widths and 4 µm gaps on a planar probe (A) and (B) are not clearly defined, while features of the edge microelectrode array design (C) are resolved with clean edges.

defined bigger features (≥ 10 μm) on the edge microelectrode arrays probe produced using the same parameters on the same wafer (Figure 5.6 C). This is probably caused by the non-uniform positive photoresist coverage and therefore poor contact of the mask with the wafer during exposure.

On a smooth surface produced through the alternate exposure approach (blanket exposure of SU-8 substrate over the entire wafer in step 2), the exposure time used to produce similar results may vary by a factor of two. Another positive photoresist, AZ 4110 (AZ Electronic Materials, Somerville, NJ), which has a larger exposure constant, has also been tried. Results are similar to that of using S1805. This indicates that reproducibly resolving the sub 10 μm features on this substrate is difficult.

The wet etching process could also be problematic. Results showed that Cr and Au deposited on un-exposed SU-8 surface is more difficult to etch away. Experience has shown that it takes up to several minutes to completely etch the Au on un-exposed SU-8, during which electrode features on the probe tip will be over-etched. On a smooth surface (when the entire substrate layer is UV-exposed), a 15 s gold etch and a 5 s chromium etch are used to etch off a 80.0 nm-thick Au layer and a 8.0 nm-thick Cr layer, respectively, while a 45 s gold etch and a 15 s chromium etch are used for a 250.0 nm thick Au layer and a 10.0 nm thick Cr layer.

The device-releasing process has been tested for different types of substrates. The Al sacrificial layer can be easily etched by soaking in 0.6 M NaOH solution overnight. The released SU-8 substrate alone, SU-8 substrate covered with Cr and Au, and SU-8 substrate with a patterned metal layer are shown in Figure 5.7. Clear edges were obtained for the SU-8 substrate alone and SU-8 substrate covered with Cr and Au. Rough edges around the probe tip were obtained for the SU-8 substrate that had been processed through metal patterning step (steps 4 to 7 in both procedures). This indicates that un-exposed SU-8 near probe tip has become insoluble in SU-8 developer during the metal patterning step.

**5.5 Conclusions and Future Work**

Two types of neural probes, co-planar lateral microband arrays and vertical edge arrays, have been designed for future applications of redox cycling with dimensions and substrate material suitable for in vivo neurotransmitter detection. A special arrangement of the two types of probes was made on the photo mask design so that by rotating the mask, multiple layers of electrodes can be made during the fabrication of the edge microband array probe with a minimum set of four masks. SU-8 was used as the substrate material

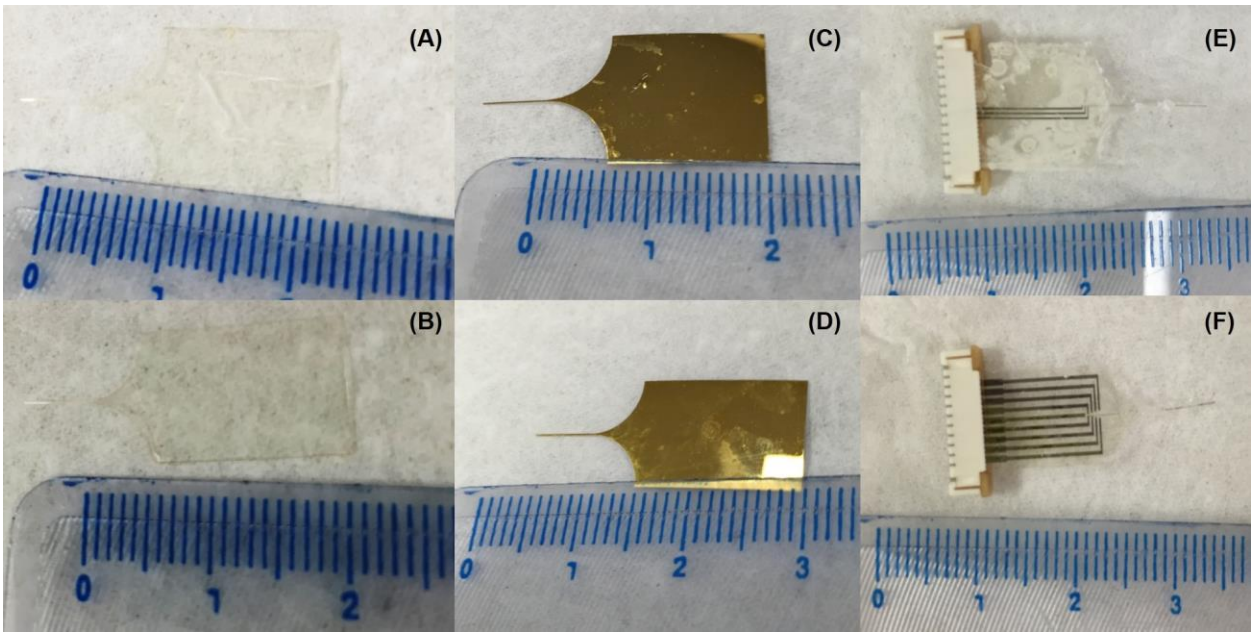


**Figure 5.7** Probe-shaped devices released from the carrier wafer: (A) and (B) SU-8 substrate alone; (C) and (D) SU-8 substrate covered with Cr and Au, and (E) and (F) SU-8 substrate with patterned metal layer inserted in ZIF edge connectors. Devices in (A), (C), (E) were made from the edge microelectrode array probe design and devices in (B), (D), (F) were made from the co-planar microelectrode array probe design. Note that electrode array on probe tip in (E) and (F) were not completely resolved.

and different microfabrication procedures were designed for the two types of probes. However, problems during the fabrication process and production of the two types of probes could not be completely overcome. Further modification and optimization of the fabrication procedure are needed.

One option is to replace the SU-8 with other polymer materials such as polyimide and BCB. As a negative photoresist like SU-8, BCB can be processed in a similar way as the SU-8, except that the thickness range is narrower. One way to overcome this problem for the substrate is to stack multiple layers of BCB to achieve the desired thickness, but the adhesion between layers and the stability of the whole substrate will need to be considered. Polyimide ~~cannot~~ be patterned by photolithography, but with the help from a sacrificial layer on top, it can be patterned by etching techniques such as RIE. For all the polymer substrates, the problems that occurred with SU-8 could still be problematic. The devices reported in the literature that used these other polymers do not have electrode features as small as those described here,[2, 8] and thus, the difficulties in resolving the small electrode features would not have been encountered.

Another option is to use a silicon substrate. As a solid substrate, the problem of an uneven surface after metal deposition will not occur. However, the use of ultra-thin silicon wafers or a wafer thinning process must be implemented. Due to the fact that the ultra-thin silicon wafers are difficult to handle and easy to break during fabrication process, the wafer-thinning procedure is preferred. DRIE can be used to thin wafers from the back side after the features has been made and also can be used to create the shape of the probe using a sacrificial layer created by the “substrate layer” mask.[12] Test runs of fabrication of co-planar microelectrode arrays probes using a standard photolithography procedure and edge microelectrode arrays using modified procedures designed here and simply stacking metal layers and thin SU-8 layers on top of silicon wafer have been performed. Results showed that wrinkles created by un-exposed thin SU-8 layers were much smaller than for the thick SU-8 layer and did not significantly affect the patterning step of the metal layer.

Other than the fabrication of neural probes, surface mounting of ZIF edge connectors to a printed circuit board (PCB) need to be performed to produce usable connecting parts. Fabricated neural probes will need to be characterized in vitro to determine their electrochemical performance. This system will also need to be tested for dopamine detection in vitro and then applied in vivo.

### 5.6 Acknowledgement

Research was supported partially through the National Science Foundation (CBET-1336853) and the Arkansas Biosciences Institute, the major research component of the Arkansas Tobacco Settlement Proceeds Act of 2000. We thank Errol Porter and Mike Glover for advice on microfabrication and AutoCAD design. The use of the High Density Electronics Center microfabrication facilities is also acknowledged. We express our appreciation to Professor Adrian Michael at the University of Pittsburgh and Dr. David Paul for insightful discussions on neural probe design and applications.

**5.7 References**

(1) Fekete, Z. *Sensors Actuators B: Chem.* **2015**, *215*, 300-315.

(2) Altuna, A.; Gabriel, G.; de la Prida, Liset Menéndez; Tijero, M.; Guimerá, A.; Berganzo, J.; Salido, R.; Villa, R.; Fernández, L. J. *J Micromech Microengineering.* **2010**, *20*, 064014.

(3) Cheung, K. C. **2007**, *9*, 923-938.

(4) Aggarwal, A. *Studies Toward the Development of a Microelectrode Array for Detection of Dopamine through Redox Cycling,* Ph.D ed.; University of Arkansas:Fayetteville, AR; 2011.

(5) Hetke, J. F.; Anderson, D. J.; Wise, K. D. **1997**, *18*, 266-267.

(6) Wassum, K. M.; Tolosa, V. M.; Wang, J.; Walker, E.; Monbouquette, H. G.; Maidment, N. T. **2008**, *8*, 5023-5036.

(7) Norlin, P.; Kindlundh, M.; Mouroux, A.; Yoshida, K.; Hofmann, U. G. **2002**, *12*, 414-419.

(8) Cheung, K. C.; Renaud, P.; Tanila, H.; Djupsund, K. **2007**, *22*, 1783-1790.

(9) Henry, C. S.; Fritsch, I. *J.Electrochem.Soc.* **1999**, *146*, 3367-3373.

(10) Sameoto, D.; Tsang, S.; Foulds, I.; Lee, S.; Parameswaran, M. *J Micromech Microengineering.* **2007**, *17*, 1093.

(11) Dentinger, P. M.; Clift, W. M.; Goods, S. H. *Microelectronic Engineering.* **2002**, *61*, 993-1000.

(12) Norlin, P.; Kindlundh, M.; Mouroux, A.; Yoshida, K.; Hofmann, U. G. *J Micromech Microengineering.* **2002**, *12*, 414.

# 6. Electrochemical Characterization of Silver-Containing Nanoparticles

## 6.1 Abstract

Nanoparticles bridge the gap in size between atoms and bulk materials, exhibiting unique physical, photonic, electronic, magnetic, and mass transport properties. They have generated tremendous interest for applications including enhanced materials, catalysis of chemical reactions, and new opportunities in medicine. Electrodes modified with nanoparticles have been used for electrochemical catalysis and sensing, where they play an important role in transduction between chemical interactions and electronic ones at the electrode-solution interface. To better understand this process at a fundamental level, electrochemical characterization of silver (Ag) containing nanoparticles (including Ag nanocubes, Ag nanocuboctahedrons, gold nanocages (derived from silver nanocubes), and Ag nanospheres) modified on electrode surface has been investigated. Anodic stripping voltammetry was used to study the characteristics of nanoparticles directly drop casted and embedded in Nafion polymer films on commercially available glassy cabon as well as Pt disk electrodes. Stripping peaks of silver were observed for all nanoparticles studied with different stripping peak potentials that depend on the surrounding electrolyte composition and type of nanoparticles. However, the reproducibility of the stripping voltammogram of the -nanoparticles modified on electrode surface remains to be a problem due to multiple factors. For example, simple drop casting does not provide a reproducible nanoparticle distribution over the electrode surface, and thus translating to the variability in the stripping voltammogram from experiment-to-experiment. Thus, caution in general should be taken in interpreting results in the literature for nanoparticle-electrochemical systems prepared in this way. Suggestions for improving procedures for electrochemical characterization of nanoparticles in the future are offered.

## 6.2 Introduction

With the long-term goal of developing electrochemical methodologies for neuroscience applications, efforts have been made in our laboratory toward detection of other neurologically-important species that do not undergo direct electron transfer at an electrode, such as glutamate, in addition to the electroactive catecholamines. We have initiated studies to combine nanoparticles for this purpose. For example, our laboratory began investigations that immobilize L-glutamate oxidase conjugated Au nanocages (Au NCs) within a matrix of PEDOT onto electrodes surface, and use the modified electrodes for L-glutamate detection, as part of collaboration with the nanoparticle expertise of Jingyi Chen's laboratory at the University of Arkansas. Upon using cyclic voltammetry (CV) to characterize the electrodes with each modification step, unique anodic stripping peaks were noted and traced to the presence of the Au NCs. Although at first this observation was surprising, an evaluation of the synthetic history of the Au NCs provided the reason for this result. The unique stripping peaks could be attributed to residual silver remaining after the galvanic replacement process of the precursor silver nanocubes (Ag NCs).[1] To test this hypothesis and to determine whether this was evidence for an opportunity to develop a method for facile electrochemical characterization of nanoparticles in general, anodic stripping voltammetry was investigated of silver-containing nanoparticles and nanocomposites that modify an electrode surface.

### 6.2.1 Electrode Surfaces Modified with Nanoparticles

Nanoparticles have unique chemical and physical properties because of their small size (less than 100 nm), and their applications in various fields, such as sensors[2] and fuel cells[3] have been explored. Nanoparticles with different compositions, sizes and shapes have been used for electrode modification and provide different functions such as catalysis of electrochemical reactions, act as the bridge for electron transfer between electrode surfaces and biomolecules (e.g. enzymes, proteins), and high surface to volume ratio.[4]

Among nanoparticles with different compositions, metal nanoparticles exhibit advantages in their excellent conductivity and catalytic properties. When modifying electrode surfaces, they act as "electronic wires" to provide direct electron transfer between redox proteins and the bulk electrode surface, and as catalysts for electrochemical reactions.[4, 5] Noble metal nanoparticles (mainly gold, silver, platinum, palladium, ruthenium and their alloys) have been explored extensively for electrochemical biosensing.[6]

Simultaneous detection of electrochemical active neurotransmitters at gold nanoparticle-modified electrodes has been reported before.[7-9] Electrodes coated with enzyme immobilized nanoparticles have been developed for detection of neurotransmitters that do not undergo direct electron transfer at an electrode, such as glucose and glutamate.[10]

Different methods have been used to modify electrode surfaces with nanoparticles. They can be grown in situ on the surface by chemical reduction from solution[11] or by electrochemical deposition.[12, 13] Deposition methods of nanoparticles post synthesis have also been used. One simple and widely used way is to drop cast nanoparticles from solution on the electrode surface.[14] Self-assembling of monolayers is another approach and provides modification with a relatively good control of thickness and composition. Another frequently used method is the co-modification of nanoparticles and biomolecules with a polymer matrix, which can facilitate electron transfer between the biomolecule active sites and the electrode.[5, 6, 10]

### 6.2.2 Characterization Methods for Electrode Surfaces Modified with Nanoparticles

Nanoparticles that are electrochemically-active may interfere with the target electrochemistry. Also, the modification process may lead to different surface morphologies of the modified electrode surface. However, the characterization of electrodes modified with nanoparticles found in the literature is quite limited. Normally, microscopic methods such as transmission electron microscopy, scanning electron microscopy (SEM), and atomic force microscopy are used to study the morphology of the modified electrode surface.[12] X-ray photoelectron spectroscopy has also been used to provide chemical compositions of nanoparticles.[11] Also, electrochemical characterization has been established for nanoparticles with electrochemical active compositions (e.g. Au, Ag).[12, 13]

Ag nanoparticles have been previously characterized by others using electrochemical stripping.[15, 16] A size-dependent electrochemical oxidation of the metal nanoparticles was reported. A reason for this behavior has been attributed to a change in surface free energy, as predicted by Plieth.[17] Another explanation is that there is a change in the patterns diffusion layer around the particles caused by the difference in the surface coverage of nanoparticles amount, as offered by Compton's group, in their study of Ag NPs in seawater by examining the impact of nanoparticles with electrodes.[15] As predicted by theory and supported by experimental data, there is a negative shift in the anodic stripping (oxidation of silver) potential with a decrease in radius for small nanoparticles (with radius below 30 nm). Thus, it appears to

be possible to discriminate between Ag nanoparticles of different sizes by the difference in the anodic stripping potential.

The electrochemical characterization of nanoparticles with other shapes such as cubes and cages has not been reported before. Because of the nature of the synthetic processes, nanoparticles usually are not perfectly spherical and can have a relatively wide distribution of size. On the other hand, cubes are better controlled during synthesis and have a more regular shape and crystal structure. Here, anodic stripping voltammetry is used to characterize Ag nanocubes (Ag Cs), Ag nanocuboctahedrons (Ag CTs) and Au NCs. Ag nanospheres (Ag NPs) is also examined as a comparison to existing literature.[15] Two methods of nanoparticle modification (drop casting, with and without coverage of Nafion film) were investigated.

## 6.3 Experimental

### 6.3.1 Chemicals and Materials

Potassium ferricyanide (EM Science, Gibbstown, NJ, USA), KCl (BDH, Radnor, PA, USA), $NaNO_3$ (AMRESCO, LLC, Solon, OH), and $KNO_3$ (Mallinckrodt Baker, Inc, Phillipsburg, NJ) were used as received. Nafion® perfluorinated ion-exchange resin (5 wt. % in mixture of lower aliphatic alcohols and water, contains 45% water) was obtained from Sigma-Aldrich (Saint Louis, MO) and diluted with deionized water before use. Water (ACS reagent grade, 18 MΩ cm or greater) was obtained from Ricca Chemical (Arlington, TX, USA).

Commercially-available disk electrodes (3 mm diameter GCE obtained from Bioanalytical Systems, Inc (Lafayette, IN) and 1.6 mm diameter Pt obtained from CH Instruments (Austin, TX)) were used for nanoparticle modification and anodic stripping experiments. Materials used for all disk electrode polishing including Nylon PSA polishing pads, 1 µm polycrystalline diamond suspension, microcloth PSA polishing pads and 0.05 µm alumina suspension were obtained from Buehler, Lake Bluff, IL. All anodic stripping experiments were performed with a bipotentiostat (CHI 750A, CH Instruments, Austin, TX), equipped with a Faraday cage and a picoamp booster. SEM images were obtained by a Philips XL30 ESEM in the Arkansas Nano & Bio Materials Characterization Facility at the University of Arkansas.

All of the nanoparticles used in this study were obtained from Jingyi Chen's laboratory (synthesized by Eric Taylor and Dr. Jingyi Chen).[1] In general, Ag Cs were were prepared by polyol reduction. PVP was

used as the capping ligand. The as-synthesized Ag Cs were then allowed to react with HCl to induce corner truncation and produce Ag CTs. The same Ag Cs were also used as templates to prepare Au NCs using galvanic replacement reaction with $HAuCl_4$. During this process, Au grows on the surface of the Ag Cs and adopts its morphology, forming a hollowed structure. The resulting Ag and Au nanoparticles were washed with acetone and ethanol several times and finally re-dispersed in deionized water for further use. PVP was used as a capping ligand for all the three types of nanoparticles. Citrate-capped Ag NP were also made to use for comparison to results by Toh et al.[15]

### 6.3.2 Deposition and Characterization of Nanoparticles on Electrode Surface

Electrodes were polished and characterized in a solution containing 1.0 mM potassium ferricyanide and 0.100 M KCl by cyclic voltammetry (CV) before nanoparticles were deposited. After use for nanoparticle modification, electrodes are cleaned by soaking in acid solution and polishing. To modify the electrode, 3 µl (or 2 µl for the 1.6 mm diameter Pt electrode) of the aqueous nanoparticle solution was dropped onto the electrode and air-dried for 1 h at room temperature. In some cases, this step was followed by covering with a 1% wt. Nafion solution (3 µl on GCE and 2 µl on Pt disk) and air-drying for several hours until dried.

The modified electrodes were characterized in 0.1 M electrolyte by three segments of CV in electrolyte containing $Cl^-$ or $NO_3^-$ to study the relationship between anodic stripping of the silver and different nanoparticle morphologies. In general, the modified disk electrode was scanned at 0.050 V/s or 0.100 V/s, anodically from 0.000 V to 1.000 V in the first segment, then cathodically to -0.200 V in the second segment, and then anodically again back to 1.000 V in the third segment, unless otherwise stated. A Ag/AgCl (saturated KCl) reference electrode and a Pt flag auxiliary electrode were used for all electrochemical experiments.

SEM was used to take a closer look at the deposited nanoparticles. Pt foil electrodes, instead of the commercially-available ones, were used to accommodate the restricted stage of the SEM instrument. The Pt foils were modified with the nanoparticles under similar conditions. For the same type of nanoparticles, two sample spots were made on different locations of the Pt foil: one of them had been through the electrochemical characterization process and the other one was just as prepared.

## 6.4 Results and Discussion

### 6.4.1 Anodic Stripping of Drop-Casted Nanoparticles

The effects of the electrolytes 0.1 M KCl and 0.1 M $KNO_3$ on anodic stripping voltammetry of nanoparticles (Au NCs, Ag Cs and Ag CTs) that had been drop-casted on a 1.6 mm diameter Pt electrode were investigated. The modified electrodes were swept from 0.000 V to 0.800 V in the first segment of the voltammetry, then to - 0.2 V during the second segment, and back to 0.8 V in the third segment at 0.100 V/s. The voltammograms are shown in Figure 6.1. The peak potentials of the anodic sweeps, the first segment (solid lines) and the third segment (dashed lines), are listed in Table 6.1. More positive peak potentials were observed in the electrolyte containing $NO_3^-$ than in that containing $Cl^-$ for all silver nanoparticles, expect for the first sweep of the Au NCs. Peak potentials in the third sweep are different from those in the first sweep, because the $Ag^+$ generated during the first can be redeposited during the second and change the morphology at the electrode surfaces. This phenomenon of peak shift between different electrolytes can be explained by the fact that $Cl^-$ helps to stabilize $Ag^+$ by forming AgCl precipitate. The concentration of $Ag^+$ in solution decreases, thus lowering the energy of oxidation of Ag and causes a negative shift of the peak potential.[18] To eliminate this effect, anodic stripping in nitrate-containing electrolyte was used for subsequent studies. Also, small reduction spikes between 0 and -0.2 V were observed on both cathodic and anodic segments in some of the stripping voltammograms, mostly in $Cl^-$ containing electrolytes. This can be attributed to the presence of extra ligand on nanoparticles surface, or reduction of $Ag^+$ in local environment.

Factors such as size, shape (cube vs. cuboctahedron), and surface coverage were analyzed. However, due to reproducibility problems, clear conclusions cannot be drawn. Three replicates of stripping voltammograms for each type of nanoparticle with similar total silver content (17 µg for Ag Cs and Ag CTs) are shown in Figure 6.2. Peak potentials of the first sweep (solid lines) and the third sweep (dashed lines) are listed in Table 6.2. Different types of nanoparticles showed different potentials of the anodic stripping peaks in the first sweep (solid line), but they also differ within the three replicates of their own type. This makes it difficult to conclude if the shifts in peak potential are significant for the different types of nanoparticles or due to the difference in nanoparticle size and/or shape. Also, broader peaks for Ag NP indicate the wide size distribution and possible particle aggregation.

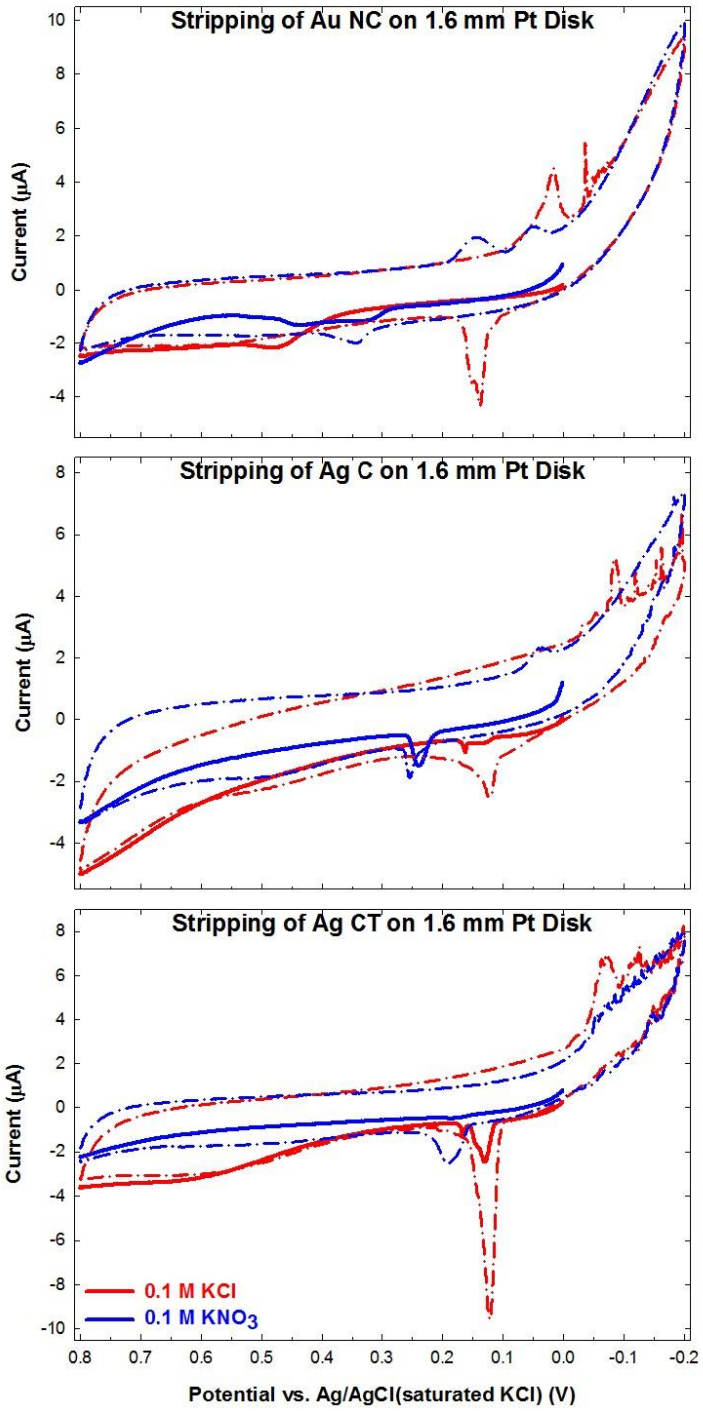


**Figure 6.1** Overlay of voltammograms obtained in 0.1 M KCl (red) and 0.1 M $KNO_3$ (blue) of nanoparticles drop casted on a 1.6 mm diameter Pt electrode surface. The modified electrodes were swept at 0.1 V/s from 0 V to 0.8 V in the first segment (solid curves), then to -0.2 V in the second segment (dashed curves), and finally to 0.8 V in the third segment (dashed curves), vs Ag/AgCl (saturated KCl). The nanoparticles were (a) Au NCs, (b) Ag Cs, and (c) Ag CTs

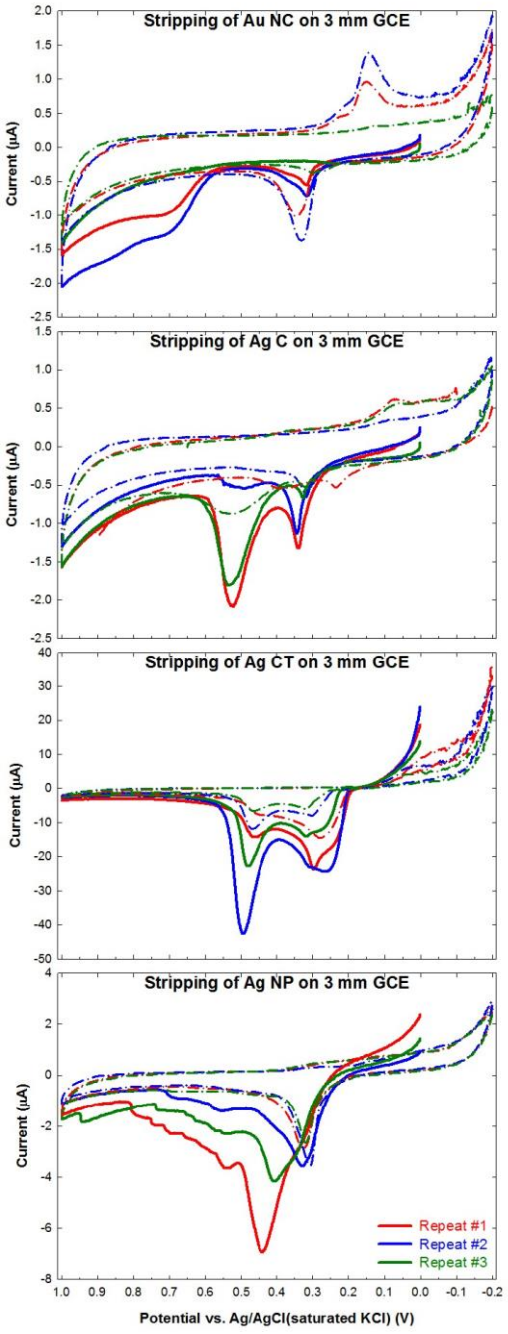


**Figure 6.2** Overlay of three replicates of voltammograms obtained in 0.1 M $NaNO_3$ of nanoparticles drop-casted on a 1.6 mm diameter Pt electrode surface. The modified electrodes were swept at 0.050 V/s from 0 V to 1.0 V in the first segment (solid curves), to -0.2 V in the second segment (dashed curves), and to 1.0 V in the third segment (dashed curves) vs Ag/AgCl (saturated KCl). The nanoparticles were: (a) Au NCs; (b) Ag Cs; (c) Ag CTs; (d) Ag NP

**Table 6.1 Stripping potentials obtained from the first and third sweeps in the anodic stripping voltammograms of nanoparticles in $Cl^-$ and $NO_3^-$ containing electrolytes shown in Figure 6.1.**

| Potential /V | Au NCs | Ag Cs | Ag CTs |
|---|---|---|---|
| KCl (1st segment) | 0.477 | 0.125; 0.162 | 0.129; 0.165 |
| $KNO_3$ (1st segment) | 0.330; 0.439 | 0.240 | 0.176 |
| KCl (3rd segment) | 0.138; 0.151 | 0.123 | 0.122 |
| $KNO_3$ (3rd segment) | 0.344 | 0.254 | 0.189 |

**Table 6.2 Stripping potentials obtained from the first and third sweeps in the anodic stripping voltammograms of nanoparticles shown in Figure 6.1.**

| Potential /V | Au NCs | Ag Cs | Ag CTs | Ag NPs |
|---|---|---|---|---|
| **#1 (1st segment)** | 0.317; 0.701 | 0.343; 0.490 | 0.261; 0.495 | 0.328 |
| **#2 (1st segment)** | 0.317; 0.688 | 0.327; 0.535 | 0.318; 0.480 | 0.407 |
| **#3 (1st segment)** | 0.247 | 0.339; 0.522 | 0.296; 0.466 | 0.440 |
| **#1 (1st segment)** | 0.346 | 0.317 | 0.301; 0.468 | 0.307 |
| **#2 (1st segment)** | 0.330 | 0.309; 0.522 | 0.318; 0.466 | 0.319 |
| **#3 (1st segment)** | 0.298 | 0.336; 0.490 | 0.279; 0.454 | 0.325 |

SEM images of the centers and edges of electrodes on which nanoparticles (Ag Cs and Ag CTs) had been drop casted and subsequently stripped on Pt foil are shown in Figure 6.3. As shown in these images, the drop-casted nanoparticles were not evenly distributed. Instead, a “coffee stain” effect was observed with more dispersed individual particles in the center of the electrode and stacked particles on the edges. In the center of the foil, no apparent changes in particle shape were observed between the images taken before and after stripping. At the edges of the electrode, where the particles were aggregated and stacked, the images of both types of particles on the edges after stripping showed a significant difference in their shapes–the particles had fused together after stripping. The nanoparticles are not completely stripped off after one and half cycles.

### 6.4.2 Anodic Stripping of Nanoparticles Embedded in Polymer

One of the standard methods of modifying electrodes with nanoparticles is to cover the drop-casted nanoparticle layer with a film of Nafion to prevent the particles from coming off the electrode.[12] Comparisons of voltammetry of drop-casted nanoparticles with and without the Nafion coating were performed. With the Nafion coating, the stripping peak shifted and became broader (Figure 6.4, blue curves). This suggests that the Nafion coating changes the interaction between nanoparticles and the surrounding solution, as would be expected. The film decreases the diffusion rate of $Ag^+$ into the surrounding solution (ions have to go through an anion-repelling film), stabilizes the cation, increases its local concentration, and lead to a positive shift of the peak potential.

## 6.5 Conclusions

Electrochemical characterization of four different types of silver-containing nanoparticles was performed by anodic stripping voltammetry. These include PVP-capped nanoparticles of Ag Cs, Ag CTs, and Au NCs and citrate-capped Ag NPs. Two types of electrode-modification methods were investigated: simple drop-casting and embedding in Nafion polymer. Stripping peaks of silver were observed for all the nanoparticles and with different peak potentials. The peaks for Au NCs indicate the presence of silver remaining on the particles after the synthesis procedure. Thus, the anodic stripping has served a valuable purpose in understanding the Au NCs composition.

The different stripping potentials obtained from replicates of experiments using the same conditions indicate that obtaining reproducible electrode modification by nanoparticles is challenging. This highlights

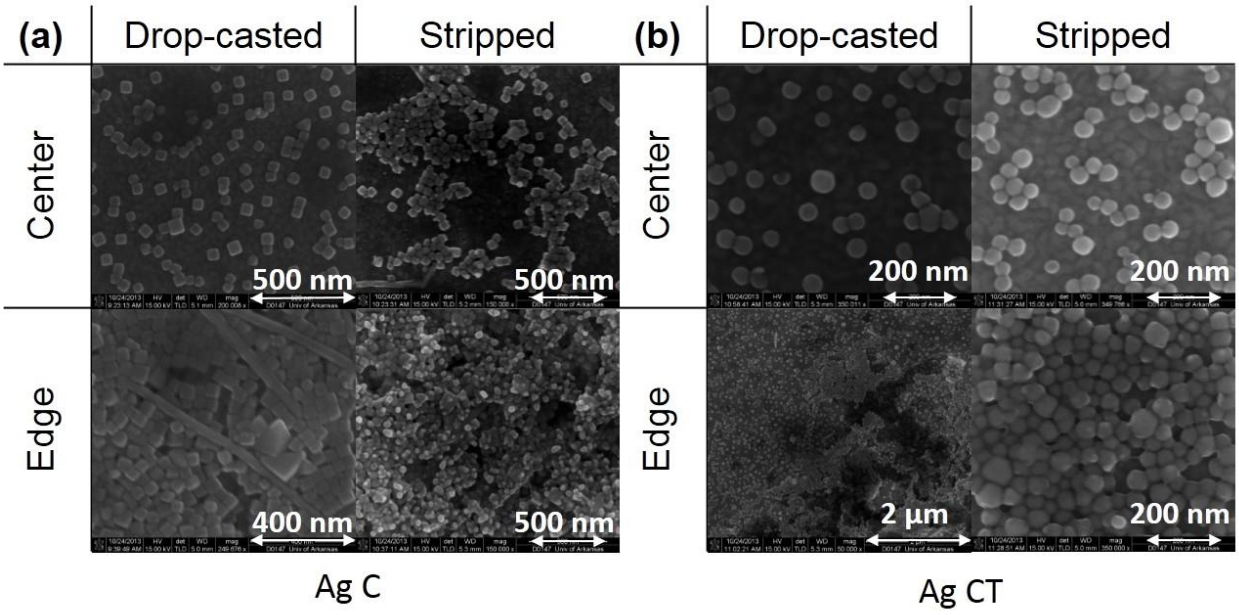


**Figure 6.3** SEM images of the center and edge locations on the Pt foil electrode on which nanoparticles had been drop-casted, both before and after stripping voltammetry, where the nanoparticles were (a) Ag Cs, and (b) Ag CTs

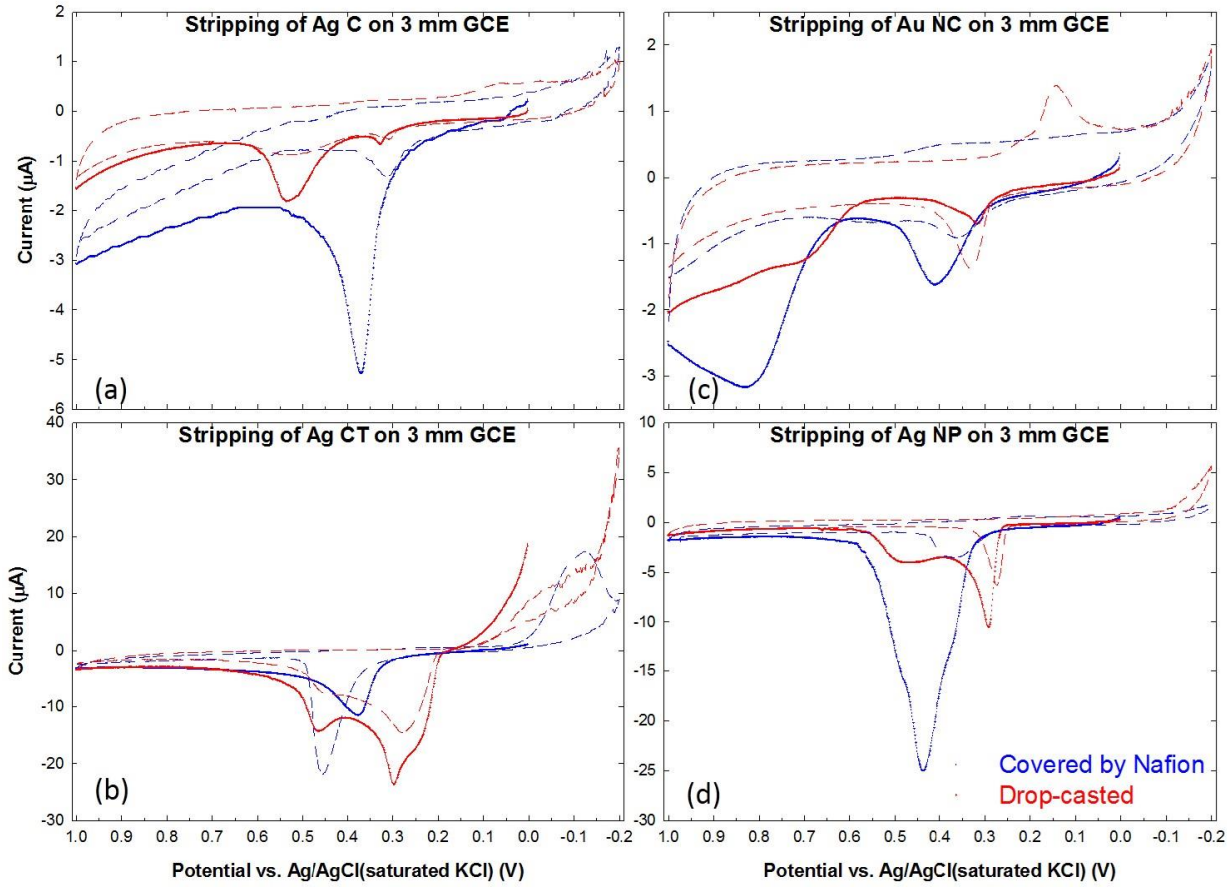


**Figure 6.4** Anodic stripping voltammogram of nanoparticles drop casted on electrode surface with (blue) and without (red) Nafion coverage in surface in 0.1 M $NaNO_3$. The modified electrodes were swept from 0 V → 1.0 V → -0.2 V → 1.0 V at 0.05 V/s vs a Ag/AgCl (saturated KCl) reference electrode. The first sweep in each voltammogram is label as solid lines and the following segments are shown in dashed lines: (a) Ag Cs; (b) Ag CTs; (c) Au NCs; (d) Ag NP

the importance of several factors in using an electrochemical approach for screening and characterization. These include the nature of how the nanoparticles are interfaced with the electrode surface and the homogeneity of that interface, the size distribution, the variation of the original properties, ligand type, and extent of washing. Future work will involve fundamental studies that gain better control over the many factors of nanoparticle solutions so that a more distinctive correlation between shape, size, and surface coverage can be made with the anodic stripping peak potentials, shapes, and magnitudes. Electrochemical investigation of the nanoparticles themselves will be expanded to include direct detection of nanoparticles from solution via impact at the electrode/solution interface at microelectrodes, where uniform deposition onto an electrode is not an issue, and which has been reported with success for other kinds of nanoparticles.[18, 19]

**6.6 Acknowledgements**

This work was supported in part by the Ralph E. Powe Jr. Faculty Enhancement Award and startup funds from the University of Arkansas to J.C. Support has also been provided in part by the Arkansas Biosciences Institute, the major research component of the Arkansas Tobacco Settlement Proceeds Act of 2000. The authors greatly appreciate the help from Dr. Mourad Benamara and the use of the Arkansas Nano & Bio Materials Characterization Facility for the SEM studies

**6.7 References**

(1) Chen, J.; McLellan, J. M.; Siekkinen, A.; Xiong, Y.; Li, Z.; Xia, Y. *J.Am.Chem.Soc.* **2006**, *128*, 14776-14777.

(2) Saha, K.; Agasti, S. S.; Kim, C.; Li, X.; Rotello, V. M. **2012**, *112*, 2739-2779.

(3) Rabis, A.; Rodriguez, P.; Schmidt, T. J. *Acs Catalysis.* **2012**, *2*, 864-890.

(4) Luo, X.; Morrin, A.; Killard, A. J.; Smyth, M. R. **2006**, *18*, 319-326.

(5) Pingarron, J. M.; Yanez-Sedeno, P.; Gonzalez-Cortes, A. **2008**, *53*, 5848-5866.

(6) Wang, J. *Microchimica Acta.* **2012**, *177*, 245-270.

(7) Goyal, R. N.; Gupta, V. K.; Oyama, M.; Bachheti, N. *Talanta.* **2007**, *72*, 976-983.

(8) Mathiyarasu, J.; Senthilkumar, S.; Phani, K. L. N.; Yegnaraman, V. **2007**, *7*, 2206-2210.

(9) Zhang, Y.; Ren, W.; Zhang, S. *Int J Electrochem Sci.* **2013**, *8*, 6839-6850.

(10) Putzbach, W.; Ronkainen, N. J. *Sensors.* **2013**, *13*, 4811-4840.

(11) Thanh, T. D.; Balamurugan, J.; Hwang, J. Y.; Kim, N. H.; Lee, J. H. *Carbon.* **2016**, *98*, 90-98.

(12) Welch, C. M.; Compton, R. G. *Analytical and bioanalytical chemistry.* **2006**, *384*, 601-619.

(13) Rad, A. S.; Mirabi, A.; Binaian, E.; Tayebi, H. *Int J Electrochem Sci.* **2011**, *6*, 3671-3683.

(14) Serafín, V.; Agüí, L.; Yáñez-Sedeño, P.; Pingarrón, J. *J Electroanal Chem.* **2011**, *656*, 152-158.

(15) Toh, H. S.; Batchelor-McAuley, C.; Tschulik, K.; Uhlemann, M.; Crossley, A.; Compton, R. G. **2013**,

(16) Ivanova, O. S.; Zamborini, F. P. **2009**, *132*, 70-72.

(17) Plieth, W. **1982**, *86*, 3166-3170.

(18) Stuart, E.; Rees, N.; Cullen, J.; Compton, R. *Nanoscale.* **2013**, *5*, 174-177.

(19) Lees, J. C.; Ellison, J.; Batchelor-McAuley, C.; Tschulik, K.; Damm, C.; Omanović, D.; Compton, R. G. *ChemPhysChem.* **2013**, *14*, 3895-3897.

# 7 Conclusions and Future Work

## 7.1 Conclusions

The investigations described in this dissertation demonstrate that the electrochemical method of redox cycling is promising for monitoring concentrations of neurotransmitters in vivo. Redox cycling has shown advantages in amplification of signals, selectivity of species based on their electrochemical reaction mechanism and no background subtraction, which are features compatible with monitoring basal level neurotransmitter concentrations in extracellular fluid of the brain. The studies in this dissertation also showed the ability of redox cycling for simultaneous detection of dopamine (DA) and norepinephrine (NE) without electrode modification, which contributes to the field of in vivo voltammetry of neurotransmitters.

First, fundamental studies were performed to evaluate the redox cycling behavior of individual and binary mixtures of catecholamines. Microelectrode arrays with 4 µm gaps between individually addressable, 4-µm wide gold microband electrodes were used for this study. Electrode configurations with different separations between the activated generator and collector electrodes were explored. By taking advantage of their different intramolecular cyclization rates, the three catecholamines could be distinguished by examining their relative contributions to the signals at collector electrodes located at different distances from the generator electrodes. With a 4 µm gap, epinephrine (EP) showed low redox cycling efficiency, which is different from DA and NE, and therefore is silent at the collector. Further studies of DA and NE with other gap conditions demonstrated differentiation between these two neurotransmitters, as well.

Second, in vitro detection of DA in the presence of multiple electrochemically-active interfering species, including ascorbic acid (AA), uric acid (UA), L-3,4-dihydroxyphenylalanine (L-dopa), homovanillic acid (HVA), 3-methoxytyramine (3-MT) and 5-hydroxyindoleacetic acid (5-HIAA), was investigated. With the microband electrode arrays having 4 µm separations between two generator and three alternating collector electrodes, DA can be selectively detected at the collector, where all of these interfering species are silent. Detection limits of 0.730 ± 0.013 µM and 0.086 ± 0.002 µM were achieved for DA detection with and without the presence of interfering species, respectively. This is in the range of physiological levels of DA reported (5-100 nM[4]).

Third, to apply redox cycling to in vivo studies, SU-8 based neural probes with dimensions suitable for insertion into the brain were designed. Probe designs for co-planar microelectrode arrays and vertical edge microelectrode arrays have been made. Microfabrication procedures have been tested for both types

of probes, and future work is needed to modify the fabrication procedure to resolve challenges encountered with the present one. It is likely that alternative substrate materials will need to be identified to accommodate new fabrication protocols.

Moreover, studies on electrochemical characterization of silver-containing nanoparticles by anodic stripping voltammetry were employed to better understand processes to modify electrodes with nanoparticles. These investigations were inspired by an interest in expanding the library of neurochemicals for electrochemical detection at probes, such as glutamate with enzyme-conjugated nanoparticles. Results from this study showed that the commonly used drop-casting technique for nanoparticle deposition on an electrode surface is problematic and modification methods that produce more uniformed nanoparticles deposition are needed.

## 7.2 Future Work

The work contained in this dissertation explores the fundamental chemistry and application of in vitro detection of catecholamines by redox cycling. The foundation is now set for future in vivo testing and applications. To gain a better understanding of the catecholamine redox cycling mechanism and apply this detection method in vivo, future work is proposed.

### 7.2.1 Digital Simulation of Redox Cycling System

Digital simulations of electrochemical systems under redox cycling conditions are desired to understand the experimental data and optimize the design of microelectrode arrays on a neural probe. COMSOL Multiphysics modeling software with the electrochemistry module can be used for this purpose. Initial efforts have already begun but are not included in this dissertation. A geometry that reflects the microfabricated electrode arrays can be established. Starting conditions and constants can be set up according to the literature.[1] Electrode reactions and homogeneous reactions in solution will be set up according to the ECC' mechanism of catecholamines.[2, 3] Only a few constants needed for the simulation can be found in the literature, including the rate constants of catecholamines for their intramolecular cyclization ($k_{DA}$ = 0.13 ± 0.05 $s^{-1}$, $k_{NE}$ = 0.98 ± 0.52 $s^{-1}$, $k_{EP}$ = 87 ± 10 $s^{-1}$, in phosphate buffer at pH 7.4),[4] $E_{1/2}$ value for the two-electron reduction of aminochrome (-0.207 V vs. Ag/AgCl (saturated KCl) for EP.[2, 5]) and diffusion coefficient of dopamine in aqueous solution (D = 6.0 × $10^{-6}$ $cm^2/s$,[25]). Estimation of other constants (such as the reaction rates of the C' reactions of each catecholamine and the C' reactions between two

different catecholamines) is needed. Simulated current densities and corresponding redox cycling efficiencies will be used to compare with experimental data. Based on the simulation parameters that provide results that best fit the experimental data, further optimization of electrode geometries can then be performed. For example, electrode width, gaps between electrodes and number of electrodes can be optimized without the need of designing and fabrication of additional microelectrode arrays. This approach can be used to guide the design of new microelectrode arrays for better selectivity and sensitivity.

### 7.2.2 Optimization of Neural Probe Design and Microfabrication Procedure

Two possible solutions have been proposed here to solve the challenges encountered during microfabrication process described in Chapter 5. One is to investigate other polymer materials that can serve as a substrate for the neural probe and which are compatible with a microfabrication approach similar to that already described in Chapter 5. Other negative photoresists, benzocyclobutene and polyimide, are possible candidate material for flexible neural probe fabrication.[6, 7] Another possible solution is the use of a silicon wafer as the substrate of the probe. This substrate would make the electrode-defining process easier but would require time-consuming wafer thinning processes (e.g. deep reactive ion etching) to achieve the desired probe shape and size.

Further improvements of the design for increasing sensitivity and selectivity will also be performed to get lower detection limit for DA detection in the presence of interfering species. This could be achieved by optimization of the vertical edge microelectrode arrays proposed in Chapter 5. Another option is to create co-planar arrays with nanometer scale electrode features by electron beam lithography.

After successful fabrication, the neural probes will be connected to a zero insertion force edge connector that is surface-mounted to a printed circuit board. Characterization of electrodes on the probe using a model compound and catecholamines will be performed in vitro. In vivo performance of the probe for DA detection will also be tested in collaboration with other group with neurological expertise.

### 7.3 References


(1) Odijk, M.; Olthuis, W.; Dam, V. A. T.; van den Berg, A. **2008**, *20*, 463-468.

(2) Hawley, M.; Tatawawadi, S.; Piekarski, S.; Adams, R. *J.Am.Chem.Soc.* **1967**, *89*, 447-450.

(3) Ciolkowski, E. L.; Maness, K. M.; Cahill, P. S.; Wightman, R. M.; Evans, D. H.; Fosset, B.; Amatore, C. *Anal.Chem.* **1994**, *66*, 3611-3617.

(4) Ciolkowski, E. L.; Cooper, B. R.; Jankowski, J. A.; Jorgenson, J. W.; Wightman, R. M. *J.Am.Chem.Soc.* **1992**, *114*, 2815-2821.

(5) Zhang, Z.; Huang, J.; Wu, X.; Zhang, W.; Chen, S. *J Electroanal Chem.* **1998**, *444*, 169-172.

(6) Altuna, A.; Gabriel, G.; de la Prida, Liset Menéndez; Tijero, M.; Guimerá, A.; Berganzo, J.; Salido, R.; Villa, R.; Fernández, L. J. *J Micromech Microengineering.* **2010**, *20*, 064014.

(7 ) Cheung, K. C. *Biomed.Microdevices.* **2007**, *9,* 923-938.